PL-TR--
92-1032

ASSESSMENT OF THE NASA ORBITAL DEBRIS ENGINEERING MODEL

K.W. Yates
F.M. Jonas

ORION International Technologies, Inc.
6501 Americas Parkway, Suite 200
Albuquerque, NM 87110

February 1995

Final Report

PHILLIPS LABORATORY
Advanced Weapons and Survivability Directorate
AIR FORCE MATERIEL COMMAND
KIRTLAND AIR FORCE BASE, NM 87117-5776

PL-TR--92-1032

This final report was prepared by ORION International Technologies, Inc., Albuquerque, New Mexico, under contract F29601-89-C-0001, Job Order 31080101, with the Phillips Laboratory, Kirtland Air Force Base, New Mexico. The Phillips Laboratory Project Officer-in-Charge was Capt Albert E. Reinhardt (WSC).

When Government drawings, specifications, or other data are used for any purpose other than in connection with a definitely Government-related procurement, the United States Government incurs no responsibility or any obligation whatsoever. The fact that the Government may have formulated or in any way supplied the said drawings, specifications, or other data, is not to be regarded by implication, or otherwise in any manner construed, as licensing the holder, or any other person or corporation; or as conveying any rights or permission to manufacture, use, or sell any patented invention that may in any way be related thereto.

This technical report has been authored by a contractor of the United States Government. Accordingly, the United States Government retains a nonexclusive royalty-free license to publish or reproduce the material contained herein, or allow others to do so, for the United States Government purposes.

This report has been reviewed by the Public Affairs Office and is releasable to the National Technical Information Service (NTIS). At NTIS, it will be available to the general public, including foreign nationals.

If your address has changed, if you wish to be removed from the mailing list, or if your organization no longer employs the addressee, please notify PL/WSC, 3550 Aberdeen Ave SE, Kirtland AFB, NM 87117-5776, to help maintain a current mailing list.

This report has been reviewed and is approved for publication.

SCOTT R. MAETHNER, Capt, USAF
Project Officer

FOR THE COMMANDER

STEVEN B. DRON, Lt Col, USAF
Chief, Space Control
Technologies Division

WILLIAM G. HECKATHORN, Col, USAF
Director, Advanced Weapons
and Survivability Directorate

DO NOT RETURN COPIES OF THIS REPORT UNLESS CONTRACTUAL OBLIGATIONS OR NOTICE ON A SPECIFIC DOCUMENT REQUIRES THAT IT BE RETURNED.

REPORT DOCUMENTATION PAGE

Form Approved
OMB No. 0704-0188

1. AGENCY USE ONLY (Leave blank)	2. REPORT DATE	3. REPORT TYPE AND DATES COVERED
	February 1995	Final, Apr 91 - Jun 92

4. TITLE AND SUBTITLE
ASSESSMENT OF THE NASA ORBITAL DEBRIS ENGINEERING MODEL

5. FUNDING NUMBERS
C: F29601-89-C-0001
PE: 63215C
PR: 3108
TA:01
WU:01

6. AUTHOR(S)
K.W. Yates, F.M. Jonas

7. PERFORMING ORGANIZATION NAME(S) AND ADDRESS(ES)
ORION International Technologies, Inc.
6501 Americas Parkway
Albuquerque, NM 87110

8. PERFORMING ORGANIZATION REPORT NUMBER

9. SPONSORING/MONITORING AGENCY NAME(S) AND ADDRESS(ES)
Phillips Laboratory
3550 Aberdeen Ave SE
Kirtland AFB, NM 87117-5776

10. SPONSORING/MONITORING AGENCY REPORT NUMBER
PL-TR--92-1032

11. SUPPLEMENTARY NOTES

12a. DISTRIBUTION/AVAILABILITY STATEMENT
Approved for public release;
distribution is unlimited.

12b. DISTRIBUTION CODE

13. ABSTRACT *(Maximum 200 words)*

This report presents an assessment of the orbital-debris engineering model which predicts near- and long-term orbital-debris environments on spacecraft in low earth orbit. The model predicts debris flux environment, mass, and collision-velocity distributions. The empirically based model is a curve fit to measured data and incorporates results derived from the NASA EVOLVE code. The data base includes US Space Command orbital element sets, Aricebo and Goldstone radar observations, MIT/Lincoln Laboratory Experimental Test System and Ground-based Electro-Optical Deep Space Surveillance optical data, and surface impact data from the Solar Maximum Mission. The model is most sensitive to the small-debris particles and becomes undefined as the particle size approaches zero. The model is least sensitive to changes in orbital altitude. The model predicts essentially constant flux > 1000 km and does not reproduce measured data at these altitudes. The uncertainty is shown to be a factor of 2-4 for an altitude of 500$\pm$200 km (all particle sizes) and for sizes > 10 cm (for all altitudes), and at least an order of magnitude for all other sizes and altitudes. The collision-velocity distribution, and particle mass expressions represent extremely gross approximations of the environment. On the basis of the results of the analysis, it is recommended the model's use be restricted to altitudes < 1000 km, debris sizes from 10^{-4} to 10^{3} cm, and for projections through the year 2010.

14. SUBJECT TERMS	15. NUMBER OF PAGES
Space debris, debris engineering model, orbital debris environment, NASA engineering model.	92
	16. PRICE CODE

17. SECURITY CLASSIFICATION OF REPORT	18. SECURITY CLASSIFICATION OF THIS PAGE	19. SECURITY CLASSIFICATION OF ABSTRACT	20. LIMITATION OF ABSTRACT
Unclassified	Unclassified	Unclassified	SAR

PREFACE

The authors wish to acknowledge the aid and assistance of the NASA Johnson Space Center personnel during meetings and discussions with them on the development of their model. Specifically, the authors wish to thank Dr. Andrew Potter and Mr. Don Kessler (the author of the NASA 89 and NASA 90 models) of NASA JSC, and Dr. Phillip Anz-Meador and Mr. Greg Ojakangas of Lockheed Engineering and Services Company. Discussions were extremely open and frank, and the NASA insights to the model development aided immensely in the ORION analysis.

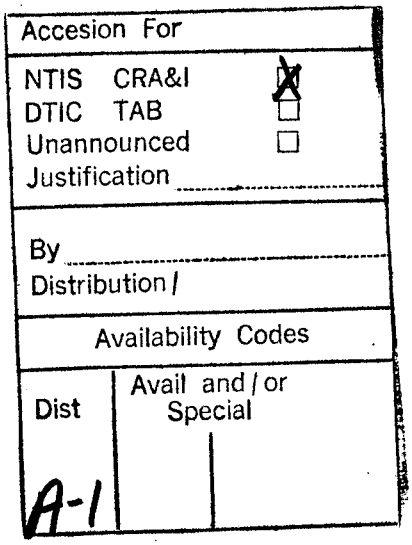

CONTENTS

CONTENTS (Concluded)

FIGURES

FIGURES (Continued)

Figure — Page

FIGURES (Concluded)

TABLES

1.0 OBJECTIVE

This report assesses the National Aeronautics and Space Administration (NASA) long-term, orbital-debris engineering model developed to predict the debris environment in low earth orbit (LEO). Specifically, this report is an assessment of the NASA orbital-debris model as described in References 1 and 2, hereafter known as the NASA 89 and NASA 90 models, respectively. This report describes the model development, presents a model sensitivity analysis, and establishes the model uncertainties. The goal of this assessment is to assist the Air Force (AF) in its task of developing a long-term debris model that can (1) operate with higher accuracy at the relevant altitudes and orbits parameters; (2) benefit from new AF and non-AF debris measurements; and (3) accommodate current and future space scenarios.

Section 2.0 presents a brief background and overview of orbital debris and why this environment is of concern to space operators, especially the Department of Defense (DoD) and the AF. The NASA 89 model and the revised NASA 90 are discussed in Section 3.0. The assessment focuses on the revised NASA 90 model. The NASA 89/90 model development is presented in Section 4.0. Included is an examination of the measurement data bases, model development rationale, and an assessment of the model limitations. The orbits of interest (altitudes and inclinations) for current and future AF and DoD operations are discussed in Section 5.0. The sensitivity analysis of the NASA 90 model is found in Section 6.0. The model sensitivities are analyzed with respect to the model variables: debris diameter, orbital altitude and inclination, time, solar activity, and debris growth. Summary comparisons and an assessment of the sensitivity are presented. The ability of the model to predict the environment, and its associated error or uncertainty, is covered in Section 7.0. This uncertainty analysis for the NASA 90 model is based upon a propagation of error analysis that uses NASA's estimated uncertainties to predict the overall model uncertainty. Section 8.0 summarizes the assessment of the NASA 90 model.

2.0 BACKGROUND

The man-made, orbital-debris environment is of increasing concern to users of space. This environment has grown since man's first steps into space. If unchecked, it will pose extreme hazards for future space operations. An essential first step in assessing potential hazards posed by the environment is to characterize the actual orbital-debris environment. A diagnostic model should be based on complete and reliable observational data. From diagnostic models, predictive models can be developed that may be based on either physics or derived empirically from the measurement data. The NASA 90 model is an empirically derived, predictive model of the debris environment for space system designers, operators, and other users. The emphasis of NASA 90 model is on the prediction of the long-term, orbital-debris environment. Before the NASA 90 model can be used with confidence, it must be assessed against the actual data or validated models to determine its limits of applicability and accuracy. The purpose of this effort is to conduct such an assessment.

Early in man's first operations in space, the principal concern with possible particle impacts was due to the natural, meteoroid environment. Meteoroids are part of the interplanetary environment and are encountered as the earth sweeps through space in its orbit about the sun (meteoroids are not in earth orbit). At any one instant, it is estimated that the meteoroid mass within 2000 km of the earth's surface is ~200 kg with most of this mass concentrated in 0.1-mm-dia meteoroids. Meteoroids move at average relative speeds of 20 km/s (Ref. 1). The natural environment is of concern, but differs from the orbital-debris environment. The man-made orbital debris remains in earth orbit and originates from the manner of space operations (intentionally or unintentionally leaving debris, boosters, spent payloads, etc., in orbit), intentional or unintentional explosions, and collisions. Estimates of orbital debris now in earth orbit within 2000-km orbital altitude ranges anywhere from 1.6 to 3.0 Mkg. Orbital debris moves at relative speeds on the order of 10 km/s. Using the value 3.0 Mkg for orbital-debris mass in orbit, it is further estimated that ~300 kg of this mass consists of particles $\leq$1 mm, 1000 kg consists of particles $\leq$1 cm, with the remainder mostly concentrated in approximately 3000 spent rockets and inactive payloads (Ref. 1). Unlike the meteoroid environment, much of the orbital debris is distributed in regions of current satellite operations. The orbital-debris environment has become at least as hazardous as the meteoroid environment for objects in LEO.

3.0 NASA ORBITAL-DEBRIS MODEL

This section describes the NASA 89 and 90 orbital-debris models. Included in these models is the prediction of (1) the orbital-debris flux (impacts per year per unit area (square meters)) as a function of the debris diameter, year of interest, solar activity, spacecraft altitude and orbital inclination, and projected growth of the orbital debris; (2) the orbital-debris collision-velocity impact and direction distribution as a function of orbital inclination; and (3) the orbital-debris mass as a function of diameter for assumed spherical shapes.

The model was developed with the goal of producing an engineering model for use by the engineering and design community to apply in their regions of interest. The model represents a curve fit to the measurement data (data sources and model development will be discussed in Section 4.0). The model is considered to be applicable only to objects in LEO (Refs. 1 and 2). This represents a nominal altitude of $h \leq 2000$ km; however, Kessler* felt it was most valid for altitudes of $h \leq 1000$ km. Subsection 3.4 examines the behavior of the model in the extreme limits of the variables on which the model is based.

3.1 NASA 89 ORBITAL-DEBRIS FLUX MODEL

The NASA 89 orbital-debris flux engineering model (Ref. 1) predicts the cumulative flux of orbital debris, for a diameter (d) and larger, for space systems in LEO at altitude (h), inclination (i), and year (t) using the following expression:

$$F(d, h, i, t, S) = k\,\Phi(h, S)\,\Psi(i)\,[F_1(d)g_1(t) + F_2(d)g_2(t)] \qquad (1)$$

where

- F = Time-averaged, cumulative, orbital-debris flux, impacts per year, and per unit area (impact/yr • m ^{2}) against a single-sided surface for diameters ($\geq$d)
- d = Orbital-debris diameter (cm)
- h = Altitude (km)
- i = Orbital inclination (deg)
- t = Time (yr)
- S = Thirteen-month, smoothed, solar radio flux at 10.7-cm wavelength expressed in 10^4 Jansky (Jy) for the previous year (t - 1), typically $70 \leq S \leq 150$ where S may exceed value of 200 at solar maximum

* Private meetings/communication with NASA/JSC, D.J. Kessler, 1990-1991.

k = Surface orientation factor where k is the ratio of the flux on a single-sided surface at a specified orientation to the flux on a randomly tumbling single-sided surface. $k = 1$ for a randomly tumbling surface and theoretically, $0 \leq k \leq 4$, for a fixed surface orientation (Ref. 1)

$\Phi(h,S)$ = $\Phi_1(h,S)/[\Phi_1(h, S) + 1]$, functional form accounting for effects of solar activity (atmospheric drag effects on debris) as a function of altitude and the solar radio flux

$\Phi_1(h,S)$ = $10^{(h/200 - S/140 - 1.5)}$

$\Psi(i)$ = Debris concentration correction factor (Table 1) where $\Psi(i)$ is the ratio of the flux at inclination i to the flux at the population's average inclination of approximately 60 deg or $F|_i / F|_{i = 60\ deg}$

$F_1(d)$ = $1.05\ (10^{-5})\ d^{-2.5}$, size distribution for small particles

$g_1(t)$ = $(1 + 2p)^{(t - 1985)}$, small-particle growth

p = Assumed annual growth rate of mass in orbit (5% or $p = 0.05$)

$F_2(d)$ = $7\ (10^{10})\ (d + 700)^{-6}$, size distribution for large particles

$g_2(t)$ = $(1 + p)^{(t-1985)}$, large-particle growth

Note that the distinction between small and large orbital-debris particles is in the range of 1 to 10 cm. No distinct boundary is specified in the NASA reports; however, diameters <1 cm are considered small by the technical community while diameters >10 cm are considered large.

The average number of impacts, N, on a surface area, A, exposed to the orbital-debris environment, F, over a period of time, t_i to t_f, is calculated using the following integral relationship:

$$N = \int_{t_i}^{t_f} FA\,dt \tag{2}$$

Note that Equation 2 determines the average number of impacts on a single-sided surface whose orientation is given by the value of k. To find the total number of impacts on a spacecraft, one must determine k for each respective surface and then sum up the impacts evaluated for each surface, e.g.,

$$N_{TOTAL} = \sum_{j=1}^{M} N_j = \sum_{j=1}^{M} \left\{ \int_{t_i}^{t_f} F_j A_j\,dt \right\} \tag{3}$$

for M surfaces. The only value changing in the orbital flux expression, (Eq. 1) is the value of k, therefore

$$N_{TOTAL} = \sum_{j=1}^{M} N_j = \left\langle \int_{t_i}^{t_f} \left(k_j \Phi \Psi [F_1 g_1 + F_2 g_2] \right) A_j dt \right\rangle \tag{4}$$

Table 1. Orbital-debris concentration correction factor, Ψ (i).

Inclination (deg)	Ψ(i)	Inclination (deg)	Ψ(i)	Inclination (deg)	Ψ(i)
25	0.900	58	1.075	92	1.400
26	0.905	59	1.080	93	1.440
27	0.910	60	1.090	94	1.500
28	0.912	61	1.100	95	1.550
28.5	0.9135	62	1.115	96	1.640
29	0.915	63	1.130	97	1.700
30	0.920	64	1.140	98	1.750
31	0.922	65	1.160	99	1.770
32	0.927	66	1.180	100	1.780
33	0.930	67	1.200	101	1.770
34	0.935	68	1.220	102	1.750
35	0.940	69	1.240	103	1.720
36	0.945	70	1.260	104	1.690
37	0.950	71	1.290	105	1.660
38	0.952	72	1.310	106	1.610
39	0.957	73	1.340	107	1.560
40	0.960	74	1.380	108	1.510
41	0.967	75	1.410	109	1.460
42	0.972	76	1.500	110	1.410
43	0.977	77	1.630	111	1.380
44	0.982	78	1.680	112	1.350
45	0.990	79	1.700	113	1.320
46	0.995	80	1.710	114	1.300
47	1.000	81	1.700	115	1.280
48	1.005	82	1.680	116	1.260
49	1.010	83	1.610	117	1.240
50	1.020	84	1.530	118	1.220
51	1.025	85	1.490	119	1.200
52	1.030	86	1.450	120	1.180
53	1.040	87	1.410	121	1.165
54	1.045	88	1.390	122	1.155
55	1.050	89	1.380	123	1.140
56	1.060	90	1.370	124	1.125
57	1.065	91	1.380	125	1.110

Finally, the probability of exactly n impacts occurring on a single-sided surface is found using Poisson statistics where

$$P_n = \frac{N^n}{n!} e^{-N} \tag{5}$$

3.2 NASA 90 ORBITAL-DEBRIS FLUX MODEL

The NASA 90 orbital-debris flux engineering model (Ref. 2) is an update to Equation 1 and is based upon more recent measurements of the orbital-debris environment. These updates will be discussed later in this report. The revised model is as follows:

$$F(d, h, i, t, S) = H(d)\ \Phi(h,S)\ \Psi(i)\ [F_1(d)\ g_1(t) + F_2(d)\ g_2(t)] \tag{6}$$

where

$F(d,h,i,t,S)$	=	Time-averaged, cumulative, orbital-debris flux on a randomly tumbling single-sided surface for diameters d and greater. Note that the parameter k is no longer associated with F, but is now only associated with the calculation of the average number of impacts, N, on a surface of A, defined in Equation 7.
$H(d)$	=	$\sqrt{10^{\exp(-(\log_{10} d - 0.78)^2/(0.637)^2)}}$
$F_1(d)$	=	$1.22\ (10^{-5})\ d^{-2.5}$
$F_2(d)$	=	$8.1\ (10^{10})\ (d + 700)^{-6}$
$g_1(t)$	=	$(1 + q)^{(t - 1988)}$ where q = 0.02 until 2010 and q = 0.04 after 2010
$g_2(t)$	=	1 + p (t - 1988) where p = 0.05

All other parameters and functions remain as previously defined.

$$N = \int_{t_i}^{t_f} \left\{ \sum_{j}^{M} k_j\ F\ A_j\ dt \right\} \tag{7}$$

The probability of exactly n impacts remains as defined in Equation 5.

A comparison of the NASA 89 model, (Eq. 1) to the NASA 90 model (Eq. 6), is shown in Figure 1 for h = 500 km, t = 1995, i = 30 deg, S = 90, and k = 1. The principal difference is due to the function H(d) in the region 1 cm $\leq$ d $\leq$ 100 cm. In Subsection 4.3.3, H(d) will be shown to increase the NASA 89 prediction for these large particles by up to a factor of 3. Other differences in the model flux predictions between the NASA 89 and 90 models are due to changes in the growth of both large and small debris. The NASA 90 model assumed growth and growth rates are less severe. For the small debris, the growth rate has been reduced from 10 percent (2 x p) to 2 percent. The reduction in growth rate is based on studies that use the NASA EVOLVE (Evolutionary Model) code (Ref. 2). EVOLVE shows fewer events and a lower source term from collisions of larger objects. This reduction in the predicted environment for the small debris can be seen in Figure 1. For the large debris, the functional form of the large-particle growth, $g_2(t)$, has been changed from compounded to linear. The reason for this will be discussed in Section 4.0. The assumed growth rate, p, remains at 5 percent. Comparisons of the NASA 90 model predictions versus the measured environment are shown in Figures 2 and 3.

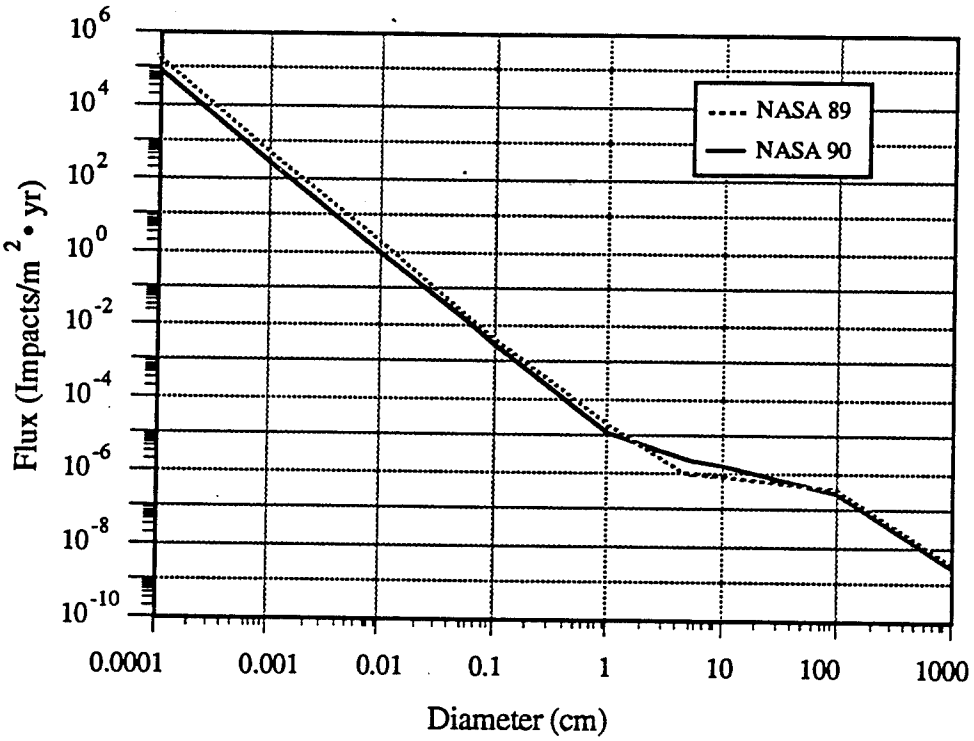

Figure 1. NASA 89 model versus NASA 90 model, flux versus diameter, h = 500 km, i = 30 deg, t = 1995, S = 90, (k = 1).

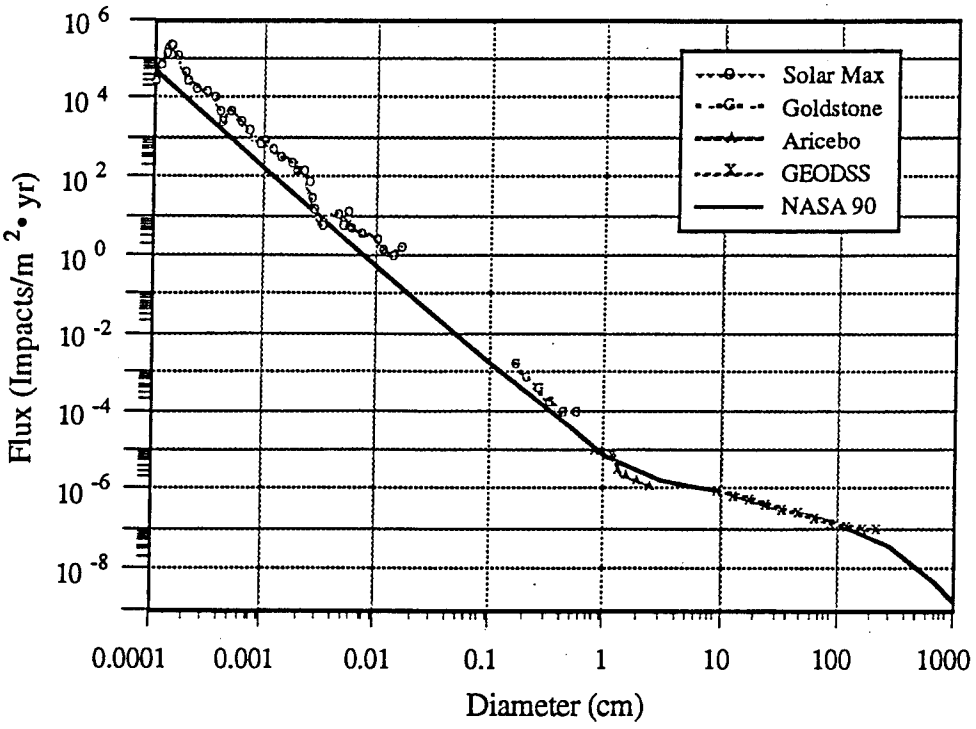

Figure 2. NASA 90 orbital-debris flux versus diameter, d (cm), compared to data from Solar Max, Goldstone, Aricebo, and GEODSS (h = 500 km, i = 28.5 deg, t = 1988, S = 140).

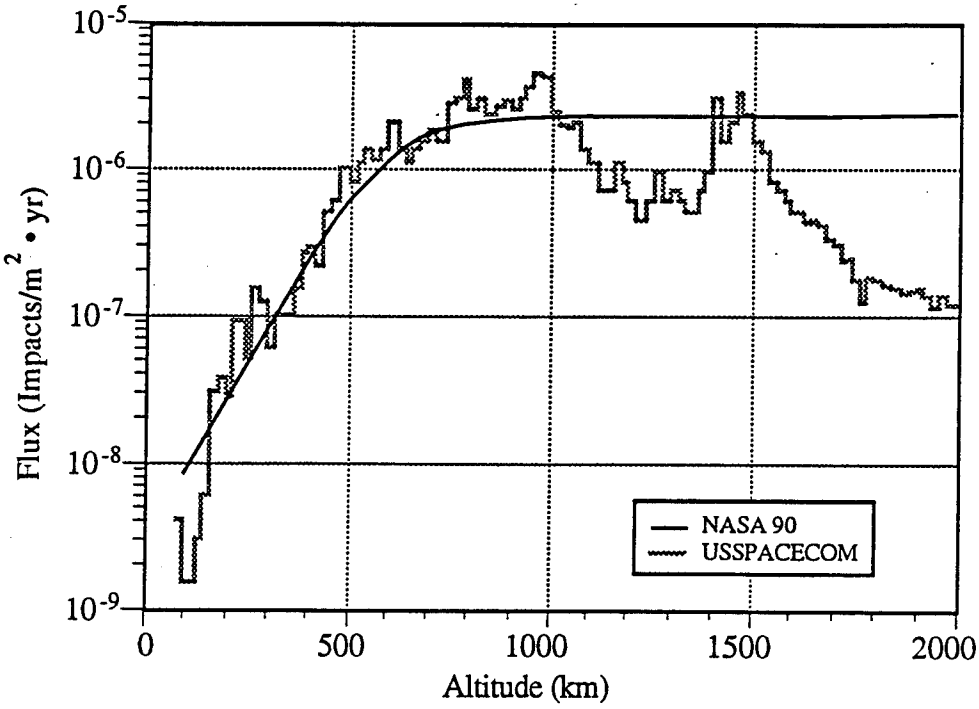

Figure 3. NASA 90 orbital-debris flux versus altitude, h (km), compared to USSPACECOM data (d ≥ 10 cm, i = 60 deg, t = 1990, S = 200).

3.3 DEBRIS IMPACT AND DIRECTION DISTRIBUTIONS, AND PARTICLE DENSITY

The orbital-debris, collision-velocity impact distribution and impact direction remains unchanged between the NASA 89 and 90 models. The collision-velocity distribution model predicts the number of impacts with collision velocities between V and V + dV relative to a spacecraft as a function of the spacecraft's orbital inclination, i, and the collision velocity, V (km/s), where

$$f(V) = \left(2 V V_0 - V^2 \right) \left\{ G\, e^{-\left[\frac{V - A V_0}{B V_0}\right]^2} + F\, e^{-\left[\frac{V - D V_0}{E V_0}\right]^2} \right\} + HC \left(4 V_0 V - V^2 \right) \qquad (8)$$

A is a constant and B, C, D, E, F, G, H, and V_0 are functions of the spacecraft orbital inclination. The parameters A through H result from the empirical curve fit while V_0 is related to the debris average orbital velocity as seen from the data for these inclinations. (Note that NASA has apparently introduced the appropriate units, i.e., impacts • s ^{2}/km ^{2}, into the coefficients to give f (V) the proper units, impacts.)

$f(V)$ = Number of impacts between V and V + dV, where $f(V) \geq 0$ (if a value of $f(V) < 0$ results from Equation 8, then set $f(V) = 0$)

$$V_0 = \begin{cases} 7.25 + 0.015\,(i - 30) & i < 60 \text{ deg} \\ 7.7 & i \geq 60 \text{ deg} \end{cases}$$

$$A = 2.5$$

$$B = \begin{cases} 0.5 & i \leq 60 \text{ deg}, \\ 0.5 - 0.1\,(i - 60) & 60 < i < 80 \text{ deg} \\ 0.3 & i \geq 80 \text{ deg} \end{cases}$$

$$C = \begin{cases} 0.0125 & i \leq 100 \text{ deg} \\ 0.0125 + 0.00125\,(i - 100) & i > 100 \text{ deg} \end{cases}$$

$$D = 1.3 - 0.01\,(i - 30)$$

$$E = 0.55 + 0.005\,(i - 30)$$

$$F = \begin{cases} 0.3 + 0.0008(i - 50)^2 & i \leq 50 \text{ deg} \\ 0.3 - 0.01\,(i - 50) & 50 < i < 80 \text{ deg} \\ 0.0 & i \geq 80 \text{ deg} \end{cases}$$

$$G = \begin{cases} 18.7 & i \le 60 \text{ deg} \\ 18.7 + 0.0289\ (i - 60)^3 & 60 < i \le 80 \text{ deg} \\ 250 & i > 80 \text{ deg} \end{cases}$$

$$H = 1.0 - 7.57\ (10^{-5})\ (i - 60)^2$$

f(V) represents an averaged, collision-velocity impact distribution over all altitudes (LEO). Figure 4 shows f(V) for an orbital inclination of 30 deg.

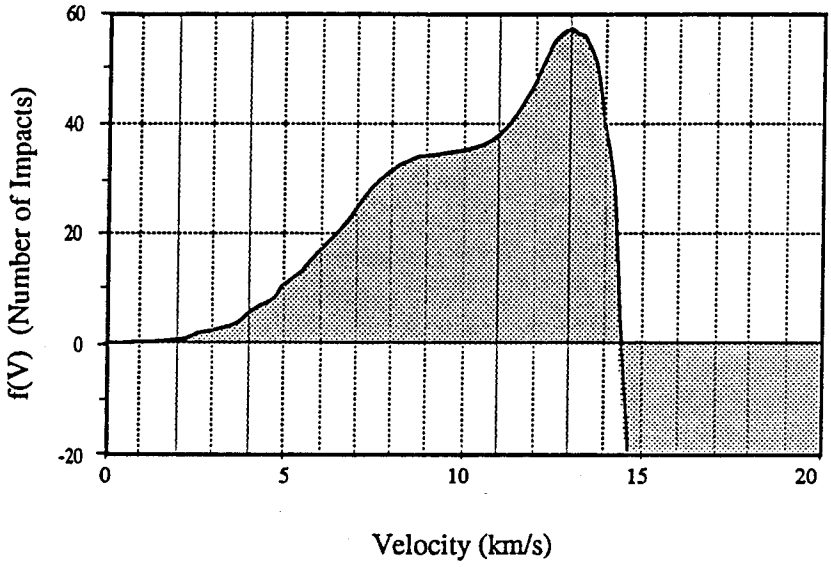

Figure 4. Orbital-debris, collision-velocity impact distribution, f(V), versus velocity (V) for i = 30 deg.

The normalized velocity distribution is given by (Refs. 1 and 2)

$$f'(V) = f(V) \Big/ \int_0^\infty f(V)\ dV \tag{9}$$

Only values of $f(V) \ge 0$ have any physical meaning, therefore, the region of f(V) that is used to specify the collision velocity impact distribution is given from $f(V) = 0$ at $V = 0$, defined as V_{min}, to $f(V) = 0$ at $V = V_{max}$. Equation 10 shows that the positive area of the curve, f(V), is used to normalize the velocity distribution. This is given as,

$$f'(V) = f(V) \Big/ \int_{V_{min}}^{V_{max}} f(V)\, dV \tag{10}$$

where V_{min} and V_{max} represent the minimum and maximum velocities at f(V) equals zero. For each orbital inclination, i, V_{max} has some value that is a function of i. The maximum V_{max}, V'_{max}, for all inclinations is 15.4 km/s.

Once the collision-velocity impact distribution and velocities are known for a given orbital inclination, then the direction of impact as well as the frequency of impact for a given direction may be estimated. This is done by first assuming the direction of impact is specified by the angle α between the spacecraft orbit and relative impact vector as shown in Figure 5. The spacecraft and debris velocity vectors are assumed to be circular orbit velocity vectors in the local horizontal plane B. The relative velocity is the resultant vector between the spacecraft and debris inertial vectors.

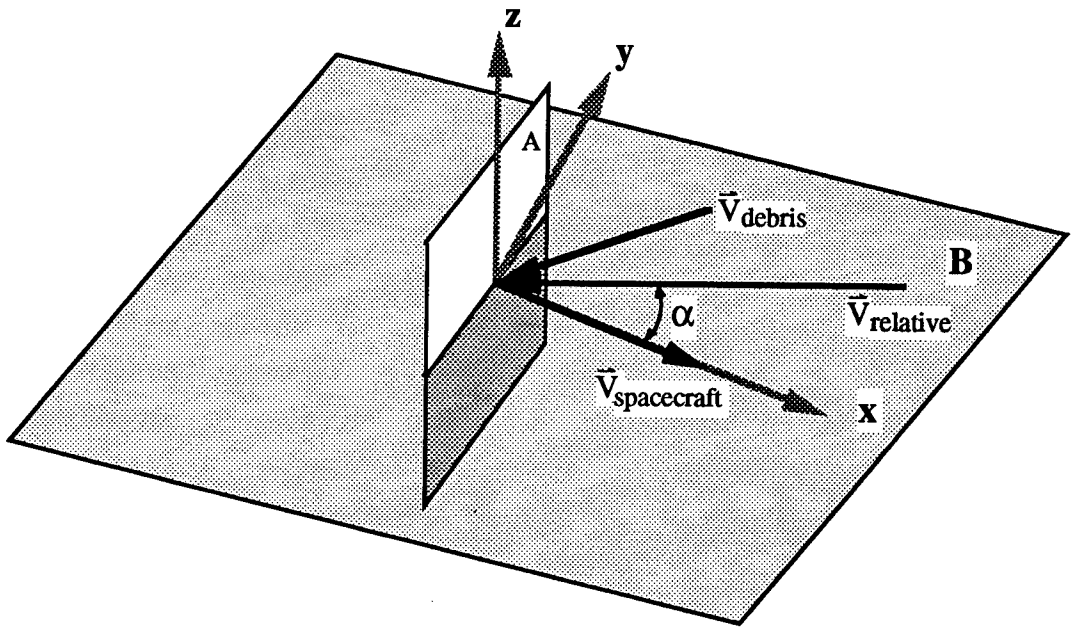

Plane A	:	Single-sided surface (represents surface of spacecraft)
Plane B	:	Parallel to Earth's surface
x-axis	:	Defined by direction of spacecraft travel (in Plane B)
y-axis	:	Orthogonal axis (in Plane B)
z-axis	:	Earth vertical (up)
$\vec{V}_{spacecraft}$	:	Surface (spacecraft) velocity vector
$\vec{V}_{debris}$	:	Debris velocity vector
$\vec{V}_{relative}$	:	Relative (impact) velocity vector
α	:	Angle between spacecraft and relative impact velocity vectors

Figure 5. Orbital-debris/spacecraft reference frame.

From the data, an average orbital velocity for objects in LEO of 7.7 km/s was used to determine the collision direction. (Note that 7.7 km/s corresponds to a circular orbit of 345 km, but the higher velocity more accurately reflects the existence of debris in elliptical orbits.) Using the geometry presented in Figure 5, it is clear that the maximum impact velocity is when $\alpha = 0$ (head-on collision) and diminishes to 0 when $\alpha \geq 90$ deg. A cosine relationship provides the direction angle of impact (α) given an impact velocity, V, and the maximum possible impact velocity, V'_{max} = 15.4 km/s (i.e., 2 x 7.7 km/s).

$$\cos(\pm\alpha) = V / V'_{max} \tag{11}$$

The range of values for V is bounded by V_{min} and V_{max} for a given inclination.

The assumption of circular orbits implies no out-of-plane (pitch angle) impacts are considered in this model. This is an approximation of the actual environment since debris does exist in elliptical orbits and will have some small pitch angle relative to the local horizontal plane containing the spacecraft velocity vector. This approximation is valid if it is assumed that the mostly near circular eccentricity distributions observed for large trackable population holds for all debris sizes.

Finally, the average mass density for orbital debris is given as follows:

$$\rho = \begin{cases} 2.8d^{-0.74}\ g/cm^3, & d>1\ cm \\ 2.8\ g/cm^3, & d\leq 1\ cm \end{cases} \text{ (NASA 89)}$$

$$\rho = \begin{cases} 2.8d^{-0.74}\ g/cm^3, & d>0.5\ cm \\ 4.7\ g/cm^3, & d\leq 0.5\ cm \end{cases} \text{ (NASA 90)} \tag{12}$$

For purposes of the model, the orbital debris particles are assumed to be spherical, thus the mass is given as follows:

$$m = \rho\left(\frac{\pi}{6} d^3\right) \tag{13}$$

3.4 OBSERVATIONS (LIMITING VALUES)

The NASA orbital-debris model is an engineering tool that is based on a curve fit to data. The model does not necessarily follow from physical laws, therefore, should not be expected to be representative in regions where there are no data to support the model. One assessment of the model's performance is to observe its behavior when its variables are taken to the limit. Physical intuition is used to assess the model's validity at those limits; this will establish the qualitative range of validity and will point out any regions where its formulation may be invalid. This examination is not meant to replace other analysis necessary to assess the model. Rewriting the NASA 90 model in terms of its variables results in the following:

$$F(d,h,i,t,S) = \sqrt{10^{\,e^{\left[(-\log_{10} d - 0.78)^2 / (0.637)^2\right]}}} \; X \left(\frac{10^{(h/200 - S/140 - 1.5)}}{10^{(h/200 - S/140 - 1.5)} + 1} \right) X \; \Psi(i)$$

$$X \left\{ \left[1.22 (10^{-5}) \; d^{-2.5} \right] (1+q)^{(t-1988)} \right.$$

$$\left. + (8.1) (10^{10}) (d+700)^{-6} [1 + p(t-1988)] \right\} \qquad (14)$$

The limits of interest can be observed by examining the behavior of F(d, h, i, t, S) as diameter (d), altitude (h), and growth (p and q) approach both zero and infinity and time (t) approaches infinity. Note, there is no physical significance in the limiting behavior of $\Psi(i)$ or F with respect to orbital inclination, i. The results of these observations are as follows:

Limiting Value		Observations
As d $\rightarrow$ 0,	F $\rightarrow \infty$	Not unreasonable
As d $\rightarrow \infty$,	F $\rightarrow$ 0	Reasonable
As h $\rightarrow$ 0,	F $\rightarrow$ Min Constant $\neq$ 0	Not unreasonable
As h $\rightarrow \infty$,	F $\rightarrow$ Max Constant	Unreasonable
As d $\rightarrow \infty$,	F $\rightarrow \infty$	Reasonable
As p,q $\rightarrow$ 0,	F $\rightarrow$ constant	Reasonable
As p,q $\rightarrow \infty$,	F $\rightarrow \infty$	Reasonable

As diameter decreases, one might expect the number of particles or flux to increase (more smaller particles than larger particles) down to some limiting diameter; therefore, this behavior in F is not unreasonable. Likewise, as diameter increases, one would expect the flux to go to zero simply based on physical reality; therefore, on this basis the behavior of F is reasonable. As altitude decreases, one would expect (due to atmospheric effects) that the flux environment will decrease, which it does. In the limit, h = 0, i.e., the earth's surface, the behavior of F is to decrease to a minimum value, as altitude decreases, which seems to comply with physical intuition and is not unreasonable. One would expect that F should decrease as altitude increases and approach zero in the limit on the basis of physical reality (because this model represents earth orbital debris). The behavior of F as altitude increases gives evidence that the model is valid only to a limiting altitude. Its use should be restricted to LEO as specified (Refs. 1 and 2). The behavior of F as time increases is reasonable assuming an ideal external space environment (no perturbations) and no change in growth rates. The behavior of F with respect to growth rates, p and q, is reasonable especially for unconstrained growth. One also should note that $\Phi(h,S)$ behaves as expected for increasing or decreasing values of h and S (as will be shown graphically in the next section). Qualitatively, the model behaves reasonably in these limits except for increasing altitude.

4.0 MODEL DEVELOPMENT/RATIONALE

This section presents the rationale and basis for the development of the NASA orbital-debris model. As mentioned previously, the NASA orbital-debris model is an engineering model and is based on a curve fit to the measurement data for objects in LEO. It is felt by its author* to be most accurate for $h \leq 1000$ km. The data base used in the development of this model will be discussed as well as the assumptions and development of the functional forms resulting from the curve fit. The estimated model uncertainties and qualitative limitations are also described.

4.1 DATA BASE

The NASA orbital-debris engineering model (Eq. 6) and the collision-velocity impact distribution (Eq. 8) represent curve fits to optical and radar ground observations of orbital debris and data from returned spacecraft surfaces. Data used in the model development and subsequent revision are as follows:

- The U.S. Space Command (USSPACECOM) radar tracking data (Ref. 3), both catalogued and uncataloged Orbital Element Sets, were used to establish altitude and solar activity effects, size distribution (large particles), historical growth rates, inclination, velocity, and directional effects. The data used represent "snapshots" of the LEO environment taken once a year from 1976 through 1988, normally in February. These data provide administrative information, period, inclination, apogee, perigee, and radar cross section of the tracked objects. Sample data from May 1990 are shown in Figure 6. The data from the orbital element sets have been converted to flux units (impacts/yr • m^2). The USSPACECOM currently tracks approximately 6500 to 7000 objects (Ref. 1).

- Optical measurements include data from the Massachusetts Institute of Technology/Lincoln Laboratory Experimental Test Site (MIT/LL ETS) in Socorro, New Mexico (Ref. 4) and the Ground-based Electro-Optical Deep Space Surveillance (GEODSS) network (Ref. 5). The GEODSS sites are located near Socorro, as well as Maui, Hawaii, and the island of Diego Garcia in the Indian Ocean. The GEODSS data were used to substantiate altitude effects and size distribution. The MIT/LL ETS data consisted of 10 hr of viewing in 1984 and 10 hr in 1985. The GEODSS data represent 80.9 hr of viewing (Ref. 5). Sample GEODSS data are shown in Figure 7.

---

* Ibid.

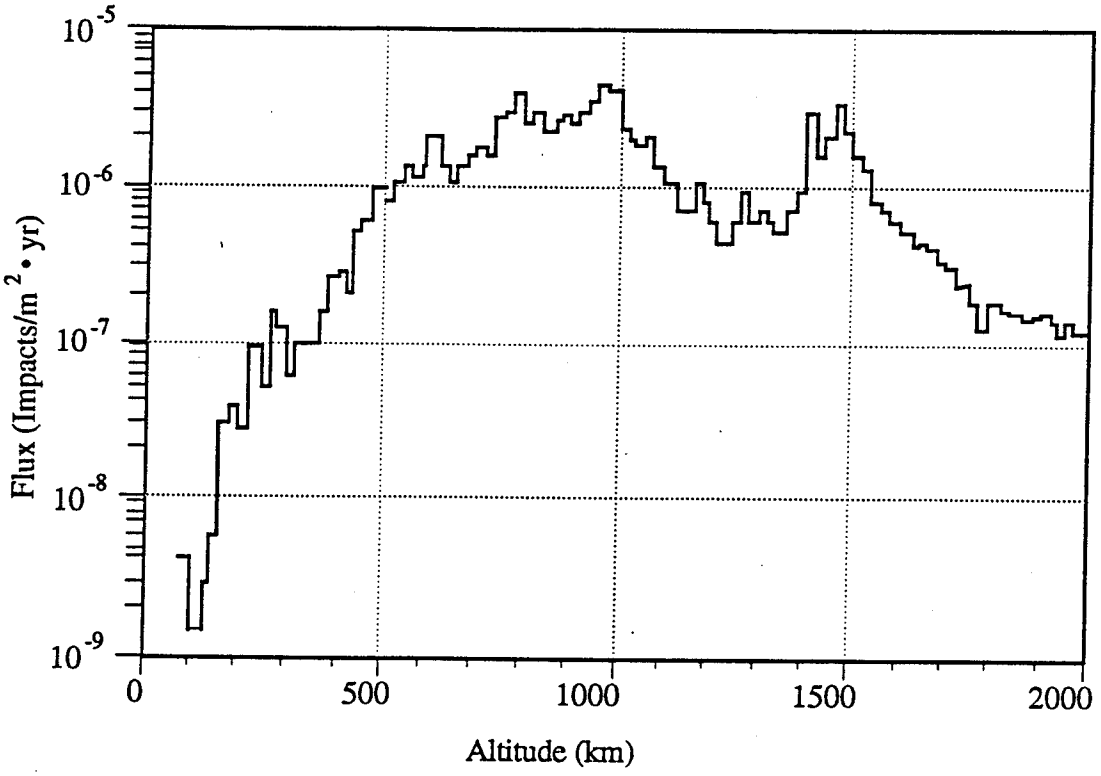

Figure 6. Sample data, USSPACECOM, flux versus altitude, May 1990.

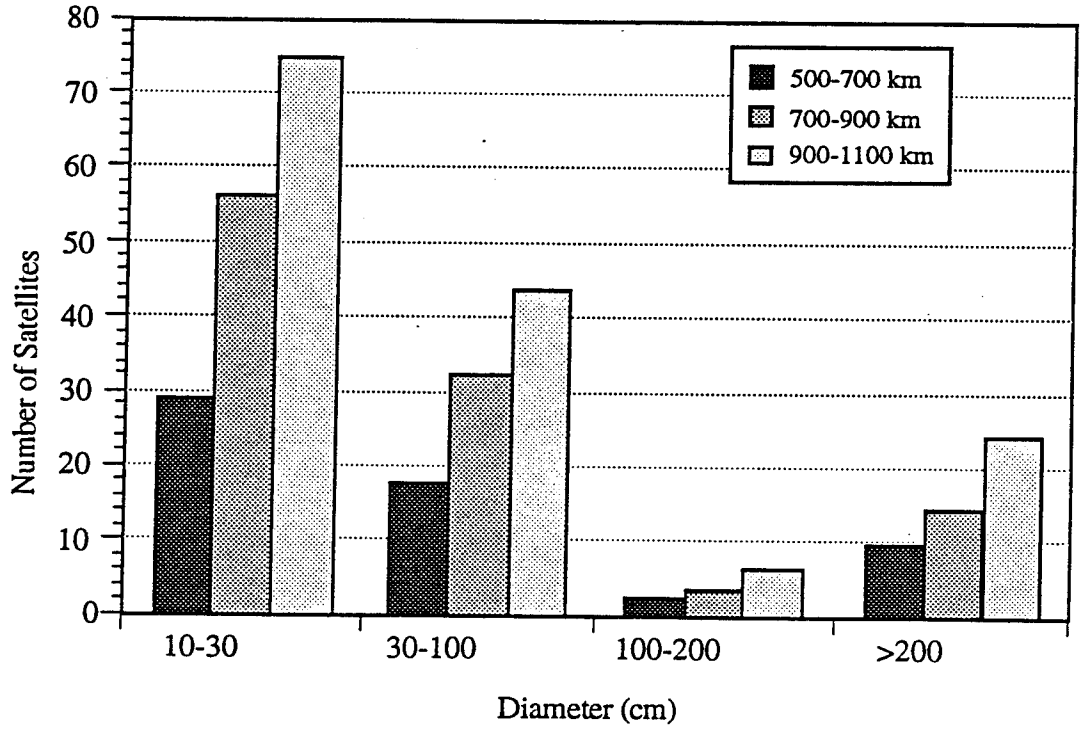

Figure 7. Sample data, GEODSS, showing the number of satellites seen in an 80.9-hr period for i > 20 deg.

- Impact data from returned spacecraft surfaces were used (Refs. 6 and 7). The primary data source was the Solar Maximum Mission (Solar Max) spacecraft that was in space for 4.15 yr (1980-84) at an orbital inclination of 28.5 deg and an altitude range of 500 to 570 km. More than 300 impact craters in the Solar Max thermal control louvres, representing ~3 m^2 of returned space-exposed surface, were examined (Refs. 6-8). Other impact data include analyses of the windows from the Skylab (orbital inclination of 50 deg at ~400-km altitude), Apollo missions (moon missions and Skylab missions), and shuttle missions (STS-1 to STS-29, nominally at 300-km altitude). Impact data must be analyzed to distinguish the natural micrometeoroid impacts from the man-made (orbital) debris impacts on the basis of analysis of the residue in the impact craters. It must then be analyzed to determine the mass of the impacting particles on the basis of this distinction. Having made these determinations, the nominal impact velocities may be estimated. The impact data were used primarily to establish the small particle-size distribution for diameters of the order of 0.05 cm and less. Sample data are shown in Figure 8.

- Recent radar measurements from Aricebo and Goldstone (Refs. 8 and 9) are used for the size ranges of 0.5 to 2 cm at altitudes of 200 to 1000 km (Aricebo), and 0.2 to 0.5 cm at a nominal altitude of 575 km (Goldstone). These data substantiated the particle size distribution for these range of particles. Aricebo data represent 18 hr of viewing while Goldstone data represent 14.5 hr of viewing. Sample data are shown in Figure 9.

- The projected growth of mass in orbit for both large and small particles is derived primarily from analyses conducted using computer models (Refs. 1 and 10), such as the NASA EVOLVE program as well as an analysis of the historical data. The analyses examine both the projected effects of various traffic models (primarily large-particle growth) and the effects the satellite breakups and random collisions (primarily small-particle growth).

- Air Force Maui Optical Station/Maui Optical Tracking and Identification Facility (AMOS/MOTIF) infrared telescope data provided orbital-debris particle albedo (Refs. 1 and 5) used to calculate particle sizes from optical measurements.

Comparisons of these data sets to the NASA 90 model flux predictions were shown in Figures 2 and 3.

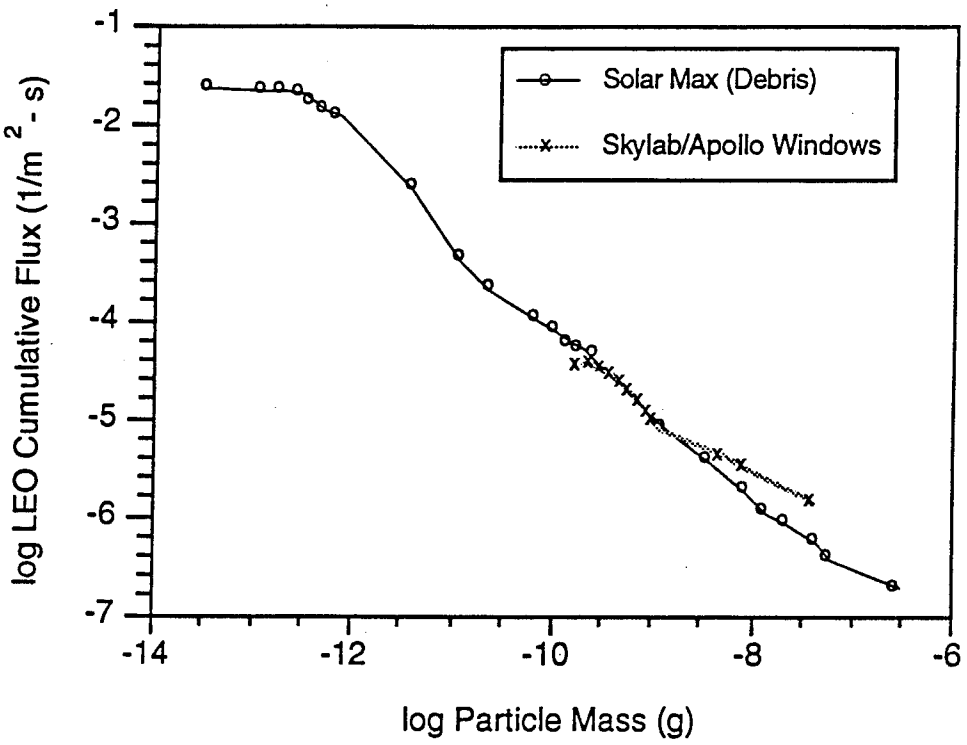

Figure 8. Sample impact data, returned spacecraft surfaces.

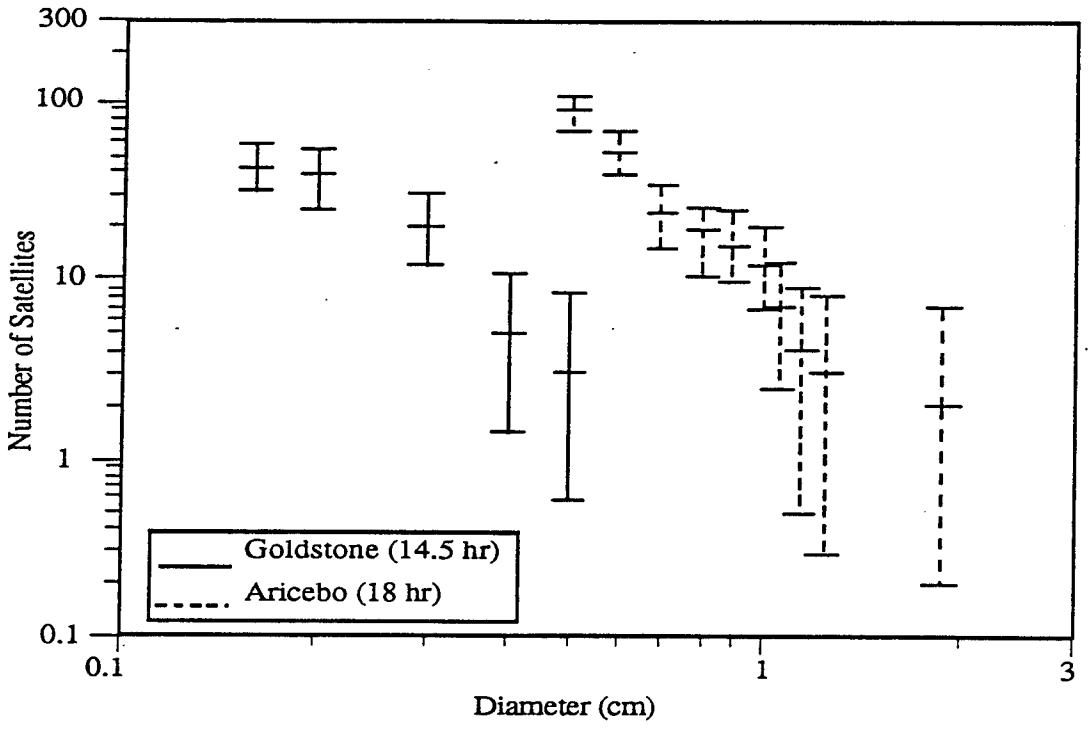

Figure 9. Sample data, Aricebo and Goldstone.

Except for the USSPACECOM and Solar Max data, the measurement periods represented by these data sources are extremely short. The total viewing time represented by the MIT/LL ETS, GEODSS, Aricebo, and Goldstone data is 133.4 hr or approximately 5 1/2 days. This observing time is judged to be an adequate sampling time to view a statistically significant number of objects in LEO. Assuming that such a sample was recorded by these measurements, an empirically derived flux model can provide meaningful results in predicting debris impacts on the time scale of years.

It has been suggested through analysis of the GEODSS data (Ref. 5) that the USSPACECOM data may be incomplete. Of the total 622 satellites found by GEODSS, only 255 were identified or found in the USSPACECOM catalog. Conversely, there are objects in the catalog that were not seen by the GEODSS telescopes (Ref. 5). On the basis of these GEODSS results, it was estimated (Ref. 5) that the USSPACECOM-derived flux environment was low by a factor of 2 to 4 for debris sizes around 10 cm in diameter.

The Solar Max data, which represent more than 4 yr exposure to the space environment, are limited to observations derived at only one orbital inclination and one mean altitude of 500 km. Other possible data, such as those from the Infrared Astronomical Satellite (IRAS) satellite observations (Ref. 11), were not useful in the model development. The IRAS sensors and data processing systems were designed to filter out transient events, such as orbital debris passing in view of these sensors, especially at close proximities to the IRAS satellite.

In summary, the data used to characterize the orbital-debris environment are at best incomplete for all LEOs and debris sizes. Characterization of the debris environment can be improved and data uncertainties reduced through a program dedicated to measure and continuously monitor the complete orbital-debris environment for all inclinations, altitudes, and debris sizes.

4.2 ASSUMPTIONS

Certain key assumptions regarding the application of the data base discussed in Subsection 4.1 were made and led to the development of the NASA orbital-debris model (Refs. 1 and 8). The key assumptions to each data set and assessment of these assumptions are as follows:

- The USSPACECOM data are assumed to be complete to a lower limiting size of 10 cm at altitudes <1000 km, and the distributions are assumed to be symmetric within each latitude observed. The variation of flux with altitude, solar activity, orbital inclination, and the velocity and direction distribution is deduced from these data. The growth of the large particle distribution is recorded over an 11-yr solar cycle of the tracked population of approximately 5 percent per year.

  Assessment: As mentioned in the previous section, the USSPACECOM data may not be complete and may be missing two to four times the actual number of objects (~10 cm diameter) in orbit compared to optical measurements. This contention has not been settled, conclusively. The diameter of the objects in orbit is derived from the radar cross-section measurements (Ref. 12). These derived sizes depend on the object's size, configuration, and orientation as well as the radar system's characteristics (Ref. 13). The limiting diameter of 10 cm has never been officially stated by USSPACECOM as the lower observing limit of their systems; however, USSPACECOM does refer to it in presentations (Ref. 3). The assumption that the USSPACECOM data are complete down to 10 cm must be verified. The derived changes in the flux environment with solar activity, etc., may be valid even though the absolute flux measurements may be in error.

- The MIT/ LL ETS, during average-seeing conditions (defined by observations of known magnitude stars), recorded twice the catalogued population (≥10-cm diameter) for ≥5-cm particles and, during excellent-seeing conditions, recorded five times the catalogued population for ≥2-cm-dia particles.

  Assessment: The size of the observed object is determined from its measured brightness and assumed albedo. Both depend greatly upon the object's shape, orientation, and surface properties, which are unknown for most orbital debris. Comparisons of GEODSS-derived diameters and radar cross-section-derived diameters have resulted in an estimated average albedo for orbital debris of 0.08 with nearly half of the objects compared falling in the albedo range of 0.05 to 0.20 (Ref. 5). This gives a wide range of uncertainty to the actual size of the object. To date, the size characteristics for this population have not been verified with radar measurements for fragments smaller than ~8 cm.

- The measured impacts on the Solar Max, which included both the meteoroid and man-made objects, were used as the basis for calculating the orbital-debris flux. The orbital-debris flux environment is 1000 times larger than the meteoroid flux for debris diameters of ≥1 μm, and 20 percent of the meteoroid flux for debris diameters of ≥0.05 cm.

  Assessment: The Solar Max panels analyzed were exposed to the space environment for more than 4 yr and should represent a good sample of the actual environment at the Solar Max's altitude and orbital inclination. The distinction between meteoroids and man- made debris can be established through the analysis of the impacting particle's residue (Ref. 6). An uncertainty arises in determining the size of the impacting object without knowing the direction and velocity of impact. (Normally the impacting object is assumed to be spherical for lack of any other information.)

- The orbital-debris flux for debris diameters between 0.05 and 2 cm is obtained by linear interpolation on a log-log plot of flux versus diameter.

  Assessment: In lieu of any other information to the contrary, a straight line is the most conservative means of interpolating, until proven otherwise.

- Initially, the growth rate of small particles was assumed to be 10 percent per year (Ref. 1); however, recent models assuming one breakup per year suggest this growth rate should be reduced to 2 percent per year (Ref. 2). It is assumed the major source of small debris is from satellite breakups.

  Assessment: As will be discussed in Subsection 4.3.4, the historic record indicates one breakup per year is a reasonable value. Modeling the resulting debris size distribution from breakups is more difficult; therefore, the growth rate of 2 percent must be validated. As will be discussed later, the estimated growth rates are the most controversial part of the flux model. The assumption that the majority of small debris is from breakups is reasonable because the only source for the majority of the small debris must result from the breakup of larger bodies.

- The ratio of large-debris particles to small-debris particles is constant with altitude, and both change at the same rate.

Assessment: Like the issue of interpolation discussed previously, there is not enough information on the debris environment, especially for the small particles, to assume otherwise. Until more information becomes available, this assumption cannot be verified.

In summary, information on the actual debris environment is scant, and the ultimate validity of the assumptions used to develop the model will be verified only with improved observations. The authors of the NASA model are aware of these limitations (Refs. 1 and 2) and understand that the model may evolve as measurements improve (as has already happened with the NASA 89 to the NASA 90 model).

4.3 DEBRIS FLUX MODEL DEVELOPMENT

With the data base defined and the assumptions presented regarding the use of this data base, the development of the NASA 89/90 model can now be presented. Each functional relationship in this model is examined. Specifically, the functions Φ (h,S), Ψ(i), F_1(d) and F_2(d), g_1(t) and g_2(t), and H(d) are discussed. Note that the orbital-debris model was assessed with respect to the parameters that were deemed the most important (Refs. 1 and 2). Those parameters are altitude, solar activity, inclination, debris size, and time.

4.3.1 Solar/Atmospheric Effects, Φ(h,S)

The function $\Phi(h,S)$, where

$$\Phi(h,S) = \Phi_1(h,S) / [\Phi_1 (h, S) + 1] \quad \text{(NASA 89/90)} \tag{15}$$

and

$$\Phi_1(h,S) = 10^{(h/200-S/140-1.5)} \qquad \text{(NASA 89/90)} \tag{16}$$

accounts for the influence of the upper atmosphere in "cleansing" or removing the orbital debris because of atmospheric drag effects. It also demonstrates the influence of the solar activity in increasing or decreasing this "cleansing" rate. The function $\Phi(h,S)$ remains unchanged between the NASA 89 (Eq. 1) and NASA 90 (Eq. 6) models. The behavior of Φ with altitude, h, and the 10.7-cm wavelength measure of the solar spectrum, S, (defined for the previous year, i.e., t - 1,

and shown to be an accurate measure of solar activity along with sunspot counts) is shown in Figure 10. Note that this function is normalized such that its maximum value is one and modifies the flux magnitude as altitude and solar activity varies. At any given altitude, when the solar activity increases (increasing S), Φ decreases, reducing the flux environment. As altitude increases for a given value of S, the effects of the atmosphere decrease. The maximum changes with respect to S appear at ≈500 km. Beyond some altitude limit, nominally 1000 km, the effects of the atmosphere are negligible. The Φ appears to behave properly.

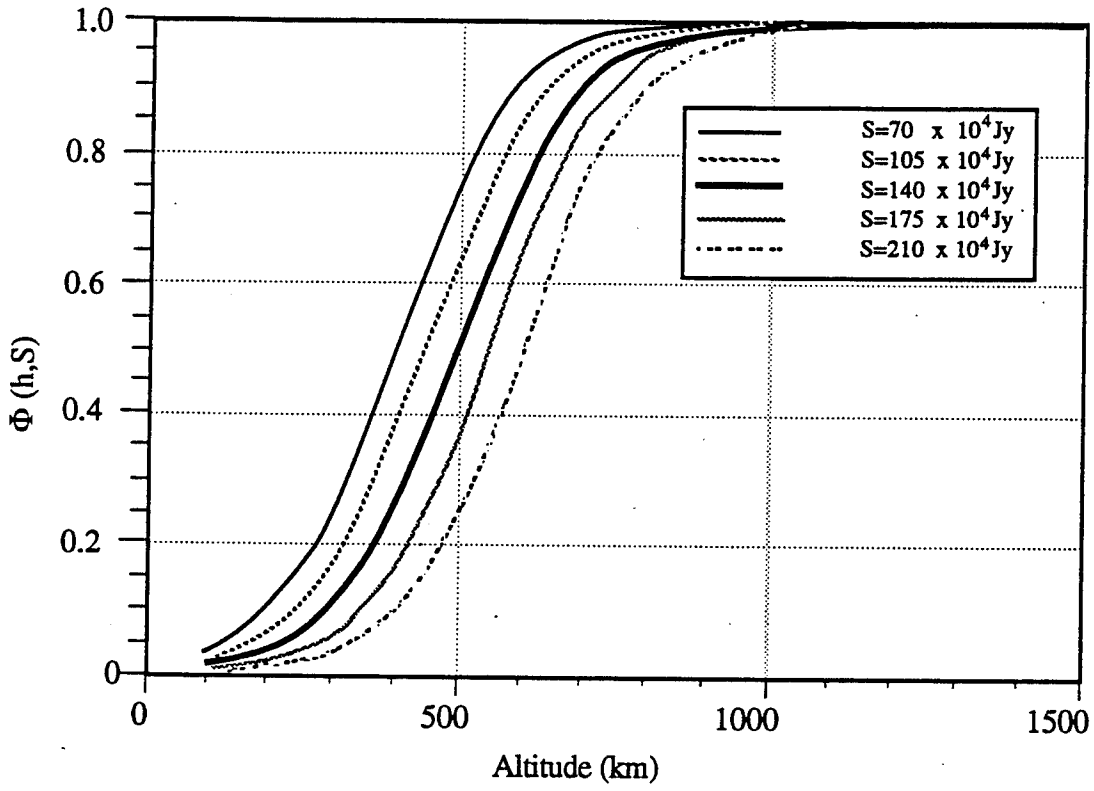

Figure 10. Solar/atmospheric effects, Φ(h,S).

The extent of upper atmosphere where orbiting objects are affected by solar activity is nominally up to 800 km (Refs. 14 and 15). The effect of the atmospheric drag is to reduce the energy of the orbiting body by first making the orbit circular. Once the orbit is circular, it then begins to decay leading eventually to the object re-entering the atmosphere. It can be shown that the lifetime of objects in circular orbits is inversely proportional to the atmospheric density (Ref. 15). One measure of solar activity is characterized by the 10.7-cm wavelength of the solar spectrum (Refs. 15 and 16) averaged over a typical 13-mo period of the 11-yr solar cycle (Ref. 16).

Nominal values of S (10^4 Jy) during a solar cycle range from a value of 70 x 10^4 Jy to 200 x 10^4 Jy; however, values exceeding 200 x 10^4 Jy and approaching 250 x 10^4 Jy have been observed (Refs. 15 and 16). The implication and result of wide variations in the maximum value of S during a solar cycle make long-term debris predictions difficult (Refs. 16 and 17).

The formulation of Φ is shown in Figure 11. The Φ is a composite function made up of $\Phi_1(h,S)$ and Φ_2 (h,S). The function Φ_1 models the effects through the altitudes where atmospheric effects are important. The Φ_2 models the debris flux at altitudes beyond the upper atmosphere. From Figure 11, Φ_2 was assumed to predict a constant flux at these altitudes. The function Φ_1 was determined by a curve fit to the USSPACECOM data through the lower altitudes where solar influences on the debris environment are important. The curve fit to the data shows an increase in the environment by an order of magnitude for every 200-km altitude increment; thus the factor, h/200. The nominal level of solar activity was picked to be 140 x 10^4 Jy and the function Φ_1 given by Equation 16 resulted from these curve fits. Because the actual magnitude of the debris flux environment is contained in F_1 and F_2 (times the growth), the function Φ_2 was set equal to one to normalize Φ. The function Φ modifies the predicted flux environment (magnitude), F, produced from the sum of the small- and large-particle fluxes, $F_1g_1 + F_2g_2$.

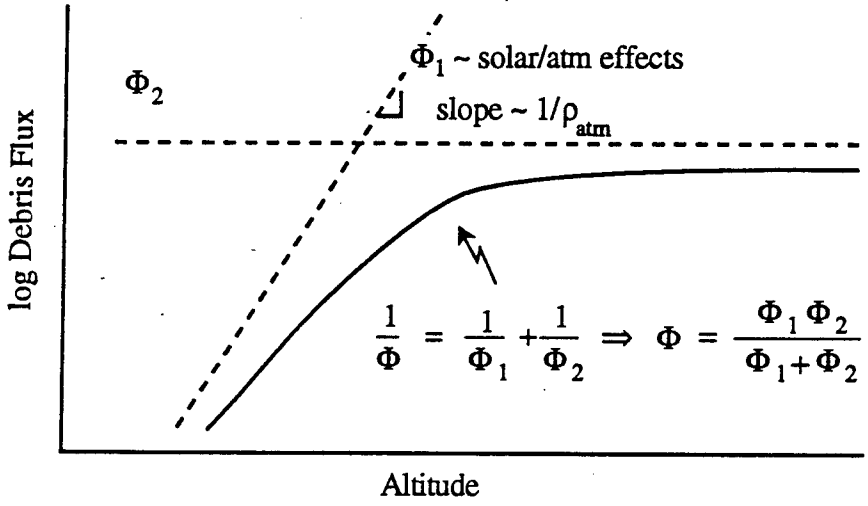

Figure 11. Construction of $\Phi(h,S)$.

4.3.2 Inclination Distribution, $\Psi(i)$

Although the orbital-debris flux environment is assumed to be symmetric in latitude (evenly distributed around the earth), observations show that it varies as a function of orbital inclination

(Ref. 18). Typical data showing these variations are depicted in Figure 12. The function $\Psi(i)$ adjusts the predicted flux environment accordingly as a function of the orbital inclination. The Ψ is shown in Figure 13 (the corresponding values were shown in Table 1). The function Ψ, in curve fitting the data, is normalized for a uniform random distribution. The peaks (polar orbits) represent inclinations where there is more traffic and where several on-orbit breakups have occurred. The overall validity of Ψ rests with the validity of the measured concentrations of debris. The most serious concern with Ψ is that it does not account for different altitude variations with i.

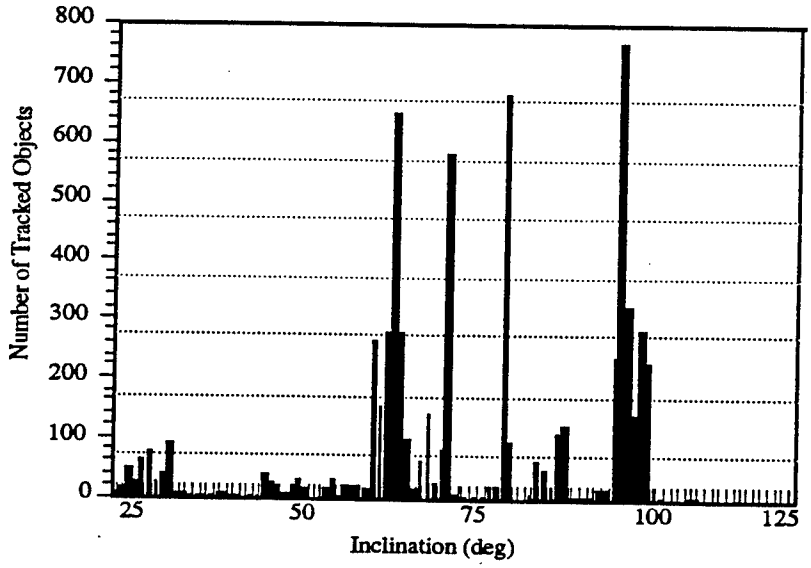

Figure 12. Inclination distribution of USSPACECOM-tracked objects August 1988 - all altitudes.

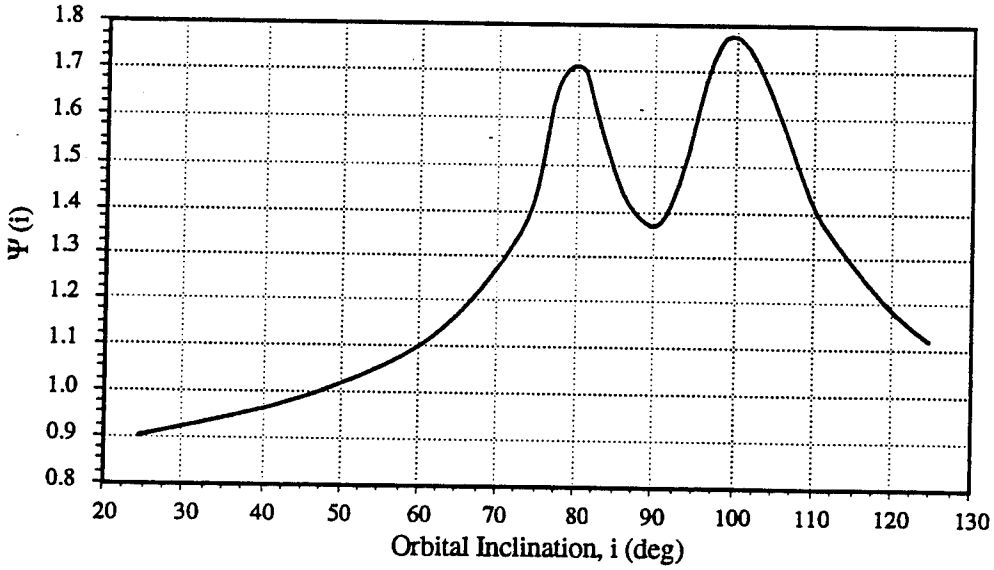

Figure 13. Orbital-debris concentration correction factor, Ψ (i), versus orbital inclination, i (deg).

4.3.3 Particle Flux, F_1 (d) and F_2 (d), H (d)

The prediction of the orbital-debris flux environment is given by F_1 for small particles and F_2 for large particles. The nominal distinction between small and large particles is in the range of 1- to 10-cm diameter. Figure 14 shows how F_1 and F_2 vary with diameter. As seen in this figure, F_1 dominates for the smaller particles and F_2 for the larger particles. They intersect at ~3.2-cm diameter, which is in the range where the distinction between large and small particles is made.

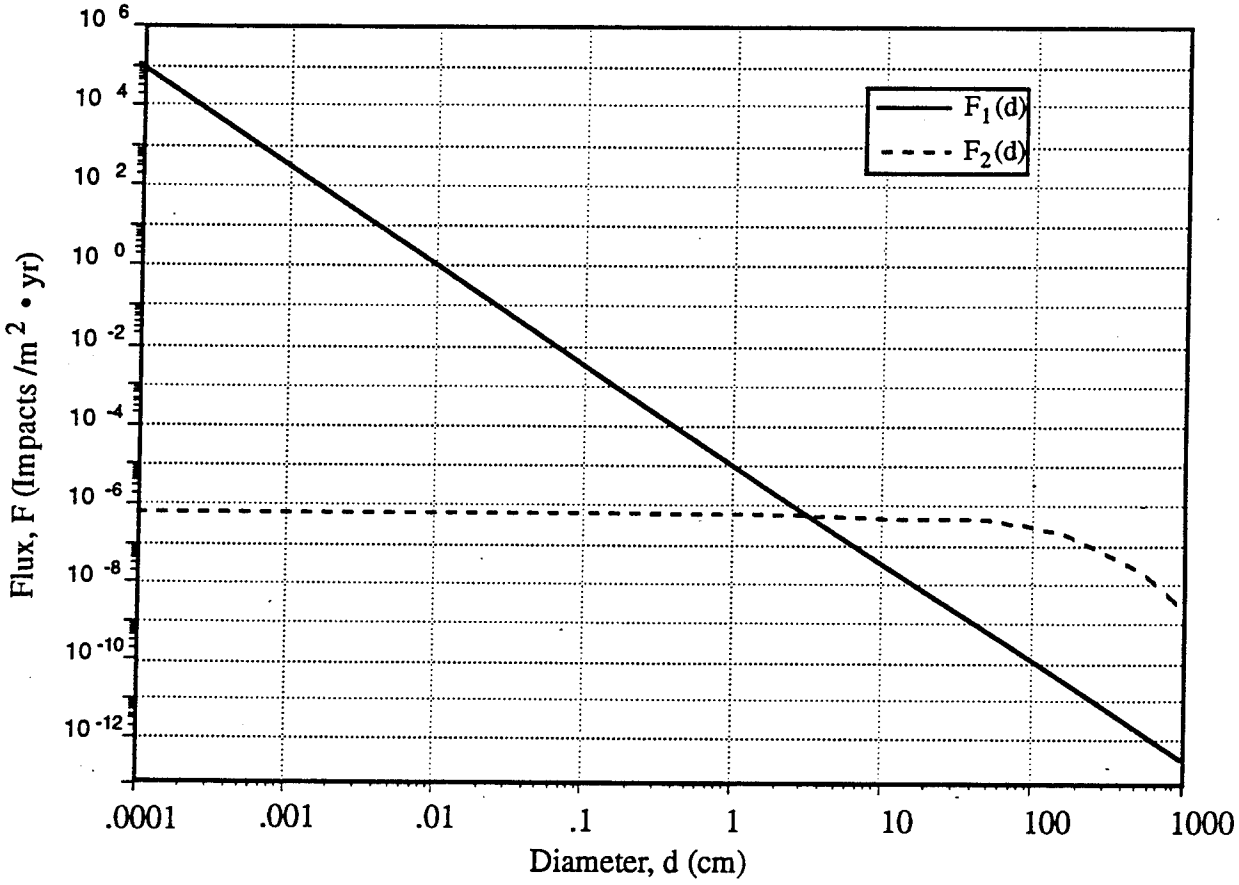

Figure 14. Small-particle flux, $F_1(d)$, and large-particle flux, $F_2(d)$, versus diameter, d(cm).

The small-particle flux distribution, F_1, was derived using data from two sources: impact data from returned spacecraft surfaces and optical data (ground observations). The impact data (Refs. 6-8) consist primarily of analyses of the returned surfaces (thermal control louvres) from the Solar Max satellite, which operated at a nominal altitude of 500 km and orbital inclination of 28.5 deg. In the analysis to determine the orbital-debris environment, it was assumed the meteoroid flux that impacted the Solar Max was a known percentage of the total flux. The orbital-debris environment

is determined from the ratio of meteoroid to orbital-debris craters/impacts as presented in Subsection 4.2. The measured impact data resulted in defining the orbital-debris flux for diameters nominally up to 0.05 cm. The optical data from the MIT/LL ETS (Ref. 4) was analyzed by NASA* . The analysis derived from these data form the "anchor" for the curve fit at the larger diameters of 2 and 5 cm. Without any other data, the curve fit between 0.05 and 2 cm is assumed to be linear (log-log relationship of flux versus diameter). It must be noted that ~8 cm is the smallest debris size whose population can be reasonably confirmed with radar measurements.

The USSPACECOM data were used to determine the large-particle flux distribution, F_2. After the formulation of the NASA 89 model, analysis of GEODSS data led NASA to an increase of the predicted environment in the 10-cm-dia range (Ref. 6). As discussed in Subsection 4.2, analysis of the GEODSS optical data in the 8- to 30-cm-dia range appears to have revealed two to four times the number of objects seen by the USSPACECOM-catalogued radar data (Ref. 5). The "Henize" function, H, represents a model adjustment that increases the environment in this range. Figure 15 shows the behavior of H versus diameter. It is a correction, peaking at a value of 3.16 for a diameter of 6.025 cm, and increasing the predicted environment for the 1- to 100-cm dia debris particles. Although the data only support corrections above 8- to 10-cm dia particles, the H correction is applied to smaller diameters and represents an extrapolation to the smaller sizes. The Aricebo and Goldstone radar data (Ref. 9) confirm the NASA 89 model predictions in the range of 0.2- to 0.5-cm diameter (Goldstone) and 0.5- to 2-cm diameter (Aricebo), within the measurement uncertainties.

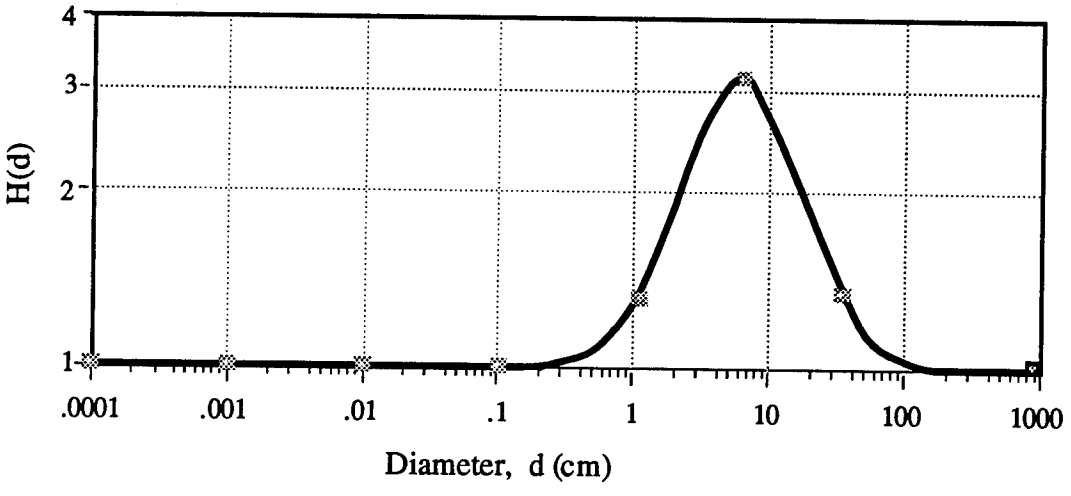

Figure 15. Flux correction, H(d), versus diameter, d(cm) for NASA 90 model.

* Internal NASA/JSC Memo by Loretta Weiss, "Reanalysis of the MIT ETS Telescope Data,"1985.

Comparisons of the NASA 90 model predictions to data from Solar Max, Goldstone, Aricebo, and GEODSS were shown in Figure 2 (model flux versus diameter, h = 500 km) and to USSPACECOM data in Figure 3 (model flux versus altitude, $d \geq 10$ cm). Figure 2 shows the fit to the small-particle data while Figure 3 shows the fit to the large-particle or USSPACECOM data. The curve fit to the small-particle data in Figure 2 shows good agreement since these data are the basis for the curve fit. Figure 3, shows a good fit to the USSPACECOM data at the lower altitudes, but illustrates the effect of the low-order curve fit and/or lack of confidence in the data at higher altitudes. The obvious peaks and valleys in the data at the higher altitudes, h > 800 km, are not represented by the curve fit.

The fluctuation in the data at ~800, 1000, and 1500 km are thought to be real. They are due to known breakups at these altitudes. Approximately 150 such events (either intentional or unintentional) have been recorded to date at various altitudes (Refs. 19 and 20). Some of the more severe breakups are shown in Table 2 (Refs. 19 and 20).

4.3.4 Debris Growth, $g_1(t)$ and $g_2(t)$

The most controversial part of the debris flux model concerns the predicted growth of the space-debris environments with time. The controversy concerns the magnitude and whether the growth rate is linear or compounded. Although the growth rate may be bracketed on the basis of historical data and model simulations, there simply is not enough data to confirm or quantify the rate. In the revision from the NASA 89 to the NASA 90 model, a major change is seen in the form of the growth functions, $g_1(t)$ and $g_2(t)$, and the growth rates, p and q. The differences are:

Function	NASA 89	NASA 90
$g_1(t)$	$(1 + 2p)^{(t-1985)}$	$(1 + q)^{(t-1988)}$
$g_2(t)$	$(1 + p)^{(t-1985)}$	$1 + p$ (t-1988)
p	~ 5%	~ 5%
q	N/A	~ 2% until 2010, then 4% thereafter

Table 2. Fragmentations/breakups.

Object (Common Name)	Breakup Date	Approximate Altitude (km)	Catalogued Objects (d ≥ 10 cm) (Approximate)	
			Initially	Still in Orbit (1988)
Titan 3C-4	1965	740	470	90
Ariane 3rd Stage	1986	820	465	460
Thor-Agena-D	1970	1080	345	295
Cosmos 1275	1981	980	300	290
Ablestar Rocket	1961	950	270	210
Thor-Agena-D	1969	920	265	140
Solwind	1985	530	250	120
Cosmos 844	1976	210	250	0
Delta 2nd Stage	1975	725	230	90
Delta 2nd Stage	1976	750	200	50
Cosmos 544	1973	310	200	0
Delta 2nd Stage	1981	900	195	175
Delta 2nd Stage	1973	1500	185	170
Cosmos 1813	1987	350-410	185	50
Cosmos 57	1965	160-700	165	0
Delta 2nd Stage	1977	1450	160	100
Cosmos-Rocket	1965	1640	150	25
Delta 2nd Stage	1975	1460	140	135
Delta 2nd Stage	1977	1510	140	135
Cosmos 252	1968	530	130	60

The small-particle growth rate has been decoupled from the large-particle growth rate through the introduction of the coefficient, q, in the NASA 90 model. Previously it was assumed the small-particle growth rate was twice that for large particles (Ref. 1). Although the growth of small particles is still compounded with time, the rate (2 percent for the NASA 90 versus 10 percent for the NASA 89) is significantly less in the NASA 90 model. Next, the large-particle growth has been changed from a compounded growth to a linear growth with time. The assumed growth rate, $p = 5$ percent, remains the same. The overall result of these changes is to reduce the projected growth rate with time as shown in Figure 16, especially for the small particles.

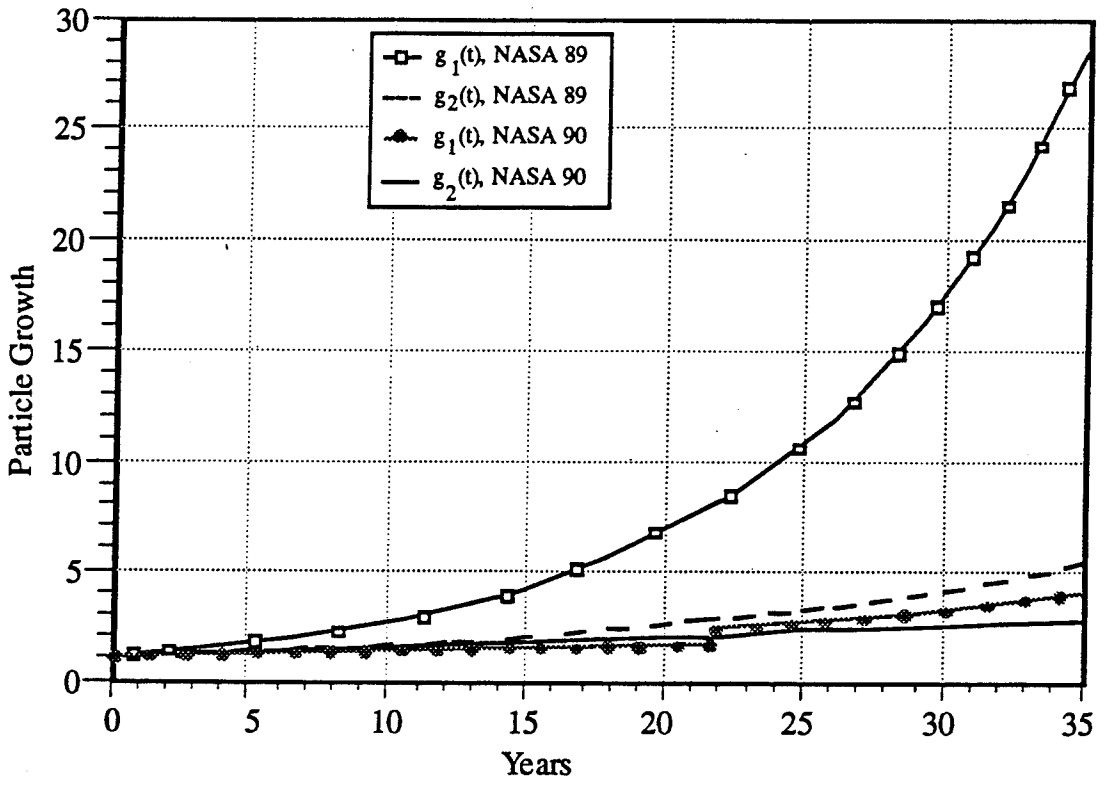

Figure 16. Small-particle growth, $g_1(t)$, and large-particle growth, $g_2(t)$, NASA 89 and NASA 90 models versus time, t (yr).

The basis for these projections is historical data such as depicted in Table 2 and model simulations to estimate the amount of small (untrackable) debris produced. The major source of small-particle debris growth is assumed to result from satellite breakups. Over the past decade, there have been 37 breakups in LEO producing 10 or more trackable fragments.* Of these 37 breakups, 11 were thought to be unintentional, and of these 11, 8 were felt to be accidental explosions. The remaining three were possible collisions. (The Cosmos 1275 is considered to be a strong collision candidate.) Assuming in the future that intentional breakups are reduced by improved operating procedures and heightened awareness by users not to create more long-term debris, one can assume (based on the historical data) the rate of one unintentional breakup per year will continue. On the basis of this breakup rate and the NASA EVOLVE model predictions, a 2-percent growth rate was estimated. This is felt to be a valid approximation through the year 2010.* Small-debris growth is still assumed to be compounded based on simulations. If current practices continue, q is projected to increase to 4 percent on or about 2010 (Ref. 2).

* Private meetings/communications with NASA/JSC, D.J. Kessler, 1990-1991.

The growth of large particles is found in historical records and is related primarily to launch rates and objects in orbit. These data, recorded by USSPACECOM, were used to determine and to project the future growth. Data are averaged over solar cycles. During the 1966-1977 solar cycle, the average increase in the catalogued population was 300 objects per year, representing approximately a 5-percent increase per year. This is the basis for the value of p. The future activity and manner in which the large-particle debris population will increase cannot be deduced from this historical record. It is clear from Figure 17 that the data do not justify either linear and compounded growth. Traffic models for a variety of conditions were examined to aid in predicting and bracketing the possible future growth trends (Refs. 1 and 2), from constrained to high world-traffic models. The linear growth was chosen based on a continued 350 launches per year and assuming a 1988 catalogued population of 7000.

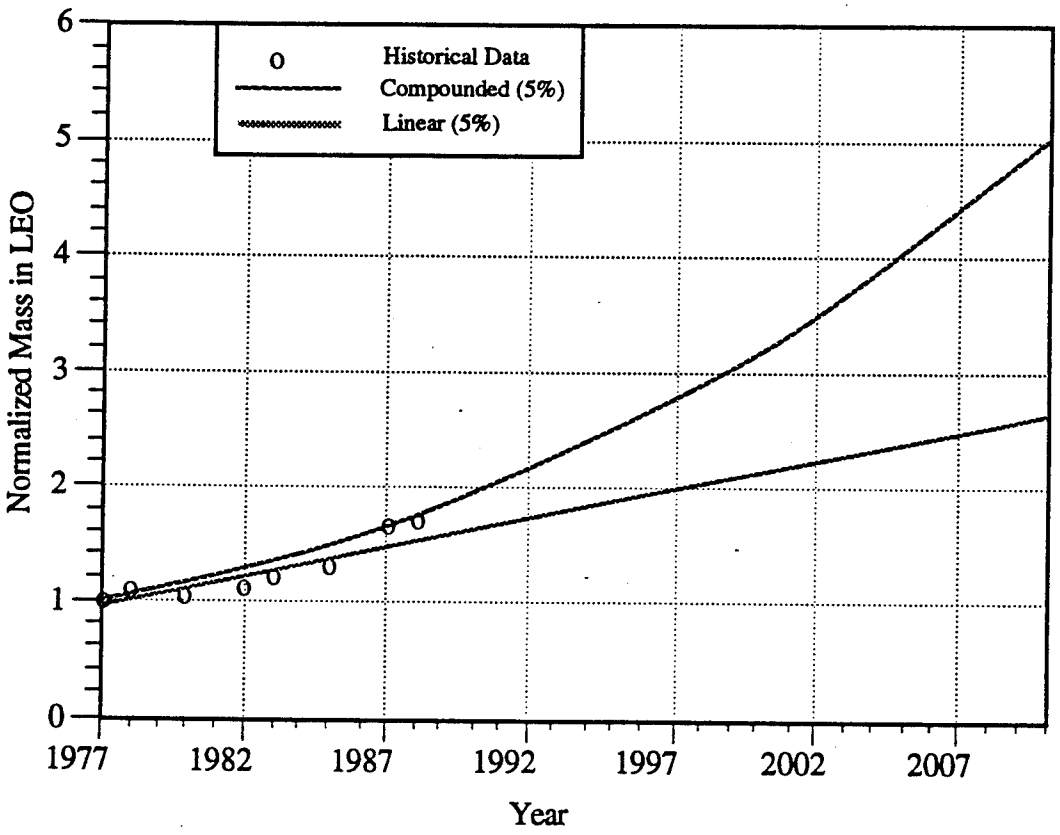

Figure 17. Historical large-particle growth.

4.4 DEBRIS IMPACT/DIRECTION DISTRIBUTION AND PARTICLE MASS

4.4.1 Collision-Velocity Impact Distribution

The expression for the collision-velocity impact distribution, f(V), as shown in Equation 8, gives the number of impacts for orbital debris having velocities between V and V + dV relative to a spacecraft with orbital inclination, i. The normalized collision-velocity impact distribution is given by Equation 10. The collision-velocity impact distribution was determined from USSPACECOM data for altitudes between 500 and 1000 km (Refs. 1 and 2). Examples of those data are shown in Figure 18 (Ref. 10). The data were examined for variations with parameters such as time, altitude, or inclination. The only significant variation that could be distinguished was the variation with respect to the orbital inclination (Refs. 1 and 2). Variations both in time and altitude appeared to look like random variations and were regarded as second-order effects*. This led NASA to formulate f (V), given in Equation 8.

The function f (V) is a double Guassian fit to the data in Figure 18. Although there may be some size dependency, data are insufficient to distinguish this effect*. The function f (V) is a complicated expression without any physical significance and whose empirically determined constants vary with inclination in a seemingly unrelated fashion. Finally, it is not an expression that is easily used.

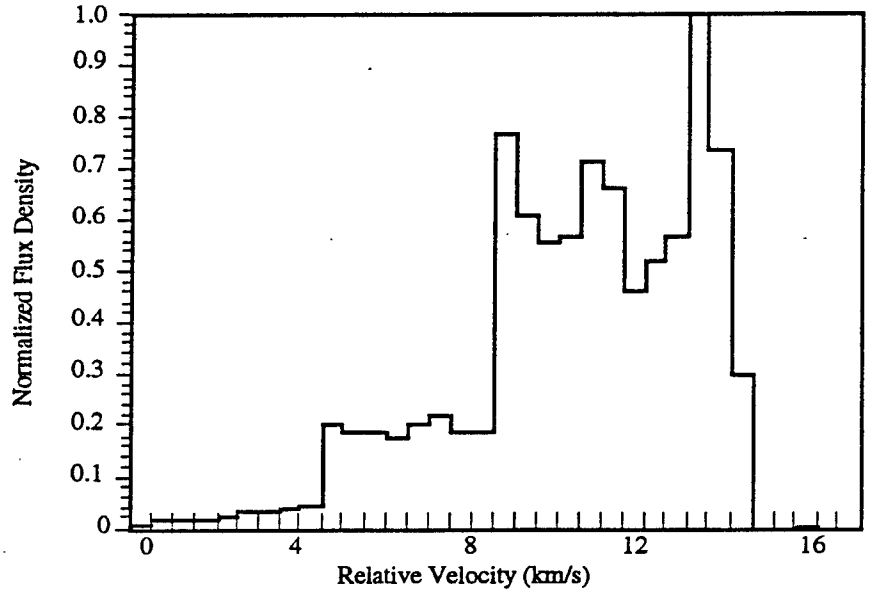

Figure 18. Velocity distribution data (h = 500 km, i = 28.5 deg).

* Ibid p. 30.

4.4.2 Impact Direction Distribution

The distribution of debris impact direction (Eq. 11) in a specified orbital inclination is symmetric and does not account for out-of-plane impacts. On the basis of measured data, the average velocity for the debris was found to be 7.7 km/s; this represents an ideal circular orbital altitude of 345 km while the data were averaged over 500 to 1000 km.

NASA has deduced that there are indeed debris with elliptical orbits. This results in an average velocity of 7.7 km/s, which is higher than expected from debris only in circular orbits. A rearward-facing surface (surface normal opposite the direction of motion) of an object in a circular orbit would not be impacted by debris unless there were debris in elliptical orbits. Returned surfaces, including the Long Duration Exposure Facility, show impacts on the rear surfaces, thus substantiating that there exists debris in elliptical orbits. There are definitely out-of-plane impacts as well as impacts on rear surfaces, thus the expression (Eq. 11) represents only an approximation of the actual in-plane debris environment.

4.4.3 Orbital-Debris Particle Density

The expression for the orbital-debris particle density assumes that the particles are spherical in shape (Eq. 12). There is little information on actual debris shapes. There does exist a data base for particle sizes >0.5 cm which consists of studies of orbital decay and fragmentation experiments involving typical spacecraft structures (Refs. 18, 21, and 22). These data, as described in Reference 21, have led to the expression (Eq. 12) for particle density ($d \geq 0.5$ cm), which is assumed to be accurate within a factor of 0.5 to 2 (Ref. 2).

For sizes <0.5-cm diameter, the data are virtually nonexistent. It is known that orbital debris consists of a variety of material types, including epoxy-glass ($\rho \sim 1.8$ g/cm ^{3}), aluminum ($\rho \sim 2.8$ g/cm ^{3}), copper ($\rho \sim 8.9$ g/cm ^{3}), and steel ($\rho \sim 8$ g/cm ^{3}). Estimates could be made of the approximate composition of the debris (by volume fraction) because of fragmentation, collision, and operational procedures (including engine operations); however, definitive studies have not been performed (Ref. 2). The value of 4.7 g/cm ^{3} for $d \leq 0.5$ cm results from Equation 12 at $d = 0.5$ cm.

The large uncertainty in particle mass has implications for impact and shielding studies. For impact and shielding studies, it is important to know not only the energy or momentum of the impacting particle, but also the mass per unit area of the impactor*. Mass is extremely important to satellite

* Private meetings/communications with PL/WSSD, Dr. Firooz Allahdadi, 1990-1991.

designers (who want to minimize mass), and unnecessary spacecraft mass due to unneeded shielding results in increase system costs. In using an expression for debris mass that may be in error by a factor of 2, a shield design may have either too little shielding or too much. Either extreme represents a dilemma to the satellite designer. The present expression for density along with the collision-velocity impact distribution and direction predictions is felt to represent extremely gross approximations of the environment.

4.5 CIRCULAR VERSUS ELLIPTICAL ORBITS

In the NASA 89/90 models, both the orbital debris and the spacecraft of interest are assumed to be in circular orbits for the purpose of computing the direction of impact, α (Eq. 11). Because V is always positive, Equation 11 allows for impact directions between only ± 90 deg (0 deg being the spacecraft direction of motion). The formulation for impact direction does not consider out-of-plane (parallel to Earth's surface) impacts. Equation 11 is plotted in Figure 19 for the range of debris-impact velocities, 0 to 15.4 km/s. The maximum impact velocity occurs at $\alpha = 0$ deg. The impact velocity is zero at $\alpha \geq \pm 90$ deg. Solving Equation 11 for V and combining with Equation 8, the expected number of impacts from any direction can be calculated. This results in the "butterfly" diagram shown in Figure 20. This figure emphasizes the directionality of impacts because of the orbital-debris flux environment (Refs. 22 and 23).

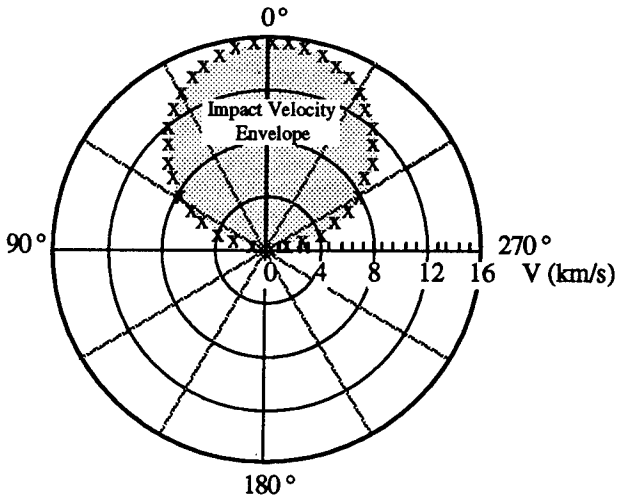

Figure 19. NASA 90 model debris-impact velocity envelope, versus direction of impact, α, where the spacecraft is in the center of polar coordinates.

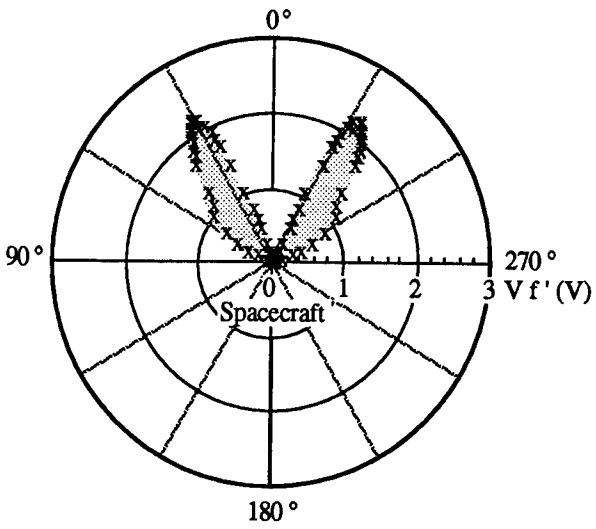

Figure 20. Debris-impact envelope, V • f '(V), NASA 90 model (i = 28.5 deg).

4.6 DATA/MODEL UNCERTAINTIES

The orbital-debris engineering model developed by NASA is based on a curve fit to debris measurement data (Refs. 1 and 2). The accuracy of this type of empirical model is related to the fidelity of the curve fit and the representativeness of the data sample used. The uncertainties due to curve fits, measurement resolution and sampling techniques have been estimated by NASA (Ref. 2) and are shown in Table 3. Values in this table will form the basis for the uncertainty analysis to be presented in Section 7.0.

The uncertainties given in this table represent the 90-percent confidence estimated values* based on the consensus of NASA investigators. The first parameter, the uncertainty in the flux measurements, reflects statistical and measurement uncertainties in the data set for the various sizes of debris. The uncertainty in the altitude distribution contributes to the total uncertainty. The uncertainty is based on the difficulty in including flux for debris in highly elliptical orbits. No altitude distribution uncertainties are presented in the 1- to 10-cm-dia size range. The uncertainty in the collision-velocity impact distribution, f(V), was estimated for the fraction of debris with impact velocities <5 km/s. The uncertainties for debris density and shape reflect the extreme lack of knowledge concerning small particles, d < 1 cm. The variations presented for growth rates and level of solar activity represent extreme values.

* Private meetings/communications with NASA/JSA, D.J. Kessler, 1990-1991.

Table 3. Estimated orbital-debris uncertainties, NASA 90 model, 90-percent confidence.

Parameter		Estimated Uncertainty
Flux Measurements	$d \geq 10$ cm	1.5 to 0.5 x Flux
	$0.05 < d < 10$ cm	3.0 to 0.33 x Flux
	$d \leq 0.05$ cm	2.0 to 0.5 x Flux
Altitude Distribution	$d \geq 10$ cm	2.0 to 0.5 x Flux
	$d \leq 1$ cm	5.0 to 0.2 x Flux per every 200 km away from h = 500 km
Velocity Distribution	$V \leq 5$ km/s	0.5 to 3.0 x f(V) only for fraction where $V \leq 5$ km/s
Debris Density	$d > 1$ cm	2.0 to 0.5 x mean density
	$d < 1$ cm	Unknown, can estimate by estimating volume/weight fractions or use +100% for $\rho = 2.8$ g/cm^3
Debris Shape		Unknown
Orbital-debris Growth	p	4 to 10%
	q	0 to 20%
Solar Activity	S	Use max and min values for nominal solar cycle where typically $70 \leq S \leq 210$

4.7 MODEL RESTRICTIONS/LIMITATIONS

Initial examination of the model development and of the corresponding assumptions resulted in the documentation of the qualitative model limitations. The limitation for use of the model to LEO was noted by NASA (Refs. 1 and 2). The use of the NASA 90 model should be limited in the temporal extent of its use. The time validity of the model, based on current projections, is assumed to extend to the year 2010.

General limitation is that this model, developed primarily using historical data, reflects the way space operations have been conducted. If one drastically changes current operational procedures or traffic model assumptions, then the model may no longer be applicable. Use of this model must be

consistent with the fundamental assumptions concerning its development. It is a tool for use by design engineers in establishing an order of magnitude orbital-debris hazard. It is not meant for sophisticated trade studies or examinations of "what ifs" in space architecture studies.

Finally, it is clear that the model does not fit precisely all fluctuations in the data, most notably those altitudes and inclinations where known breakups have occurred. If one specifically wishes to predict debris environments with higher accuracy, then a debris model with a higher order fit to the data is needed. The model will be required to simulate and integrate the effects of breakups to improve its accuracy. Model capabilities and limitations will be further quantified in Sections 6.0 and 7.0.

5.0 THE AF/DoD ORBITS OF INTEREST

The AF/DoD orbits of interest have been identified on the basis of an analysis of the historical record and projected mission requirements (Ref. 24). From this analysis, it appears that future AF/DoD traffic will operate in five orbital regimes (Ref. 24) as shown in Table 4 and depicted in Figure 21. These projections are based on the analysis of all AF/DoD requirements through the year 2010. If there is any preponderance of new traffic, it will be destined for Regimes D and E at relatively low altitudes ($h \leq 1200$ nm or $h \leq 2220$ km). Note that the Space Station Freedom is destined for operation in Regime C (460-km altitude, 28.5-deg orbital inclination).

Table 4. The AF/DoD orbits of interest.

Regime	Description	Orbital Inclination (deg)	Altitude (h)
A	High Altitude/ Geosynchronous	$0 \leq i \leq 67$	~19330 nm (~35800 km) [Synchronous]
B	Mid Altitude/ Midinclination	$55 \leq i \leq 67$	5600 nm $\leq h \leq$ 11000 nm (10400 km $\leq h \leq$ 20400 km)
C	Low Altitude/East	$28 \leq i \leq 32$	$h \leq$ 1000 nm ($h \leq$ 18540 km)
D	Low Altitude/ Midinclination	$60 \leq i \leq 80$	$h \leq$ 1000 nm ($h \leq$ 1850 km)
E	Low Altitude/Polar	$90 \leq i \leq 100$	$h \leq$ 4000 nm ($h \leq$ 7400 km)

On the basis of the analysis of the preceding sections, NASA 90 orbital-debris prediction for the AF/DoD orbits of interest will be made only for those regimes where the results are applicable as shown in Figure 21: Regimes C, D, E for $h \leq 2000$ km.

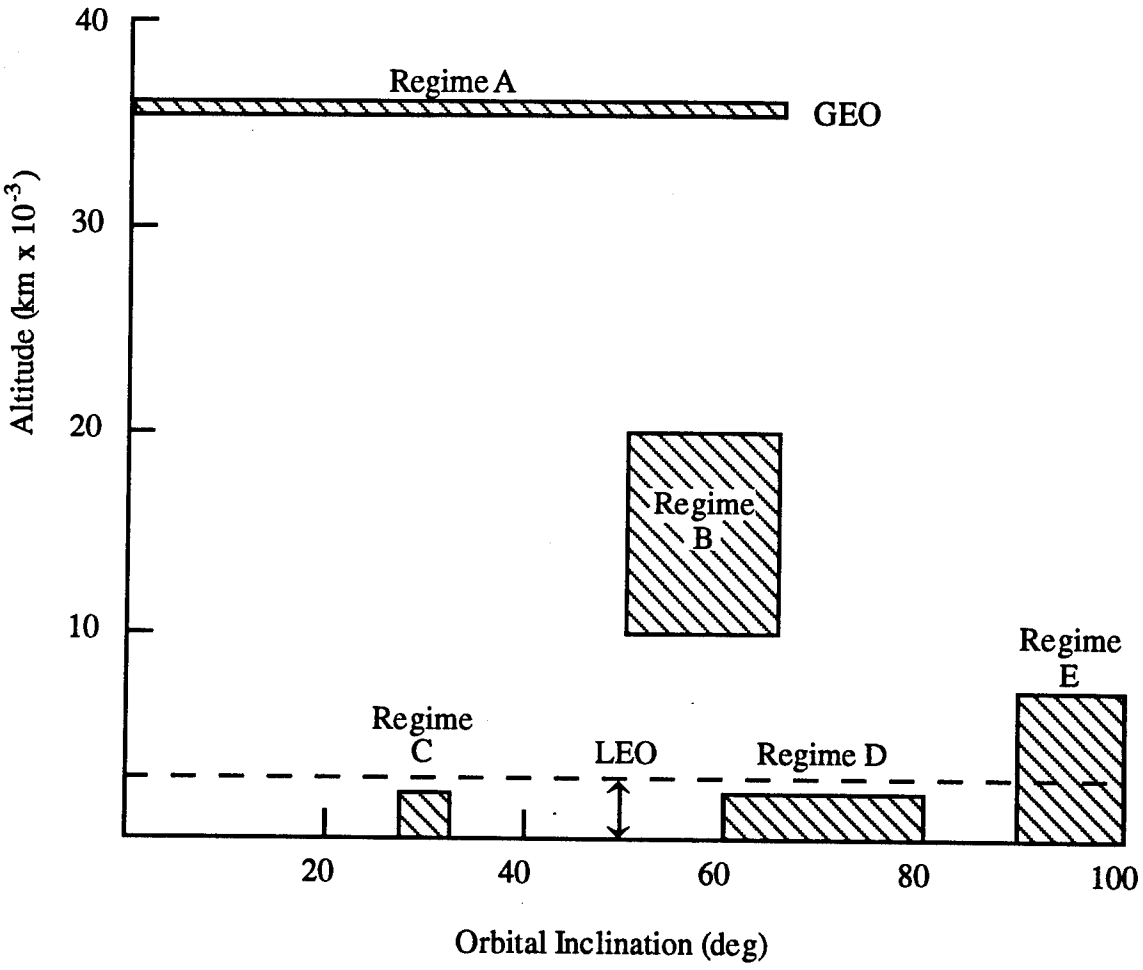

Figure 21. The AF/DoD orbits of interest.

6.0 SENSITIVITY STUDY

A sensitivity study of the NASA 90 model is discussed in this section. The sensitivity or variation of the orbital-debris flux prediction is calculated by examining the first partial derivative of F (d ,h ,i ,t ,S) with respect to the variables d, h, i, t, S, p, and q. The derivative gives the relative change of F with respect to the change in each parameter. The purpose of the sensitivity study is to identify those variables that cause the greatest change in F for given changes in the variables. The more sensitive parameters will cause the greatest change in F. Any anomalous behavior is also examined, especially any singularity in the function, F. The derivative equations are presented in Subsection 6.1 while the analyses are presented in Subsection 6.2. Subsection 6.3 summarizes the results of the sensitivity study.

6.1 SENSITIVITY PARAMETERS/ANALYTIC EXPRESSIONS

The function F(d, h, i, t, S) is composed of several distinct, empirically derived functions. Because the majority of functions that make up F are smooth and continuous, it is expected that the first-order derivatives also will be smooth and continuous. The function $\Psi(i)$ is based on tabular values, which when plotted results in a smooth continuous curve over the range $25 \text{ deg} \leq i \leq 125$ deg. The function $g_1(t)$ is piecewise continuous with the discontinuity occurring where q changes value at the year 2010. The functional forms making up F (d, h, i, t, S) are shown in Figures 10 and 13 through 16 for $\Phi(h, S)$, $\Psi(i)$, $F_1(d)$ and $F_2(d)$, H(d) and $g_1(t)$ and $g_2(t)$, respectively.

The first-order partial derivatives of F with respect to each variable are as follows:

$$\frac{\partial F}{\partial d} = (-F)\left\{\frac{(\log_{10} d - 0.78)}{d(0.637)^2}\, e^{-\left(\frac{\log_{10} d - 0.78}{0.637}\right)^2} + \left(\frac{\left(\frac{2.5}{d}\right) F_1 g_1 + \left(\frac{6}{d+700}\right) F_2 g_2}{F_1 g_1 + F_2 g_2}\right)\right\} \tag{17}$$

$$\frac{\partial F}{\partial h} = \left(\frac{\ln 10}{200}\right)\left(\frac{\Phi}{\Phi_1}\right) F \tag{18}$$

$$\frac{\partial F}{\partial i} = \frac{(\partial \Psi / \partial i)}{\Psi} F \cong \frac{(\Delta \Psi / \Delta i)}{\Psi} F \tag{19}$$

where $\Delta\Psi/\Delta i$ is determined by numerical finite differencing.

$$\frac{\partial F}{\partial t} = \left[\frac{F_1 g_1 \ln(1+q) + pF_2}{F_1 g_1 + F_2 g_2}\right] F \tag{20}$$

$$\frac{\partial F}{\partial S} = \left(-\frac{\ln 10}{140}\right)\left(\frac{\Phi}{\Phi_1}\right) F \tag{21}$$

$$\frac{\partial F}{\partial p} = \left[\frac{(t-1988) F_2}{F_1 g_1 + F_2 g_2}\right] F \tag{22}$$

$$\frac{\partial F}{\partial q} = \left[\frac{\frac{(t-1988)}{(1+q)} F_1 g_1}{F_1 g_1 + F_2 g_2}\right] F \tag{23}$$

6.2 SENSITIVITY ANALYSIS AND RESULTS

In performing the sensitivity analyses, variations of the parameters for two base line cases were made as follows:

Case I: d = 1 cm, h = 500 km, i = 47 deg (Ψ (i) = 1.0), t = 1988, S = 140, p = 0.05, and q = 0.02

Case II: d = 1 cm, h = 500 km, i = 47 deg, t = 1995, S = 90, p = 0.05, and q = 0.02

There is no particular significance in the choice of these two cases other than selecting a value of unity for debris diameter and the orbital inclination. One selects the model starting year, 1988, and some future year, 1995, to ensure that significant changes with respect to time are identified (the values of S are representative of those years). Finally, the values of p and q represent the model nominal values.

From these base line values, variations with respect to each derivative functional relationship were calculated for the following ranges:

- $\frac{\partial F}{\partial d}$ versus d for $10^{-3} \leq d \leq 10^{2}$ cm
- $\frac{\partial F}{\partial h}$ versus h for $100 \leq h \leq 2000$ km

- $\frac{\partial F}{\partial i}$ versus i for $25 \leq i \leq 125$ deg
- $\frac{\partial F}{\partial t}$ versus t for 1988 or $1995 \leq t \leq 2010$
- $\frac{\partial F}{\partial S}$ versus S for $70 \leq S \leq 250$
- $\frac{\partial F}{\partial p}$ versus p for $0 \leq p \leq 0.20$
- $\frac{\partial F}{\partial q}$ versus q for $0 \leq q \leq 0.20$

6.2.1 $\partial F/\partial d$ versus d

The variation of $\partial F/\partial d$ versus diameter is shown in Figure 22 for Cases I and II and Figures 23a and b for Case I. From Figure 23,

$$\frac{\partial F}{\partial d} \sim \left(-\frac{1}{d}\right)$$

i.e., the flux becomes more sensitive to particles with smaller diameters. Note that there are 16 orders of magnitude change in $\partial F/\partial d$ for the range of diameters, 0.001 to 100 cm. The rapid change of $\partial F/\partial d$ is especially apparent when plotted on linear axes in Figure 22b. The expression $|\partial F/\partial d| \cong 10^{6}$ at d = 0.001 cm, 10^{-4} at d = 1 cm, and 10^{-9} at d = 100 cm. Note that $|\partial F/\partial d| < 1$ for diameters >0.05 cm. There is a slight change in slope of $\partial F/\partial d$ versus diameter at $d \cong 5.0$ cm. For diameters <0.1 cm, F_1 (and thus its derivative) dominates while for diameters >10 cm, F_2 dominates; thus, the reason for the change in slope. Note, in the limits (for the absolute values),

$$\frac{\partial F}{\partial d} \rightarrow \infty \text{ as } d \rightarrow 0$$

This means that the flux increases rapidly for the smallest diameter particles. The derivative is negative throughout the diameter space indicating a decrease in the flux as diameter increases. Cases I and II (Fig. 22) show the similar characteristics.

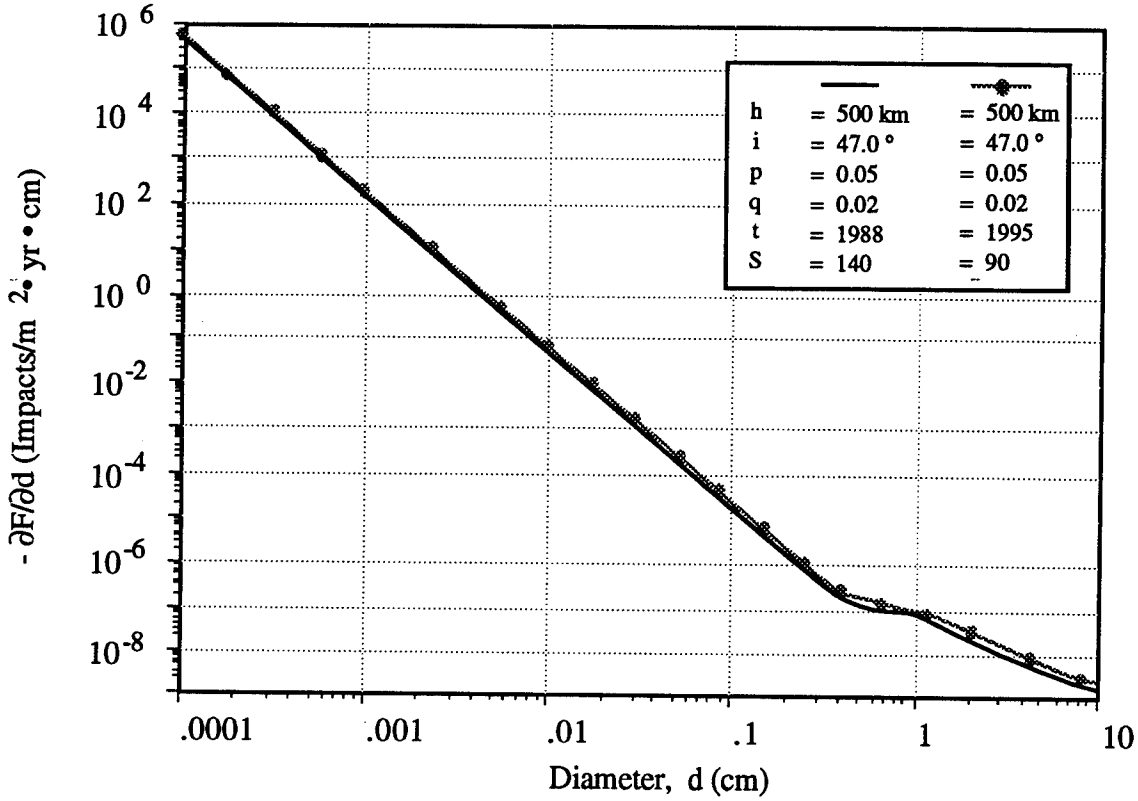

Figure 22. Flux model sensitivity with respect to debris diameter (Cases I & II).

The flux is extremely sensitive to changes in diameter for the smaller particles, especially beginning where $|\partial F/\partial d| > 1$ at $d < 0.05$ cm. This is due to the nature of the curve fit, F_1, through the data (Fig. 1). The function F(d, h, i, t, S) predicts an infinite flux as diameter approaches zero (discussed in Subsection 3.4). Because of this behavior, it is recommended that the model be limited to the range of diameters, $10^{-4} \leq d \leq 10^3$ cm, where the basis is measured data.

6.2.2 ∂F/∂h versus h

The variation of ∂F/∂h versus altitude is shown in Figure 24 for the two base line cases. The magnitude of ∂F/∂h is very small, i.e., $|\partial F/\partial h| << 1$; thus, while there is change, the predicted flux is relatively insensitive to changes in altitude. From Figure 24, it is seen that the sensitivity of ∂F/∂h increases through the lower altitudes and peaks at ~500 km where much of the data base lies. Then the sensitivity decreases with increasing altitude.

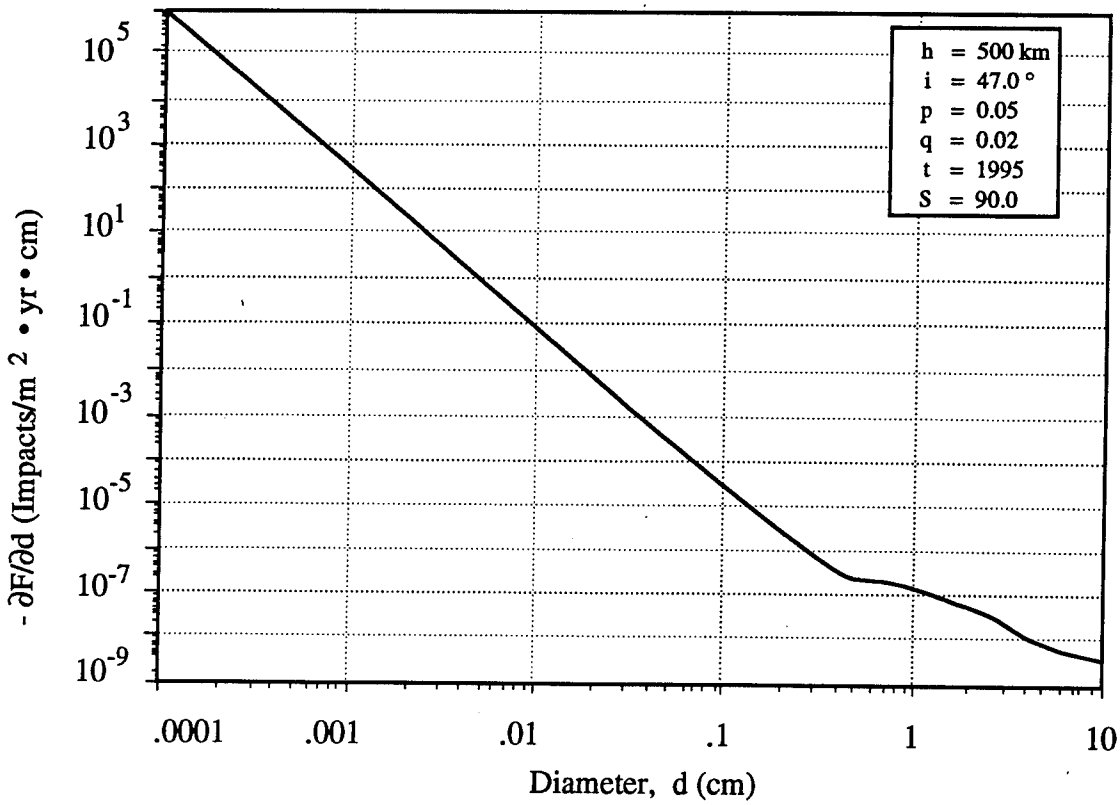

(a). log-log

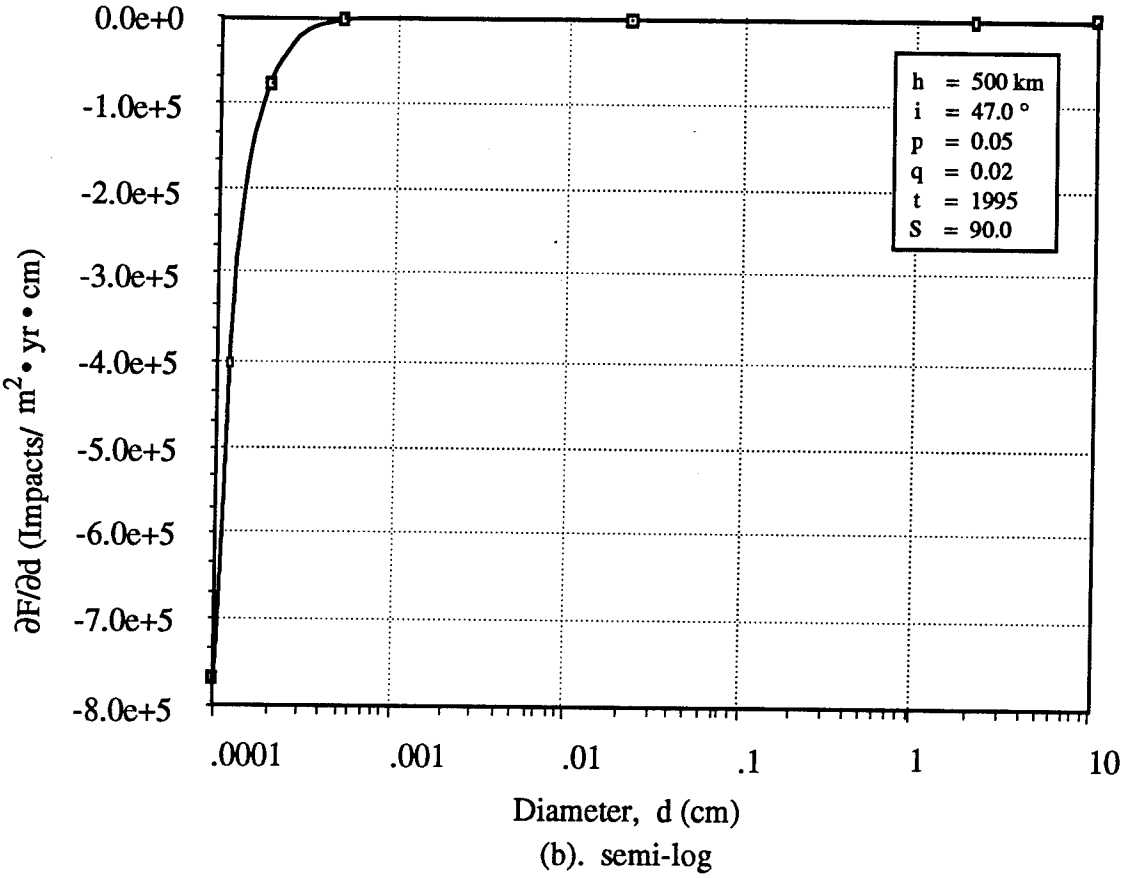

(b). semi-log

Figure 23. Flux model sensitivity with respect to debris diameter (Case II).

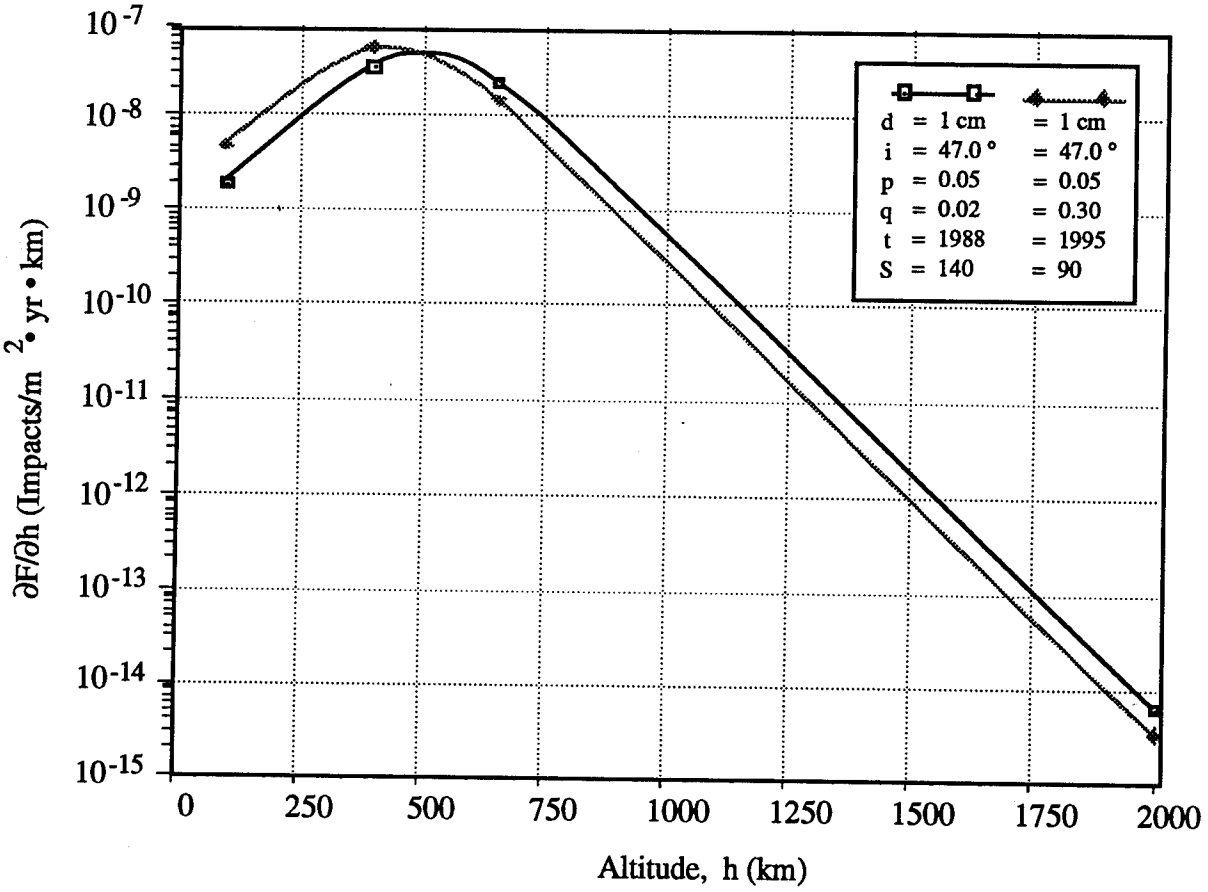

Figure 24. Flux model sensitivity with respect to orbital altitude (Cases I & II).

The predicted flux is relatively insensitive to changes in altitude, especially as altitude increases. The lack of flux changes with altitude beyond 1000 km suggests that the model be limited to altitudes <1000 km. The sensitivity increases through the lower altitudes, up to ~500 km, then decreases (becoming less sensitive) as altitude increases beyond 500 km.

6.2.3 $\partial F/\partial i$ versus i

The variation of $\partial F/\partial i$ versus orbital inclination is shown in Figure 25 for the two base line cases. The curves shown reflect the nature of Ψ. The expression $\partial F/\partial i$ is equal to zero at 80, 90, and 100 deg where Ψ has local maximums and a minimum. The function is relatively insensitive to changes in orbital inclination, i.e., $\partial F/\partial i << 1$.

The flux prediction is relatively insensitive to changes in orbital inclination and mirrors the variation in Ψ with respect to i.

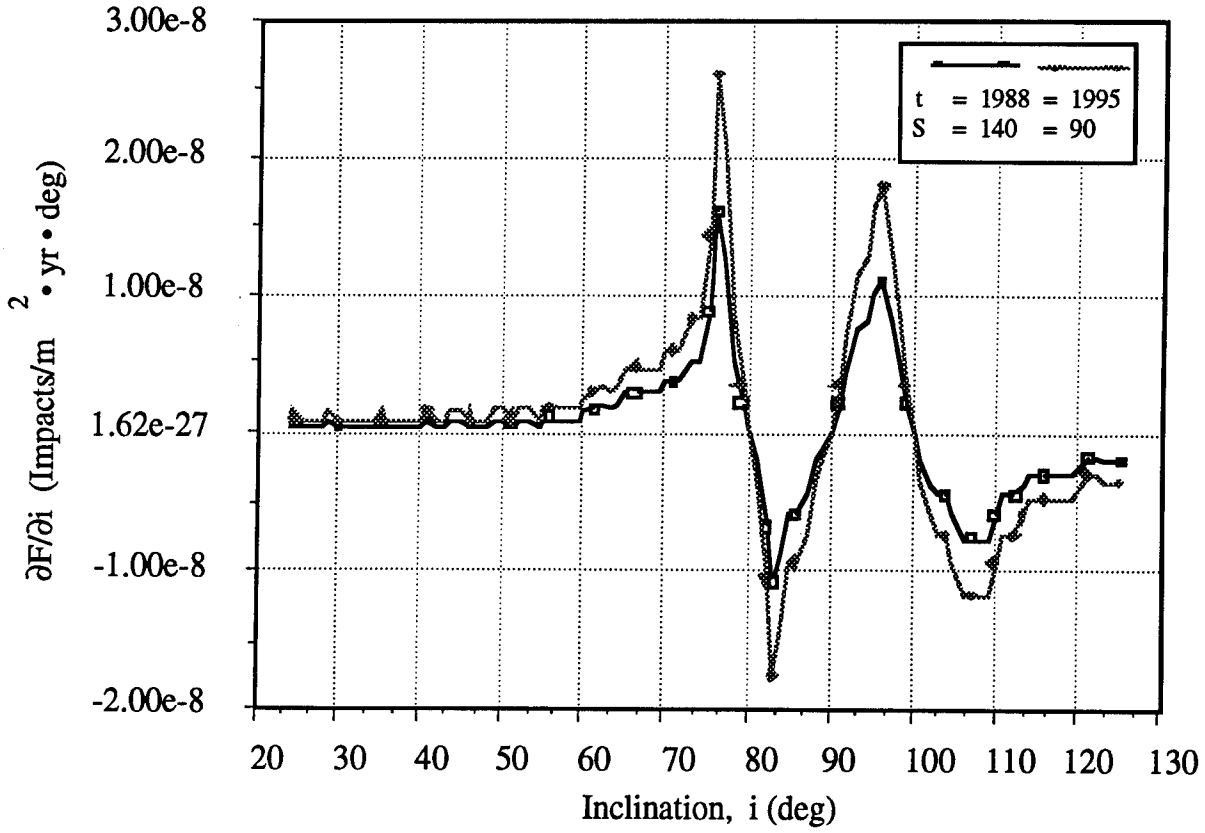

Figure 25. Flux model sensitivity with respect to orbital inclination for Cases I & II, where d = 1 cm, h = 500 km, p = 0.05, and q = 0.02.

6.2.4 ∂F/∂t versus t

The variation of ∂F/∂t versus time (yrs) is shown in Figure 26 for the two base line cases. The curves show an increase in sensitivity with time, but the magnitude (10^{-7}) is extremely small, i.e., $\partial F/\partial t << 1$.

The flux prediction sensitivity increases with time, but the overall magnitude is extremely small. This increased sensitivity is negligible over the period of time for which the model is being considered valid.

6.2.5 ∂F/∂S versus S

The variation of ∂F/∂S versus the measure of the solar activity, S, is shown in Figure 27 for the two base line cases. The magnitude of the sensitivity is extremely small, i.e., $\partial F/\partial S << 1$. As seen in Figure 27, $|\partial F/\partial S|$ reaches a maximum at approximately S = 140, which is the value used to normalize S in Φ_1.

The flux prediction sensitivity with respect to S is extremely small and on the same order of magnitude as the previous sensitivities.

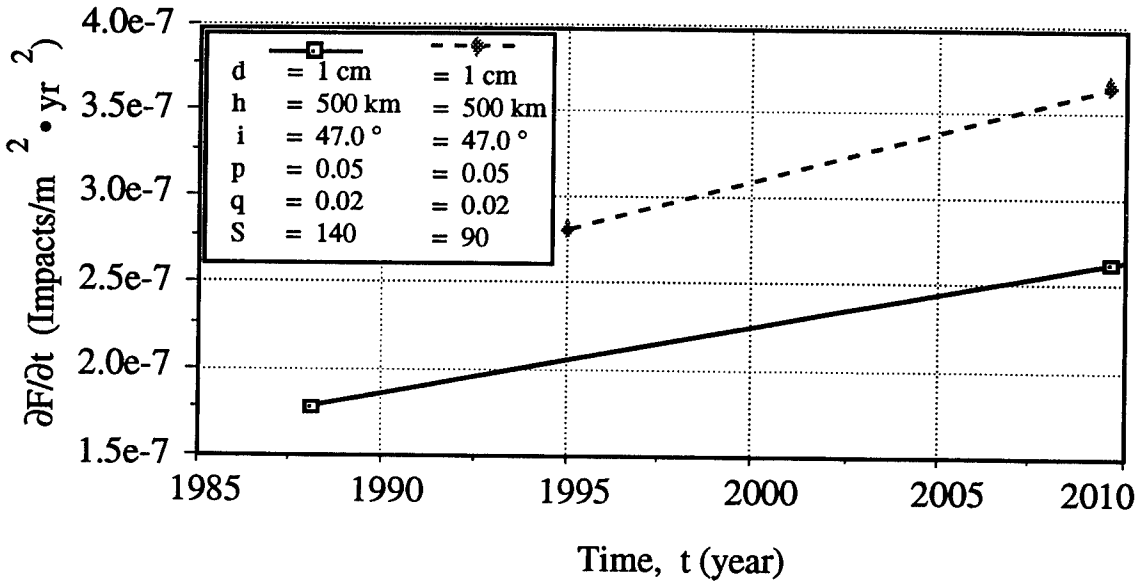

Figure 26. Flux model sensitivity with respect to time (Cases I & II).

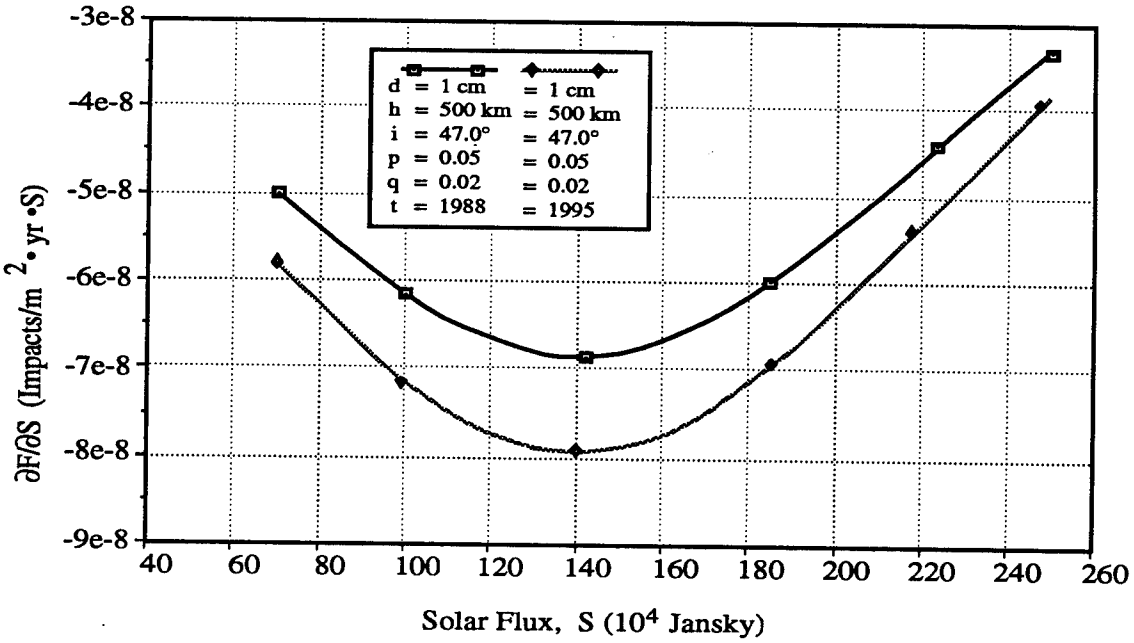

Figure 27. Flux model sensitivity with respect to solar activity (Cases I & II).

6.2.6 $\partial F/\partial p$ and $\partial F/\partial q$

The variations of $\partial F/\partial p$ versus p and $\partial F/\partial q$ versus q are shown in Figure 28 for Case II only (t = 1995). Case I is trivial since both g_1 and g_2 equal one for t = 1988, i.e., no change in the sensitivities with either p or q. As can be seen in Figure 28, $\partial F/\partial p$ is constant with respect to changes in p. This is due to the linear nature of g_2. The function $\partial F/\partial q$, however, changes with q and increases when q is increased, reflecting the compounded nature of g_2. This points out another difference between compounded growth (g_1) or linear growth (g_2), discussed in Subsection 4.3. The flux prediction sensitivity does not change for linear growth, while its sensitivity increases with compounded growth (increases with increasing q). The relative order of magnitude of $\partial F/\partial q$ 10^{-4} ranks this sensitivity as second to $\partial F/\partial d$.

The flux prediction sensitivity does not change with the large-particle growth rate, p, and is increasingly sensitive to increases in the small-particle growth rate, q.

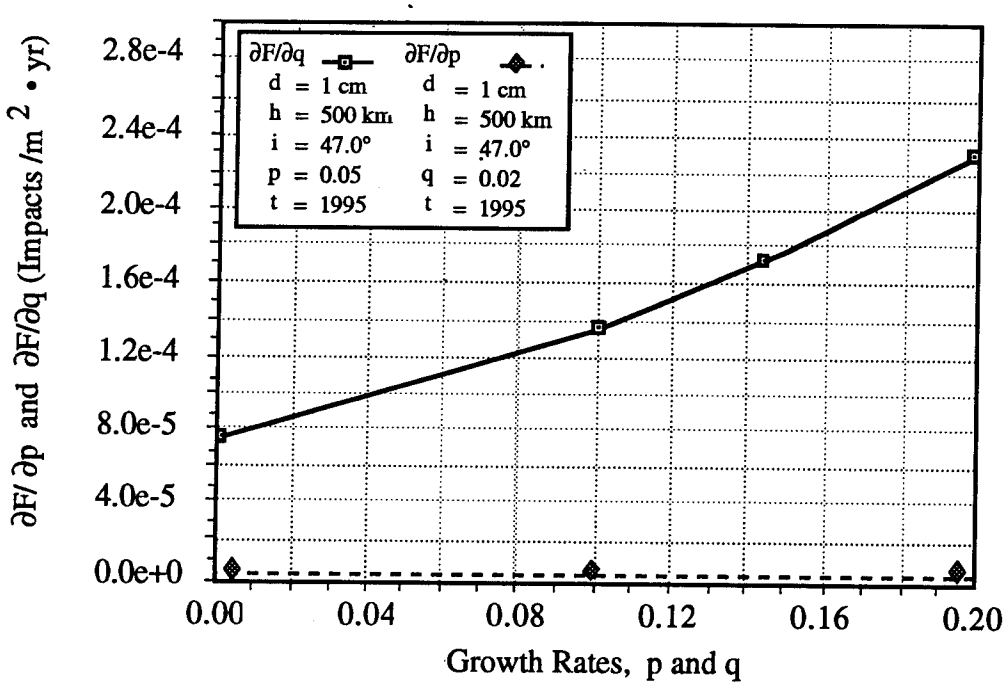

Figure 28. Flux model sensitivity with respect to particle growth rates (Case II).

6.2.7 Combined Sensitivities for $\partial^2 F/\partial h\, \partial d$, $\partial^2 F/\partial h\, \partial i$, and $\partial^2 F/\partial d\, \partial q$.

Combined or composite sensitivities are shown in Figures 29 to 31 for Case II. Because of the nature of Equation 6, the sensitivities presented are given by the following relationships:

$$\frac{\partial^2 F}{\partial h\, \partial d} = \frac{1}{F}\left(\frac{\partial F}{\partial h}\right)\left(\frac{\partial F}{\partial d}\right) \tag{24}$$

$$\frac{\partial^2 F}{\partial h\, \partial i} = \frac{1}{F}\left(\frac{\partial F}{\partial h}\right)\left(\frac{\partial F}{\partial i}\right) \tag{25}$$

$$\frac{\partial^2 F}{\partial d\, \partial q} = \frac{1}{F}\left(\frac{\partial F}{\partial d}\right)\left(\frac{\partial F}{\partial q}\right) \tag{26}$$

Figure 29 shows the flux model sensitivity versus altitude and diameter. As seen in this figure, the flux model is most sensitive for the smaller diameters at the lower altitudes and becomes extremely insensitive at the higher altitudes for the larger particles.

The flux model sensitivity versus altitude and inclination given in Figure 30 shows the flux is sensitive to variation in orbital inclination for only the lower altitudes, $h < 1000$ km. Above 1000 km, the model is insensitive to any changes in altitude or orbital inclination and a uniform debris cloud is predicted above 1000 km.

The variation of the flux model sensitivity with respect to diameter and small-particle growth rate is shown in Figure 31. Clearly the dominant sensitivity is with respect to diameter. The results of these sensitivities are consistent with the results previously presented. The flux model is most sensitive to changes in diameter, especially as diameter decreases. The flux model is least sensitive to changes in altitude, predicting a constant debris flux beyond 1000 km.

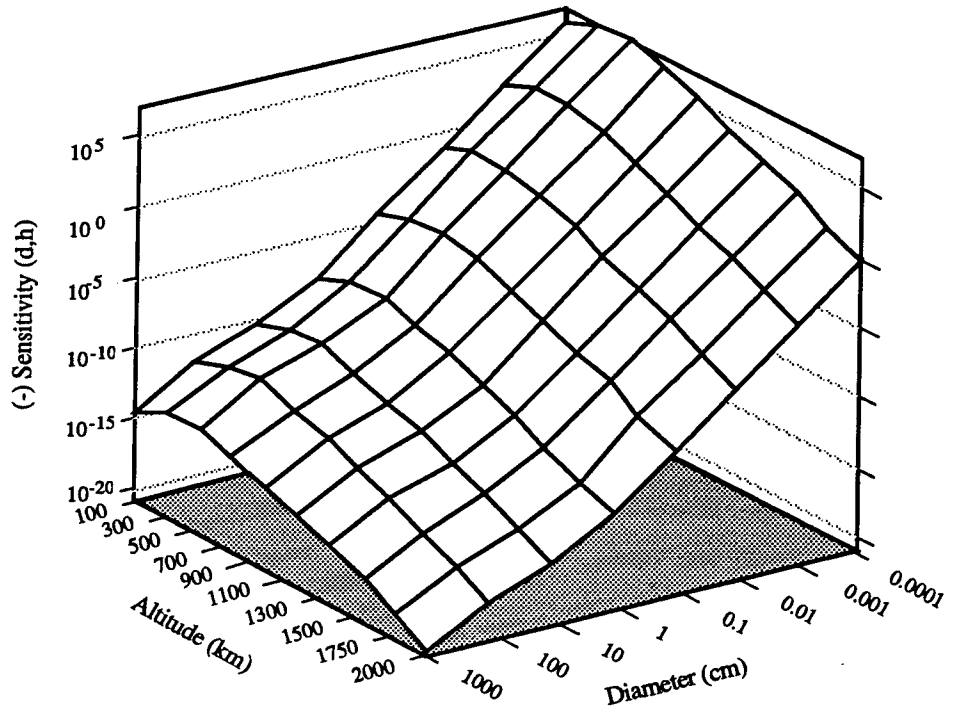

Figure 29. Flux model sensitivity with respect to altitude and diameter (Case II).

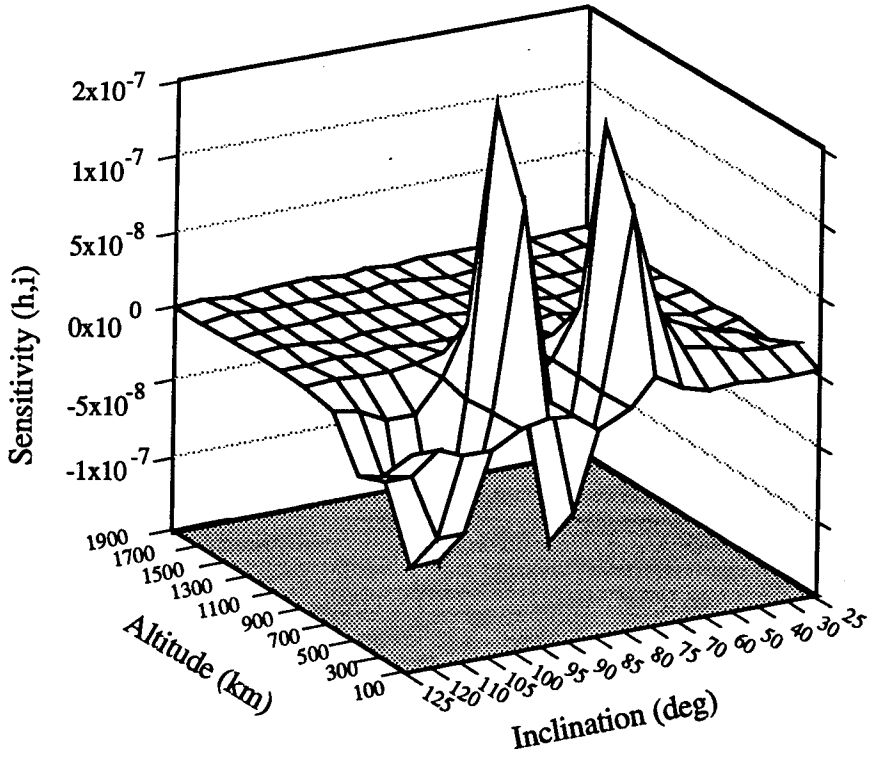

Figure 30. Flux model sensitivity with respect to altitude and inclination (Case II).

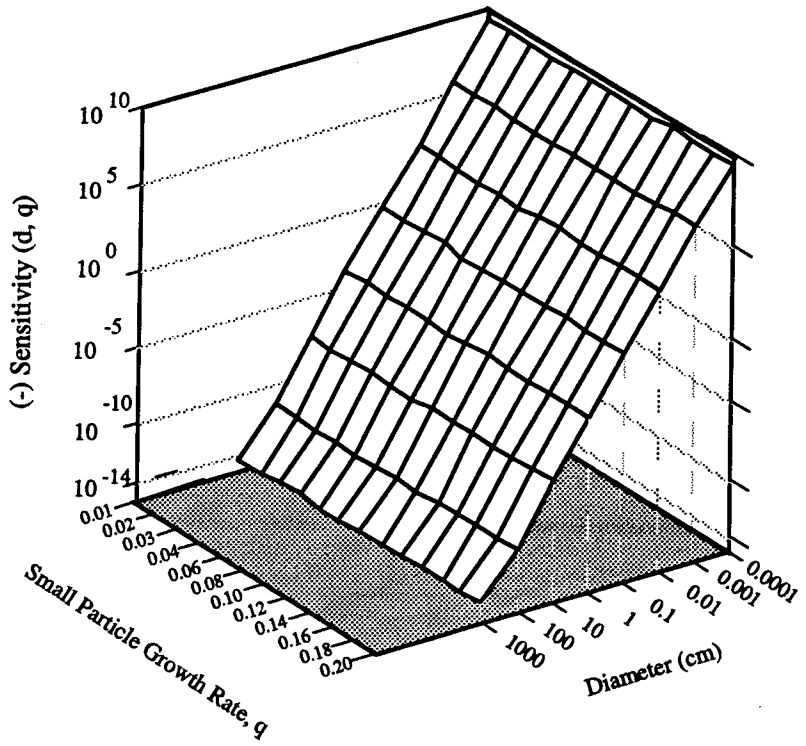

Figure 31. Flux model sensitivity with respect to diameter and small-particle growth rate (Case II).

6.3 SENSITIVITY ASSESSMENT

The sensitivities of the flux model have been analyzed with respect to the independent variables, debris diameter (d), orbital altitude (h), orbital inclination (i), time (t), solar activity (S), and the large- and small-particle growth rates (p and q). The summary results, depicted in Figure 32, show the relative magnitudes of these sensitivities. One can see the flux prediction is most sensitive to changes in debris diameter, for the small diameter debris. On the basis of the singular behavior of F as diameter decreases and the range of diameters from the data base, it is recommended the model be restricted to $10^{-4} \leq d \leq 10^{3}$ cm.

Next in importance is the sensitivity of F to the assumed growth rates for small particles, q. The sensitivity increases as the growth rate increases. The sensitivities with respect to the large-particle growth rate, p, and inclination are next in relative importance. The sensitivity with respect to p is constant. The sensitivity with respect to i at 500-km mirrors Ψ. (Note that for comparison the orbital inclination sensitivity presented in Figure 32 has the units of flux/radian.) The sensitivities with respect to time and solar activity are next in importance but are much less in magnitude than the previous variables. The least sensitive changes by an order of magnitude are with respect to

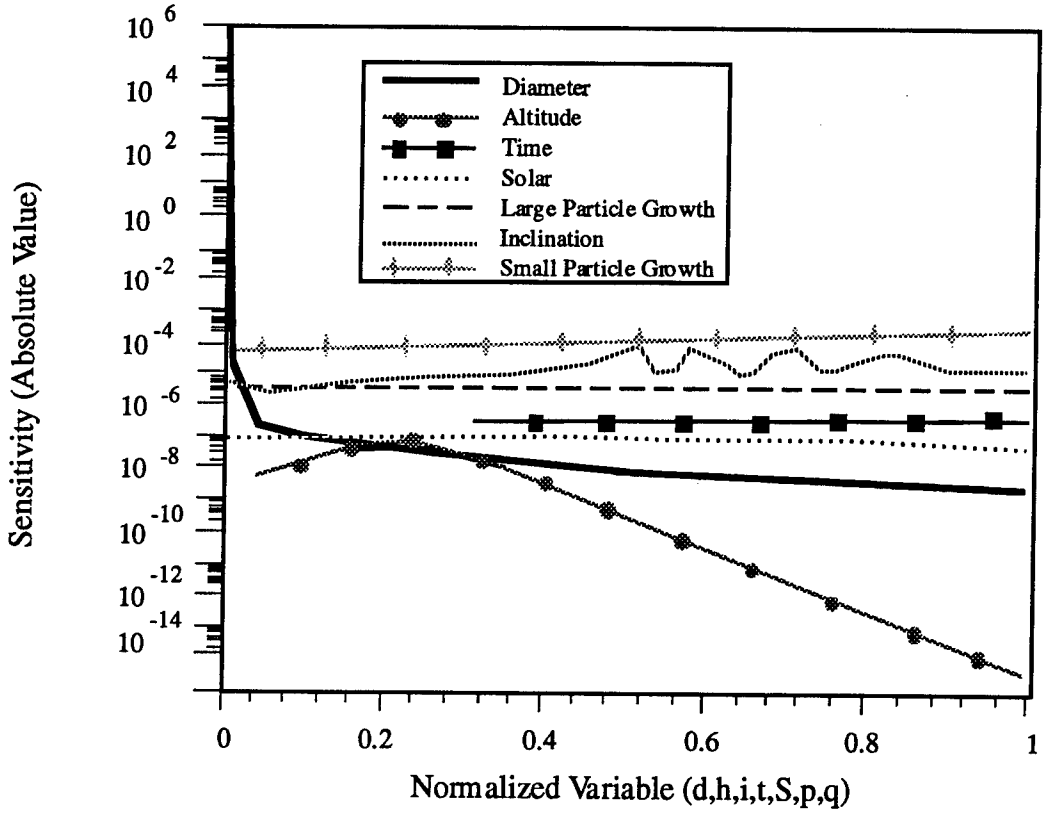

Figure 32. Flux model sensitivities, summary comparisons (Case II). (Baseline values: h = 500 km, d = 1 cm, i = 47 deg, t = 1995, S = 90, p = 5%, q = 2%.)

altitude. This suggests that the model does not account for variations with altitude in a realistic manner. In fact, F becomes nearly constant as altitude increases beyond nominally 800 to 1000 km ($\partial F/\partial h \rightarrow 0$). Recall that Equation 6 does not reproduce the published data as was shown in Figure 3 for these altitudes. This insensitivity and weakness in the model prediction with respect to altitude emphasize its limitations and suggest the model be used at altitudes ≤1000 km rather than what is typically thought of as LEO (h < 2000 km). In summary, the rank order of the flux model sensitivities is as follows:

Parameter	Relative Order of Magnitude/Comments
• d (diameter)	~10^{6} at d = 0.001 cm ~1 at d = 0.05 cm ~10^{-9} at d = 100 cm Flux prediction becomes undefined as d → 0.
• q (small-particle growth rate)	~10^{-4}, slightly increasing with increasing q

• i (orbital inclination) and p (large-particle growth rate)	~10^{-5} to 10^{-6}, sensitivity with respect to i reflects $\Psi(i)$ variation; sensitivity with respect to p is constant
• t (time) and S (solar)	~10^{-7} to 10^{-8}
• h (altitude)	~10^{-8} (h = 500 km) to 10^{-14} (h = 2000 km), predicts constant flux for h > 1000 km

7.0 UNCERTAINTY ANALYSIS

This section presents an uncertainty analysis of the NASA 90 model. The uncertainty analysis is a study of how the root-mean-square (RMS) error in the data or curve fit affects the results obtained from the use of the model. The uncertainty analysis approach is described in Subsection 7.1 while Subsection 7.2 shows the results. Subsection 7.3 presents the summary assessment.

7.1 PROPAGATION OF ERRORS

Most empirically based models will have some inherent error in the results because of the uncertainties in the measured values and because of the RMS difference of the curve fit to the data. These differences can be due to either the natural variation of parameters measured in space and time or in the model (curve fit) representation of the data. The values of the differences, or errors, can be estimated with some level of confidence from the known or quantifiable characteristics of the data or the curve fit. For example,

$\pm \varepsilon_j$ = estimated uncertainty in the parameter j at some level of confidence (e.g., 90% confidence). Note that the +/- values may not be necessarily identical.

For the NASA 90 model, the overall error, $\pm \varepsilon_F$, in F(d, h, i, t, S) is due to the uncertainties in the variables used to determine F. If one assumes that each of the variables are uncorrelated, the contribution of the individual uncertainties to ε_F may be estimated by the use of a propagation of error analysis as follows:

$$\varepsilon_F = \pm \left\{ \left(\frac{\partial F}{\partial d} \varepsilon_d \right)^2 + \left(\frac{\partial F}{\partial h} \varepsilon_h \right)^2 + \left(\frac{\partial F}{\partial i} \varepsilon_i \right)^2 + \left(\frac{\partial F}{\partial t} \varepsilon_t \right)^2 + \left(\frac{\partial F}{\partial S} \varepsilon_S \right)^2 + \left(\frac{\partial F}{\partial p} \varepsilon_p \right)^2 + \left(\frac{\partial F}{\partial q} \varepsilon_q \right)^2 \right\}^{1/2} \quad (27)$$

where

ε_F = Uncertainty in F, e.g., $F \pm \varepsilon_F$
ε_d = Uncertainty in flux with respect to particle diameters
ε_h = Uncertainty in flux with respect to altitude
ε_i = Uncertainty in flux with respect to inclination
ε_t = Uncertainty in flux with respect to time
ε_p = Uncertainty in flux with respect to large-particle growth

ε_q = Uncertainty in flux with respect to small-particle growth

ε_S = Uncertainty in the level of solar activity

Each of the individual uncertainties is estimated at the same level of confidence. In this study NASA's estimates of the individual uncertainties as presented in Subsection 4.6 were used. This led to the modification of Equation 27 as follows:

$$\varepsilon_F = \pm \left\{ (\varepsilon_{FM})^2 + (\varepsilon_{FH})^2 + \left(\frac{\partial F}{\partial S}\varepsilon_S\right)^2 + \left(\frac{\partial F}{\partial p}\varepsilon_p\right)^2 + \left(\frac{\partial F}{\partial q}\varepsilon_q\right)^2 \right\}^{1/2} \qquad (28)$$

where

ε_{FM} = Uncertainty in F because of statistical and measurement uncertainties primarily as a function of debris diameter

ε_{FH} = Uncertainty in F with respect to altitude due in part to the difficulty in determining F for debris in highly elliptical orbits

Equation 28 represents the parameters that were felt to affect significantly the uncertainty in the flux prediction, Equation 6. Note that $\partial F/\partial p$, $\partial F/\partial q$, and $\partial F/\partial S$ are given by Equations 21 through 23. The estimated uncertainties used for this study are shown in Table 5.

Rationale for Choices: Equation 28 was used to analyze the results of the error propagation because it was convenient to use the uncertainties reported by NASA (Ref. 2). The terms shown in Equation 27 are equivalent to those in Equation 28. The uncertainty in flux measurements, ε_{FM}, and the uncertainty with respect to the altitude distribution, ε_{FH}, in Equation 28 represent the measurement uncertainties given as the first four terms of Equation 27. Because ε_{FM} and ε_{FH} are reported directly by NASA (Ref. 2), there is no need to attempt to estimate ε_d, ε_h, ε_i, and ε_t directly. The remaining uncertainties in knowledge of the actual particle growth and solar activity, ε_p, ε_q, and ε_s, are estimated by NASA (Ref. 2) and were included because the state of particle growth has not yet been verified and because predicting future maximum levels of solar activity remains uncertain (Ref. 17).

An independent assessment of the NASA estimated uncertainties was not conducted as part of this task. Such an assessment may be performed by establishing uncertainties in each variable in Equation 27.

Table 5. Propagation of error analysis uncertainties.

Parameter	Estimated Uncertainty (90% Confidence)	Flux Uncertainty
• Flux Measurements:	$d \geq 10$ cm	$\pm\varepsilon_{FM} = 0.5F$
	$0.05 < d < 10$ cm	$+\varepsilon_{FM} = 2F$ $-\varepsilon_{FM} = (2/3)\ F$
	$d \leq 0.05$ cm	$+\varepsilon_{FM} = F$ $-\varepsilon_{FM} = 0.5\ F$
• Flux Measurements: Altitude Distribution	$d \geq 10$ cm	$+\varepsilon_{FH} = F$ $-\varepsilon_{FH} = 0.5\ F$
	$1 < d < 10$ cm	$\pm\varepsilon_{FH}$ = (same as $\pm\varepsilon_{FM}$ for $0.05 < d < 10$ cm)
	$d \leq 1$ cm	$\pm\varepsilon_{FH} = 4F$ for $100 \leq h \leq 300$ km $\pm\varepsilon_{FH} = 0$ for $300 < h < 700$ km $\pm\varepsilon_{FH} = 4F$, for $700 \leq h < 900$ km $\pm\varepsilon_{FH} = 9F$ for $900 \leq h < 1100$ km • • • $\pm 5F$ for each 200-km increment in altitude • • • $\pm\varepsilon_{FH} = 34F$ for $1900 \leq h \leq 2000$ km
• Large-Particle Growth ($p = 0.05$)		$+\varepsilon_p = 0.05$ $-\varepsilon_p = 0.01$
• Small-Particle Growth ($q = 0.02$)		$+\varepsilon_q = 0.18$ $-\varepsilon_q = 0.02$
• Solar Activity		$+\varepsilon_s = 250 - S$ $-\varepsilon_s = S - 70$

7.2 UNCERTAINTY ANALYSIS RESULTS

This subsection discusses the uncertainties given in Equation 28. The ε_{FM} and ε_{FH} uncertainties will be analyzed in Subsections 7.2.1 and 7.2.2. The contribution to $+\varepsilon_F$, $+\varepsilon_F{}^*$, of two of the uncertainties, $+\varepsilon_{FM}$ and $+\varepsilon_{FH}$, are plotted in Figure 33 as a function of d and h. The flux, F(h,d,i,t,p,q), has been factored out, i.e., normalized error, $+\varepsilon_F{}^*$.

$$+\varepsilon_F \propto (c_1 F^2 + c_2 F^2)^{1/2} \tag{29}$$

or

$$+\varepsilon_F{}^* = \frac{F\,(c_1 + c_2)^{1/2}}{F} \tag{30}$$

where c_1 and c_2 are the multipliers of F (Table 5) that are used to calculate $+\varepsilon_{FM}$ and $+\varepsilon_{FH}$ for varying diameters and altitudes.

Figure 33 shows that the normalized error, $+\varepsilon_F{}^*$, is greater than a factor of 5 for altitudes >700 km and particle diameters ≤1 cm. For altitudes >1000 km and particle diameters ≤1 cm, $+\varepsilon_F{}^*$ is greater than one order of magnitude. These observations will help in visualizing the overall, unnormalized error shown in Figures 34-39.

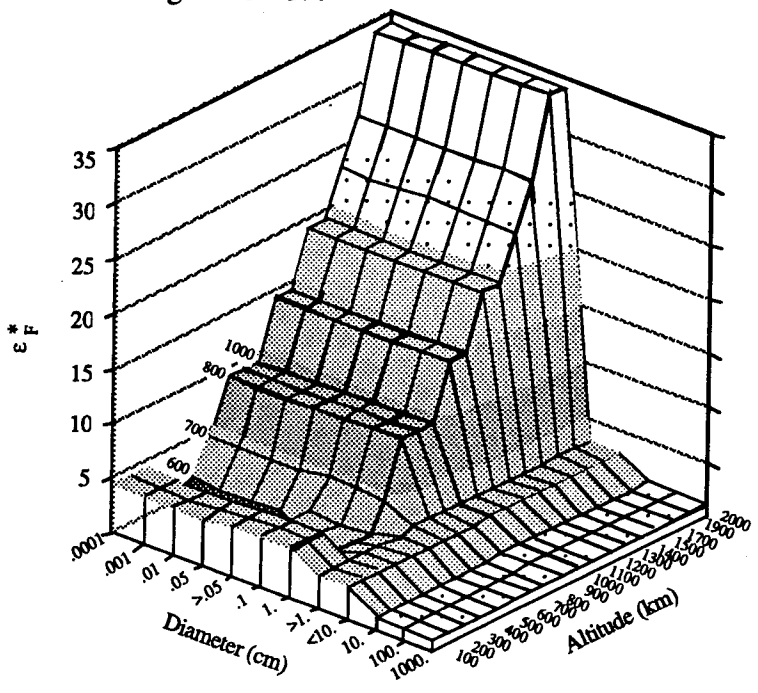

Figure 33. Flux model uncertainty, $+\varepsilon_{FM}$ and $+\varepsilon_{FH}$ components, versus diameter and altitude.

The graphical results of the absolute uncertainty, $\pm\varepsilon_F$, are presented in Figures 34-36 and Figures 37-39 for the AF/DoD orbits of interest identified in Section 5.0. Figures 34-36 present the flux versus the diameter for orbital altitudes of 500, 1000, and 1500 km and orbital inclinations of 30, 70, and 95 deg, respectively. The debris diameter is varied between 10^{-4} to 10^{3} cm. Figures 36-38 present the flux versus altitude for diameters of 0.05, 0.1, 1.0, and 10 cm and orbital inclinations of 30, 70, and 95 deg. The orbital altitude is varied between 100 to 2000 km. In all figures, the upper curve represents $F + \varepsilon_F$, the middle curve represents the nominal value of F and the lower curve represents $F - \varepsilon_F$. The uncertainties, $+\varepsilon_F$ and $-\varepsilon_F$, were determined using Equation 28 and Table 5.

7.2.1 Flux versus Diameter

The flux versus diameter results are presented in Figures 34-36 (a, b, c) for 1995 (S = 90). Figure 34 presents the results for i = 30 deg, Figure 35 for i = 70 deg, and Figure 36 for i = 95 deg for orbital altitudes of (a) 500 km, (b) 1000 km, and (c) 1500 km. An examination of these figures shows that the uncertainty increases with increasing altitude and decreases with increasing diameter. The best results (those with the least uncertainty) are for an orbital altitude of 500 km and diameters >10 cm. This is expected because much of the impact data base comes from orbital altitudes of 500 km or less (Solar Max). The best measurements with respect to size come from USSPACECOM data, which have an estimated measurement resolution of diameters down to 10 cm.

Typical of the general trends, the flux uncertainty varies by a factor of 2 to 4 for the lower altitudes and by an order of magnitude for the higher altitudes. The major contributors to this overall uncertainty can be identified by examining the individual terms of Equation 28. For example, at i = 30 deg, h = 1000 km, d = 0.1 cm (Fig. 33), and F = 0.00407 impacts/m^2 • yr,

$$\varepsilon_F = \pm\left\{(\varepsilon_{FM})^2 + (\varepsilon_{FH})^2 + \left(\frac{\partial F}{\partial p}\varepsilon_p\right)^2 + \left(\frac{\partial F}{\partial q}\varepsilon_q\right)^2 + \left(\frac{\partial F}{\partial S}\varepsilon_S\right)^2\right\}^{1/2}$$

$$= [(8.15 \times 10^{-3})^2 + (3.67 \times 10^{-2})^2 + (2.21 \times 10^{-7})^2 + (5.03 \times 10^{-3})^2 + (1.49 \times 10^{-5})^2]^{1/2}$$

$$= 3.79\ (10^{-2}) \text{ thus } [(F + \varepsilon_F)/F] = 10.3$$

The flux prediction is dominated by the first two terms which represent the uncertainties in the flux measurement capabilities. This emphasizes earlier conclusions that the accuracy of this model can be increased significantly through a reduction in the measurement uncertainties. The next term to dominate is the uncertainty in the small-particle growth (recall that this example is for d = 0.1 cm).

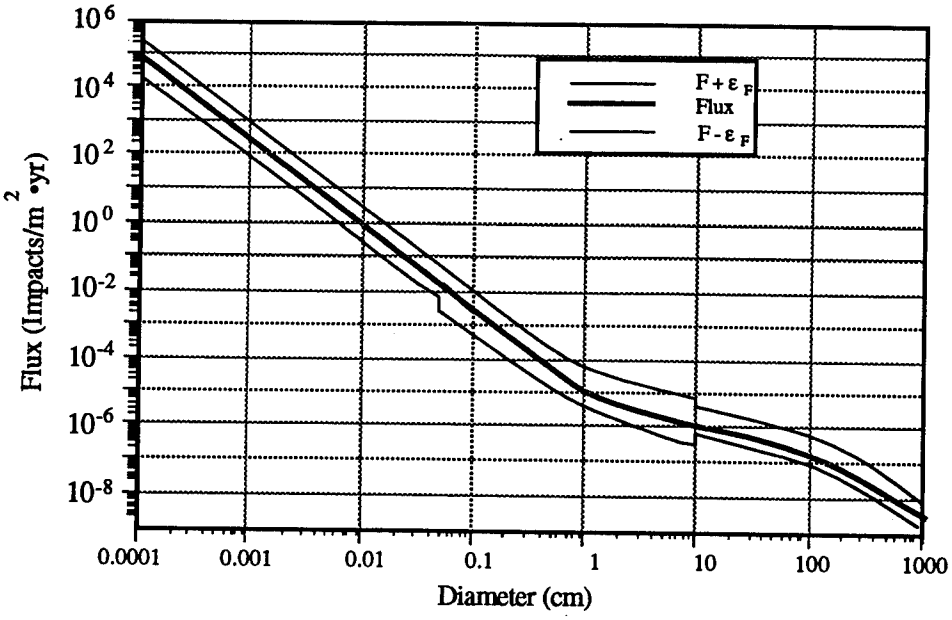

(a) h = 500 km, t = 1995, and S = 90.

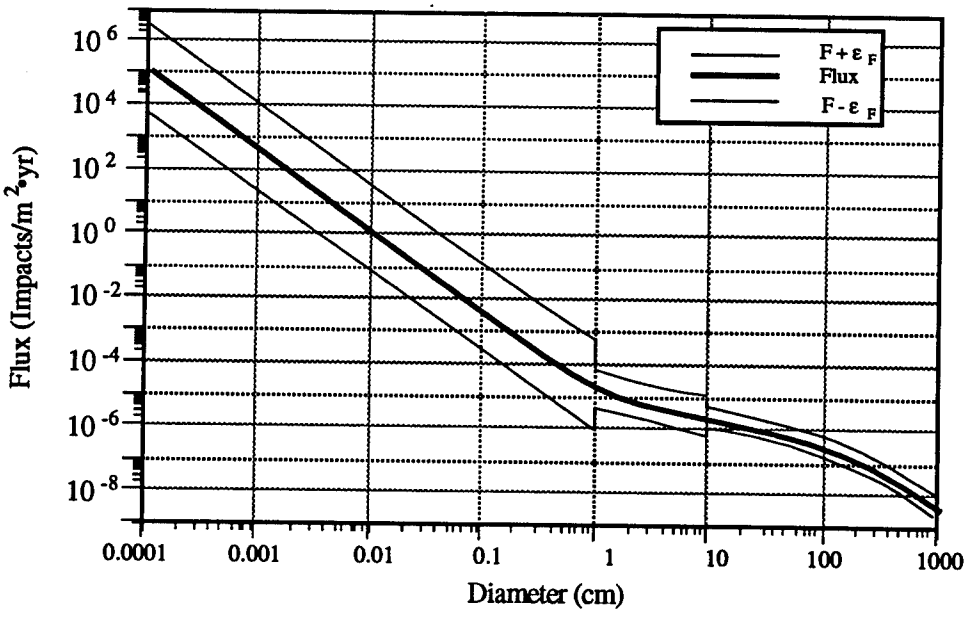

(b) h = 1000 km, t = 1995, and S = 90.

Figure 34. Flux model uncertainty versus diameter for i = 30 deg.

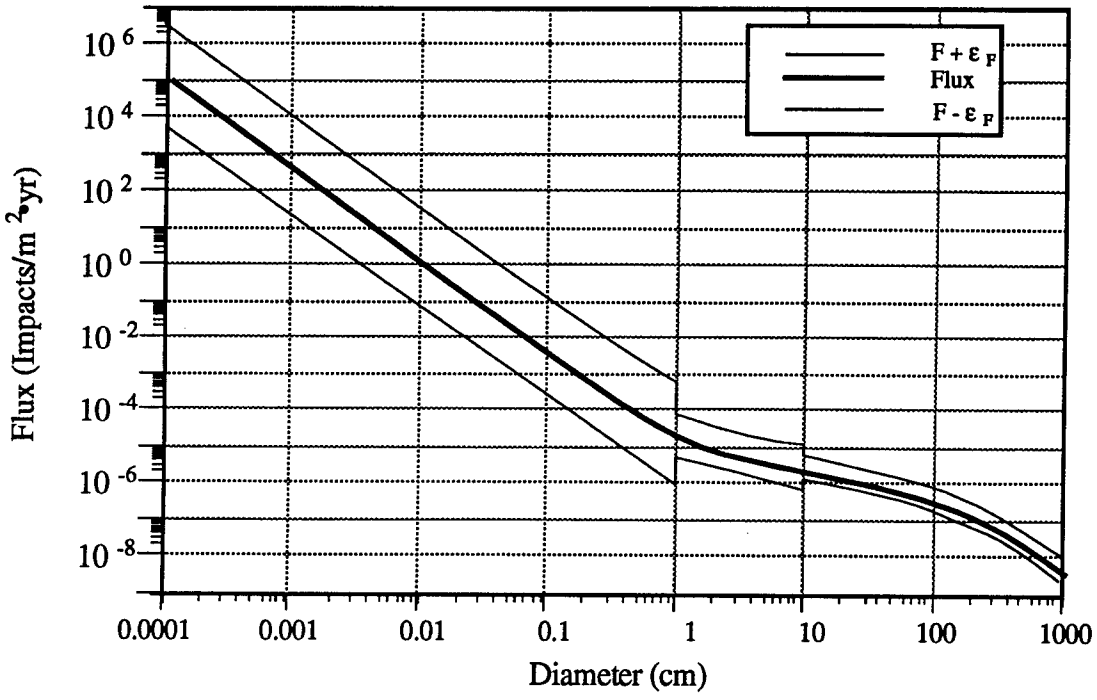

(c) h = 1500 km, t = 1995, and S = 90.

Figure 34. Concluded.

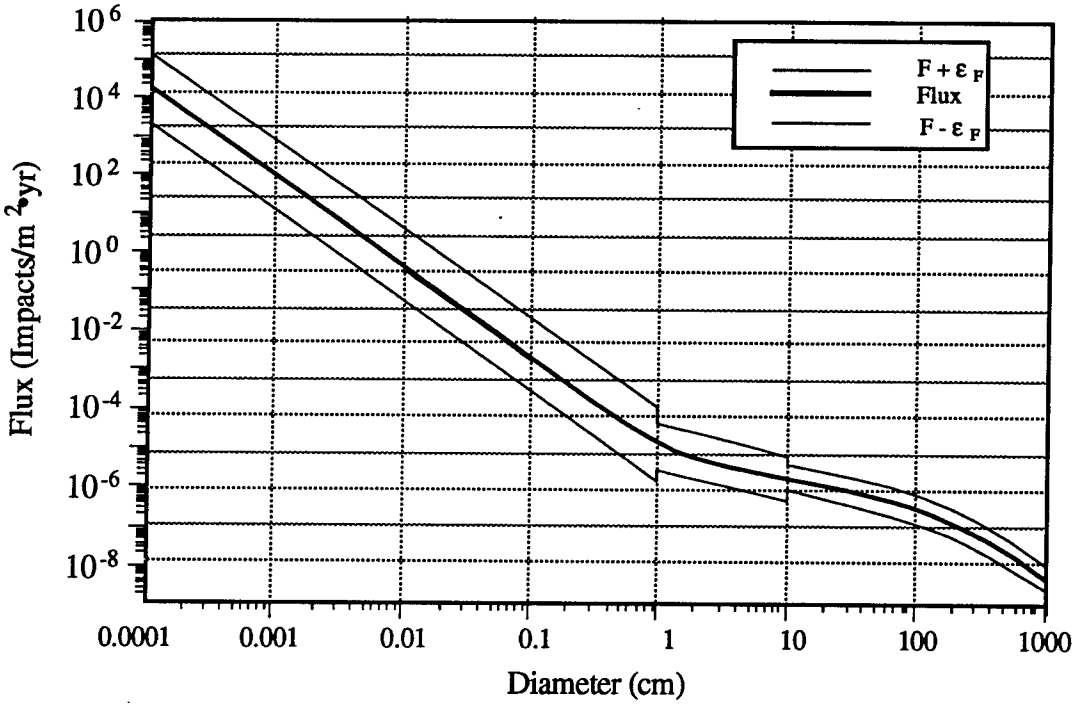

(a) h = 500 km, t = 1995, and S = 90.

Figure 35. Flux model uncertainty versus diameter for i = 70 deg.

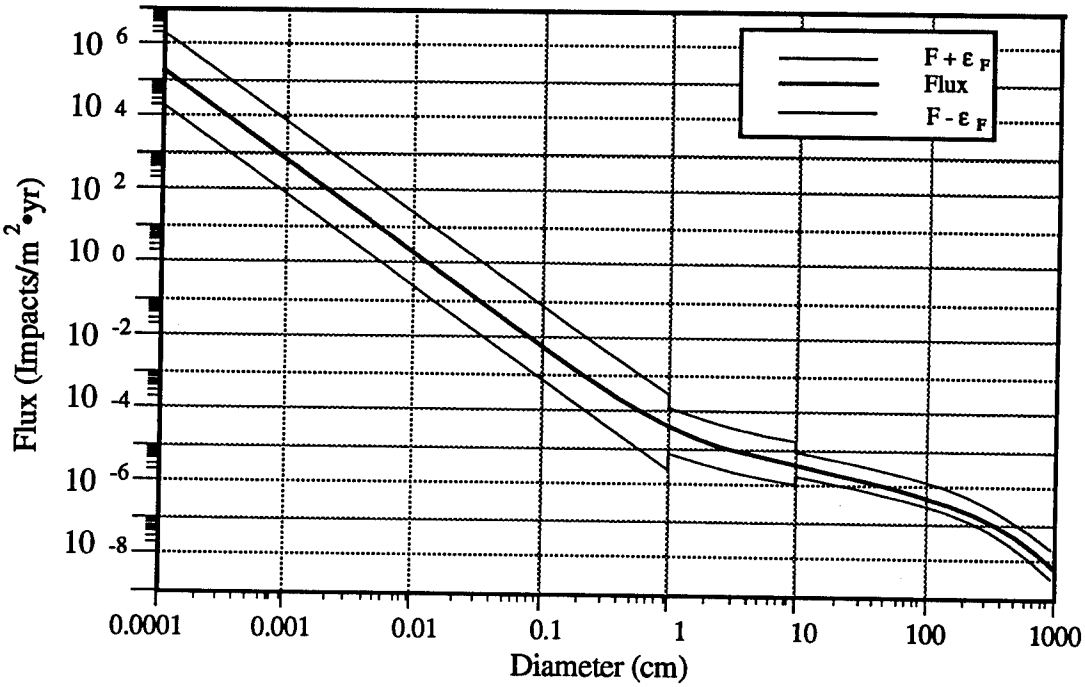

(b) h = 1000 km, t = 1995, and S = 90.

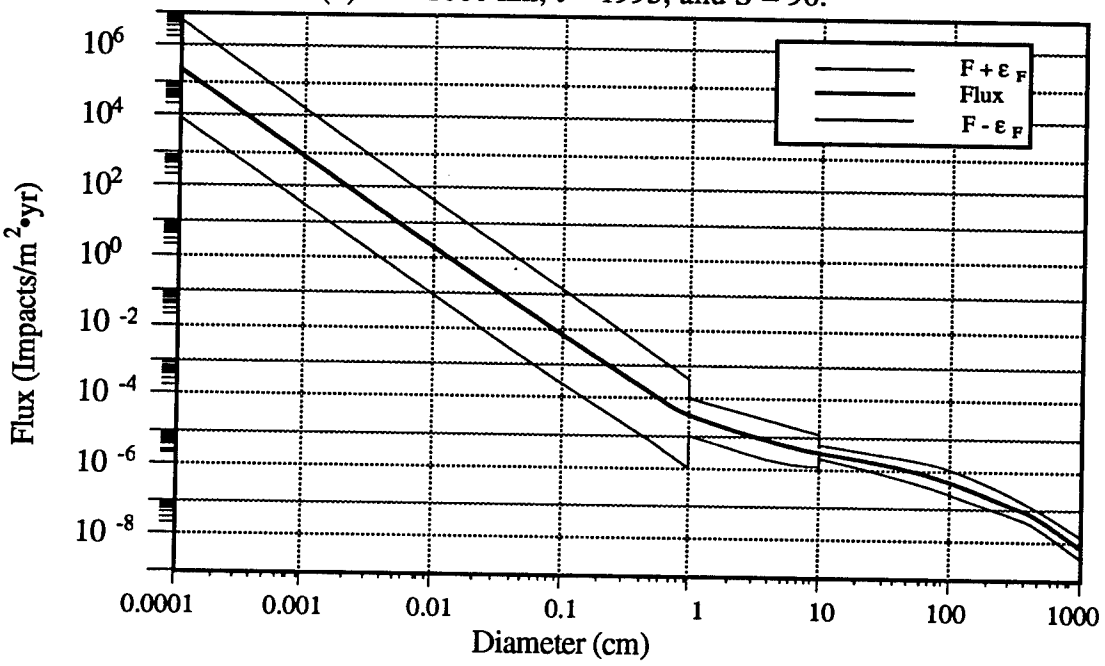

(c) h = 1500 km, t = 1995, and S = 90.

Figure 35. Concluded.

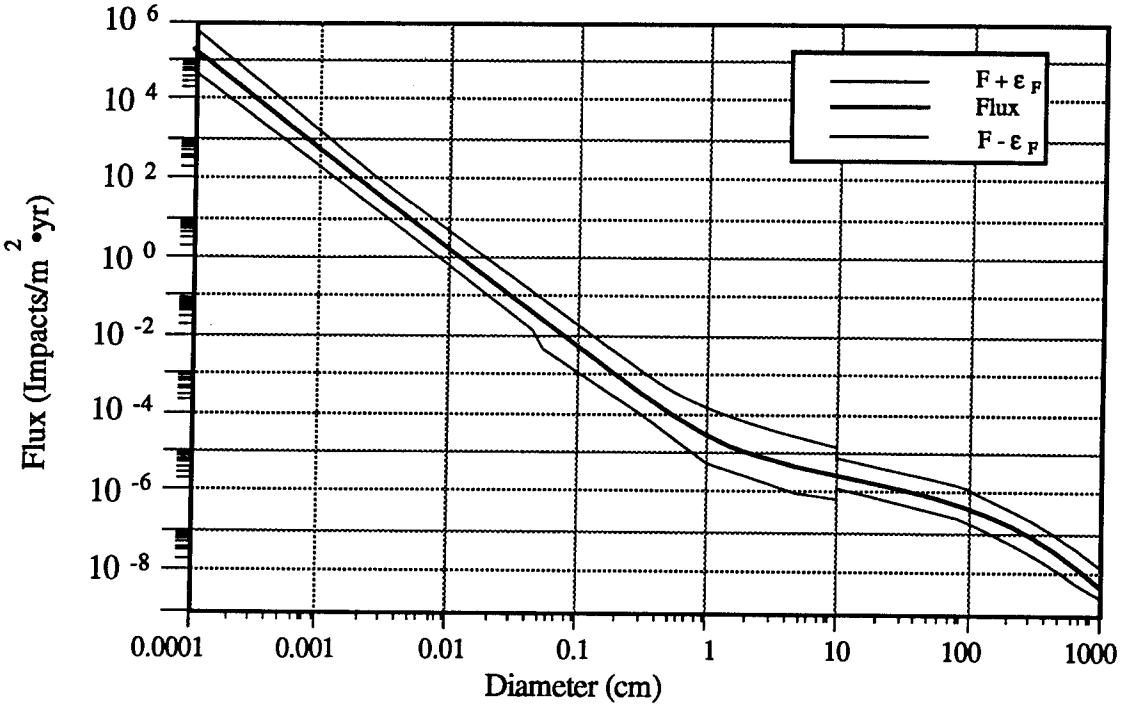

(a) h = 500 km, t = 1995, and S = 90.

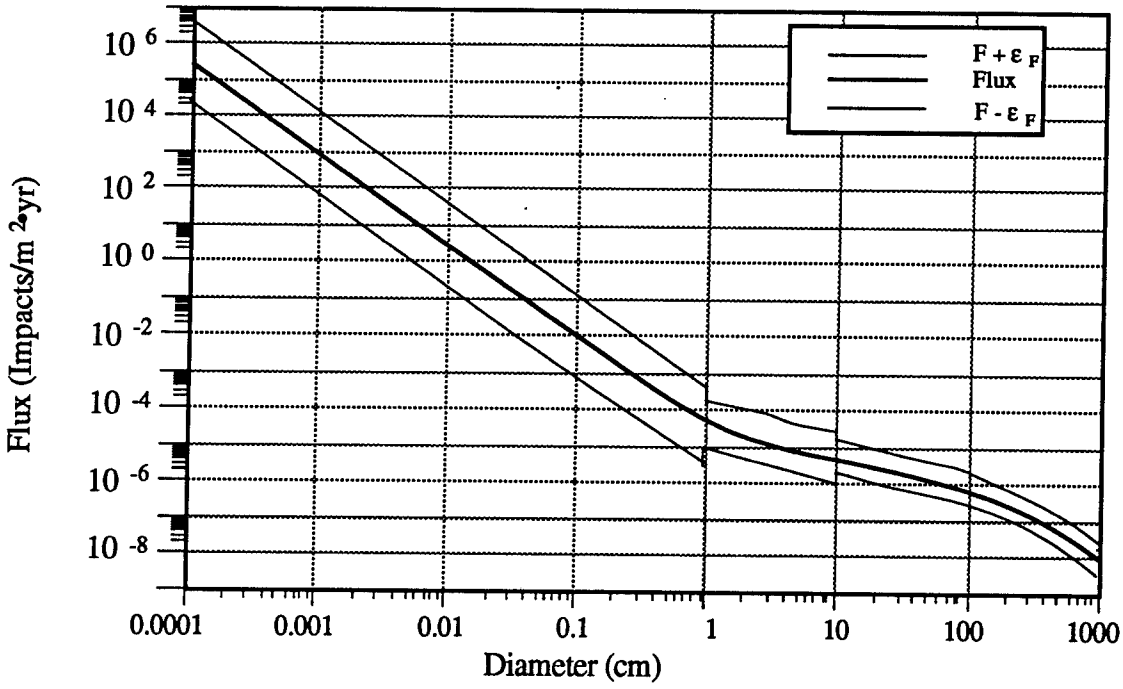

(b) h = 1000 km, t = 1995, and S = 90.

Figure 36. Flux model uncertainty versus diameter for i = 95 deg.

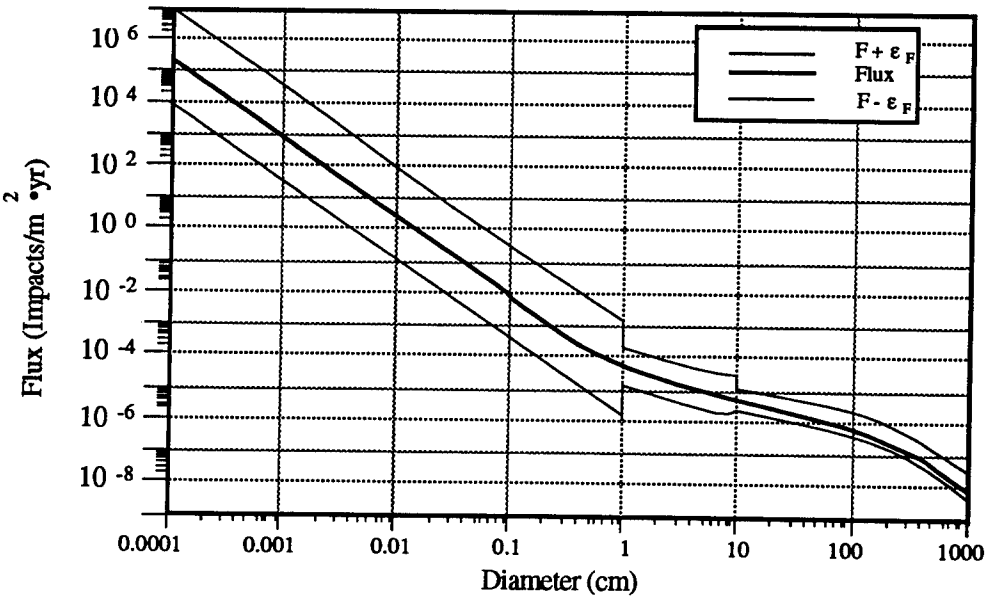

(c) h = 1500 km, t = 1995, and S = 90.

Figure 36. Concluded.

7.2.2 Flux Versus Altitude

The flux versus altitude results are presented in Figures 37-39 (a,b,c,d) for 1995 (S = 90). Figure 37 presents the results for i = 30 deg, Figure 38 for i = 70 deg, and Figure 39 for i = 95 deg for orbital-debris particle diameters of (a) 0.05 cm, (b) 0.1 cm, (c) 1.0 cm, and (d) 10 cm. Examination of these figures shows the least uncertainty for altitudes around 500 km, with the uncertainty increasing as one moves away from this altitude.

The flux uncertainty can vary by a factor of 2 for the large diameters and by an order of magnitude for the smaller diameters. The uncertainty in F, $F + \varepsilon_F$, increases as the altitude approaches 2000 km. The major contributors to these levels of uncertainty can again be identified by examining the terms of Equation 28. For example (Fig. 37a), at i = 30 deg, h = 1000 km, d = 0.05 cm, and F = 0.023 impacts/m^2 • yr,

$$\varepsilon_F = \pm\left[(\varepsilon_{FM})^2 + (\varepsilon_{FH})^2 + \left(\frac{\partial F}{\partial p}\varepsilon_p\right)^2 + \left(\frac{\partial F}{\partial q}\varepsilon_q\right)^2 + \left(\frac{\partial F}{\partial S}\varepsilon_S\right)^2\right]^{1/2}$$

$$= [(2.3 \times 10^{-2})^2 + (2.07 \times 10^{-1})^2 + (2.21 \times 10^{-7})^2 + (2.85 \times 10^{-2})^2 + (8.41 \times 10^{-5})^2]^{1/2}$$

$$= 2.11\ (10^{-1}) \quad \underline{\text{thus}} \quad [(F + \varepsilon_F)/F] = 10.1$$

As in the case for flux versus diameter, the dominant terms are the uncertainties in the flux measurements and the small-particle growth. The uncertainties with respect to large-particle growth and the level of solar activity are negligible because the choice of diameters for this example (d = 0.05 cm, small particle) and choice of altitude where solar effects are minimal.

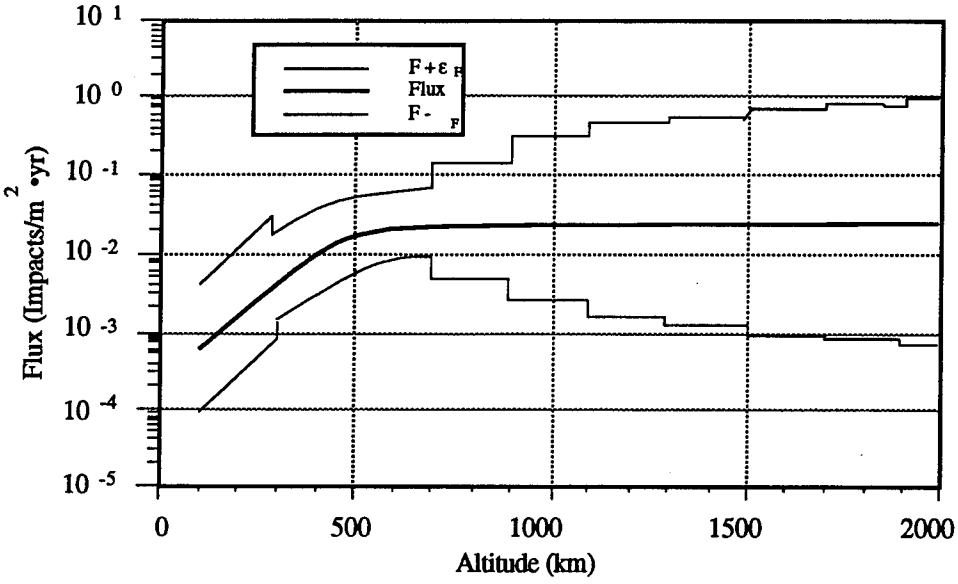

(a) d = 0.05 cm, t = 1995, and S = 90.

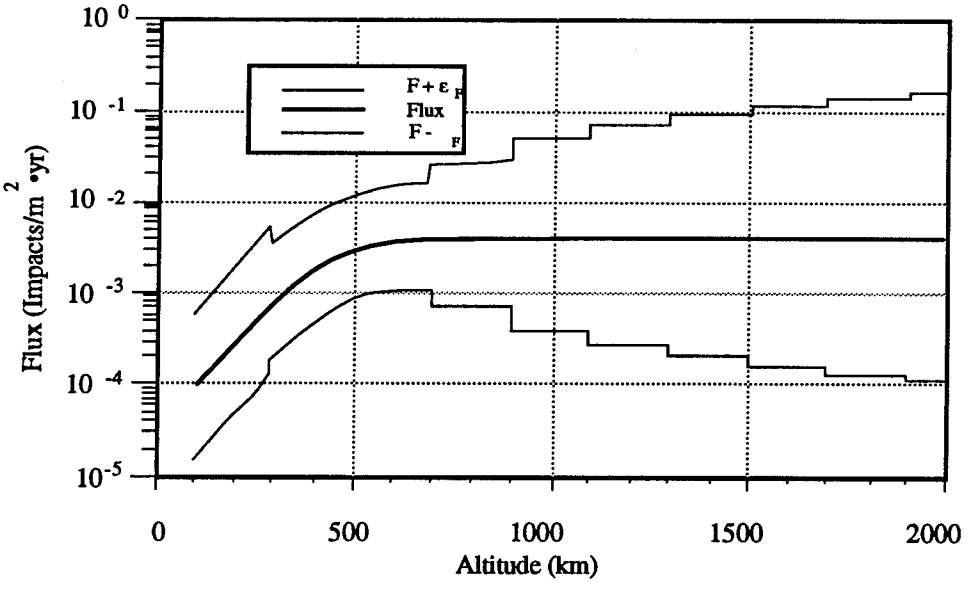

(b) d = 0.1 cm, t = 1995, and S = 90.

Figure 37. Flux model uncertainty versus altitude for i = 30 deg.

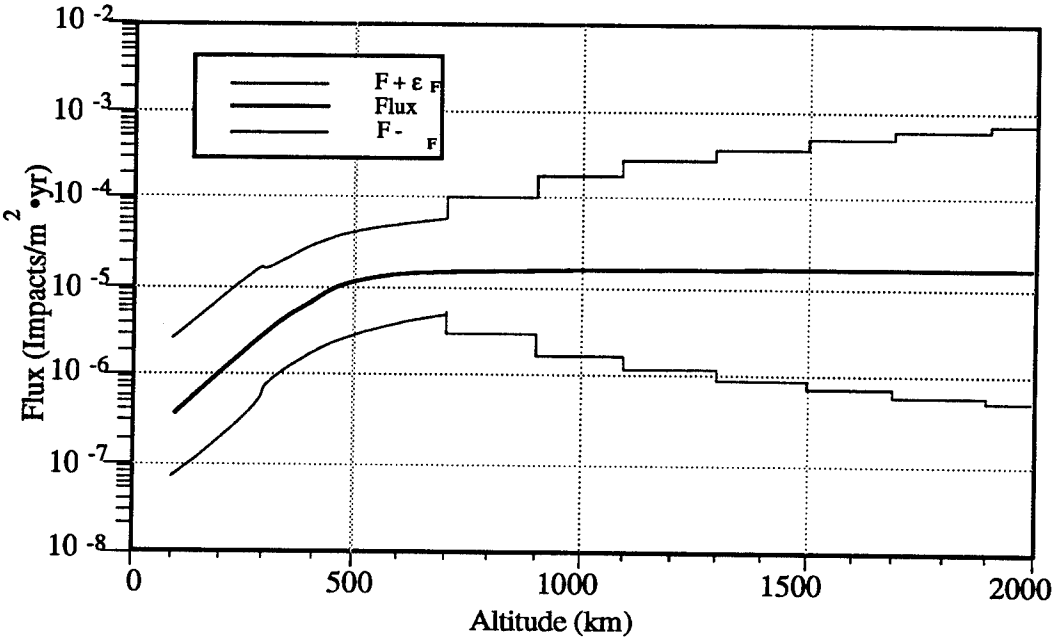

(c) d = 1.0 cm, t = 1995, and S = 90.

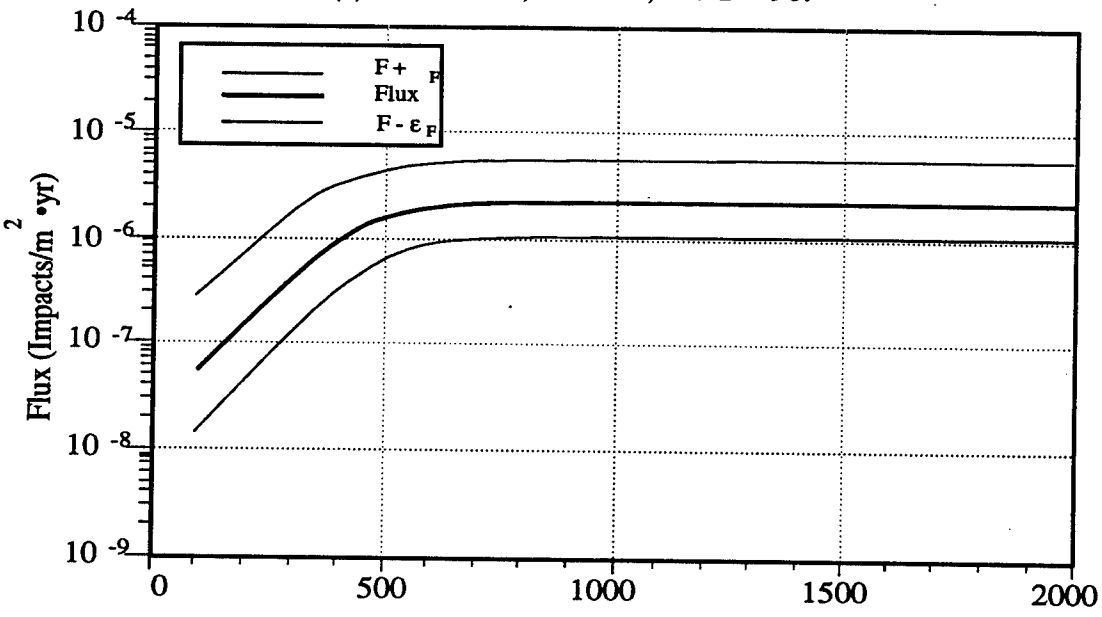

(d) d = 10 cm, t = 1995, and S = 90.

Figure 37. Concluded.

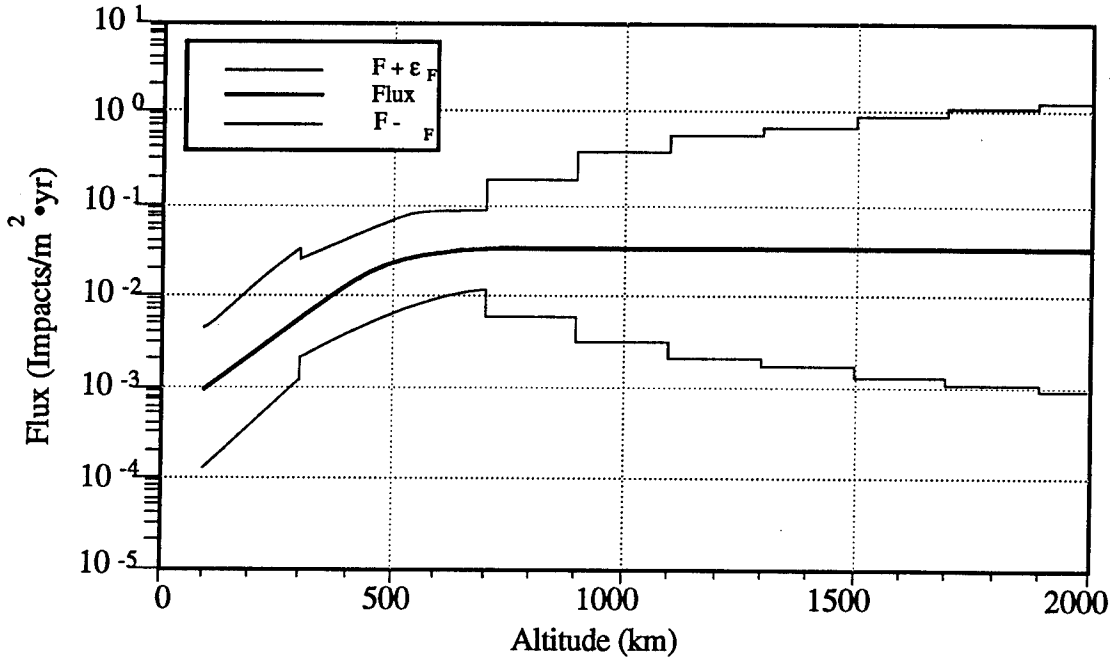

(a) d = 0.05 cm, t = 1995, and S = 90.

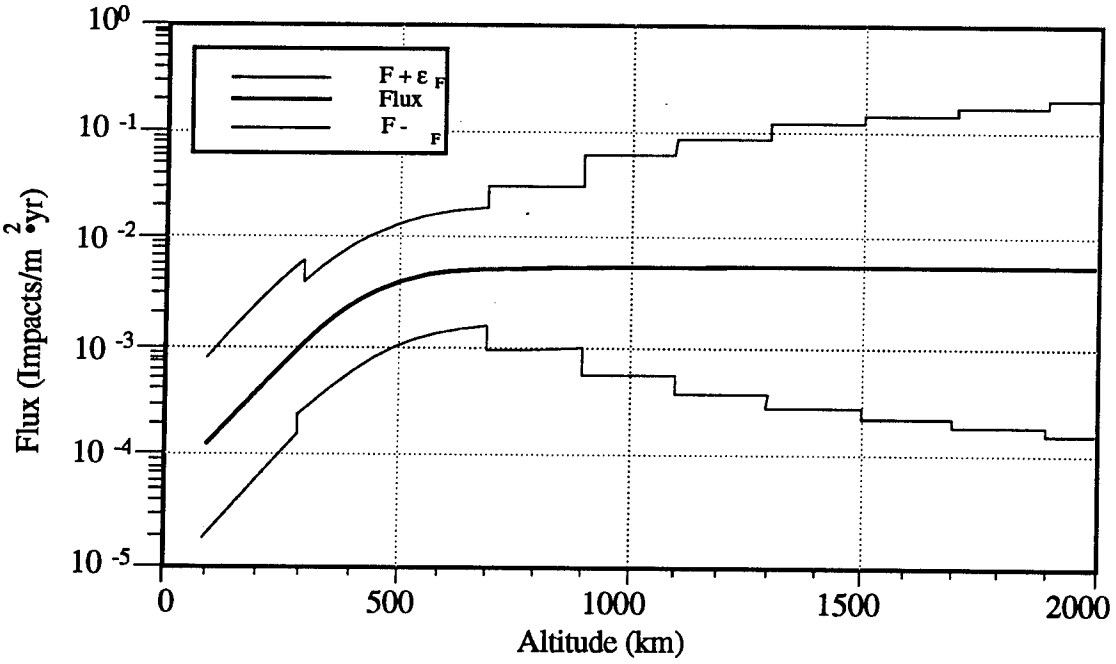

(b) d = 0.1 cm, t = 1995, and S = 90.

Figure 38. Flux model uncertainty versus altitude for i = 70 deg.

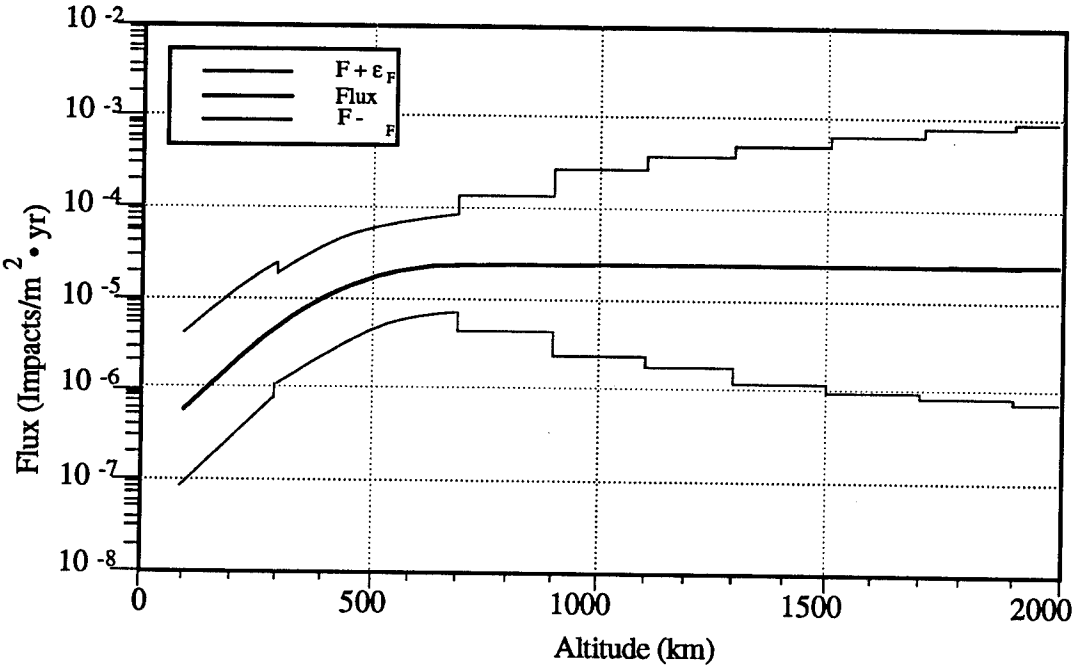

(c) d = 1.0 cm, t = 1995, and S = 90.

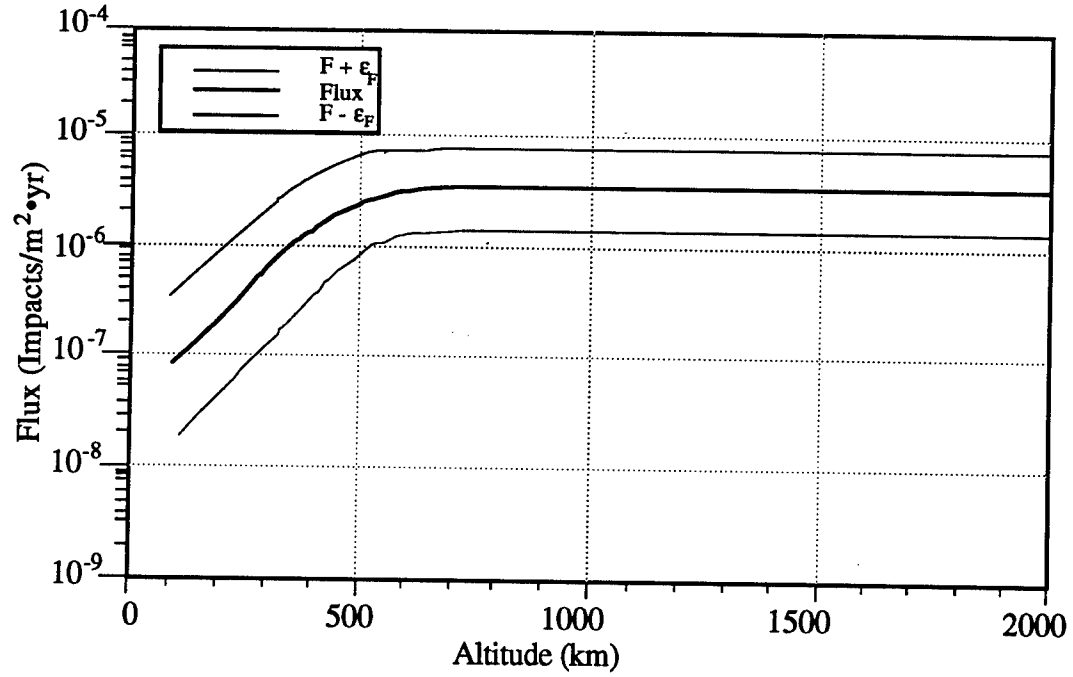

(d) d = 10 cm, t = 1995, S = 90.

Figure 38. Concluded.

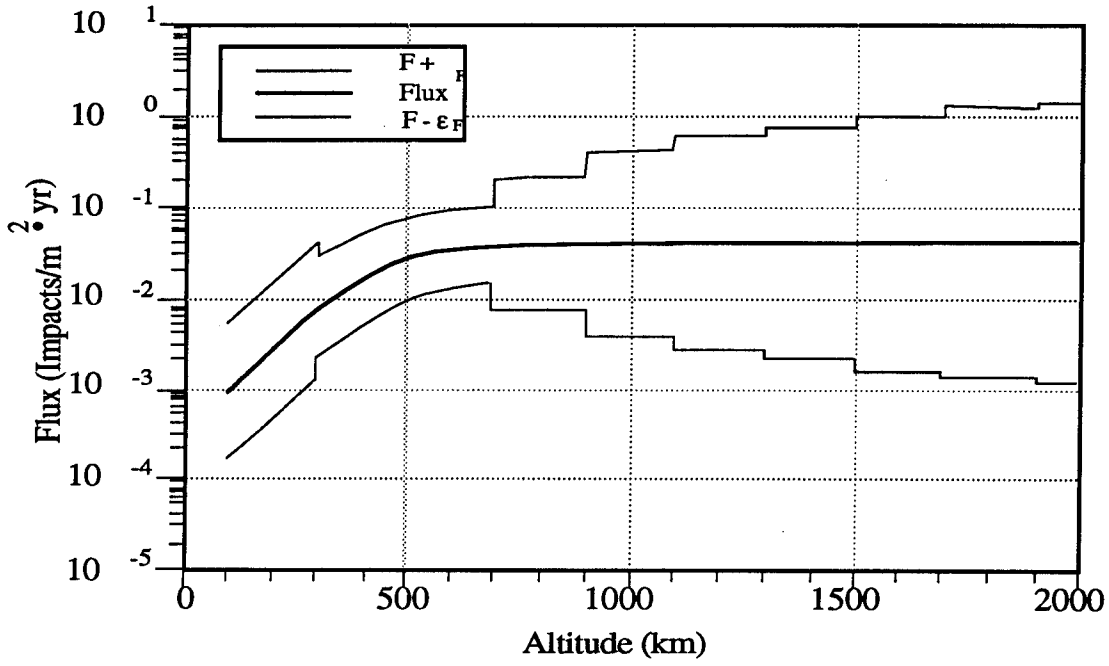

(a) d = 0.05 cm, t = 1995, and S = 90.

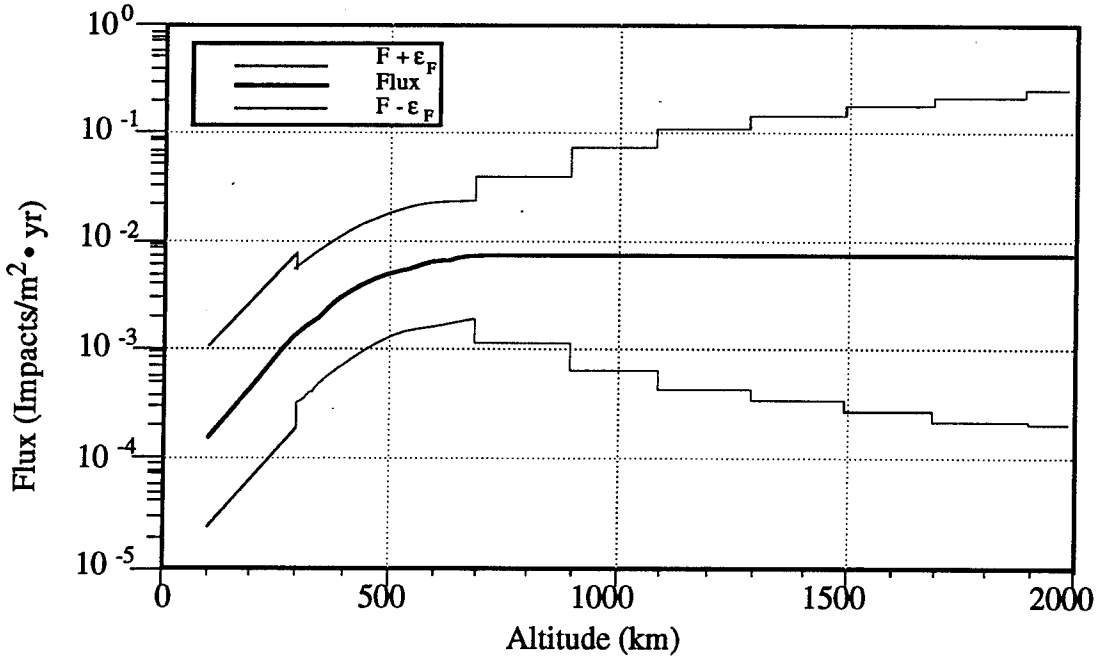

(b) d = 0.1 cm, t = 1995, and S = 90.

Figure 39. Flux model uncertainty versus altitude for i = 95 deg.

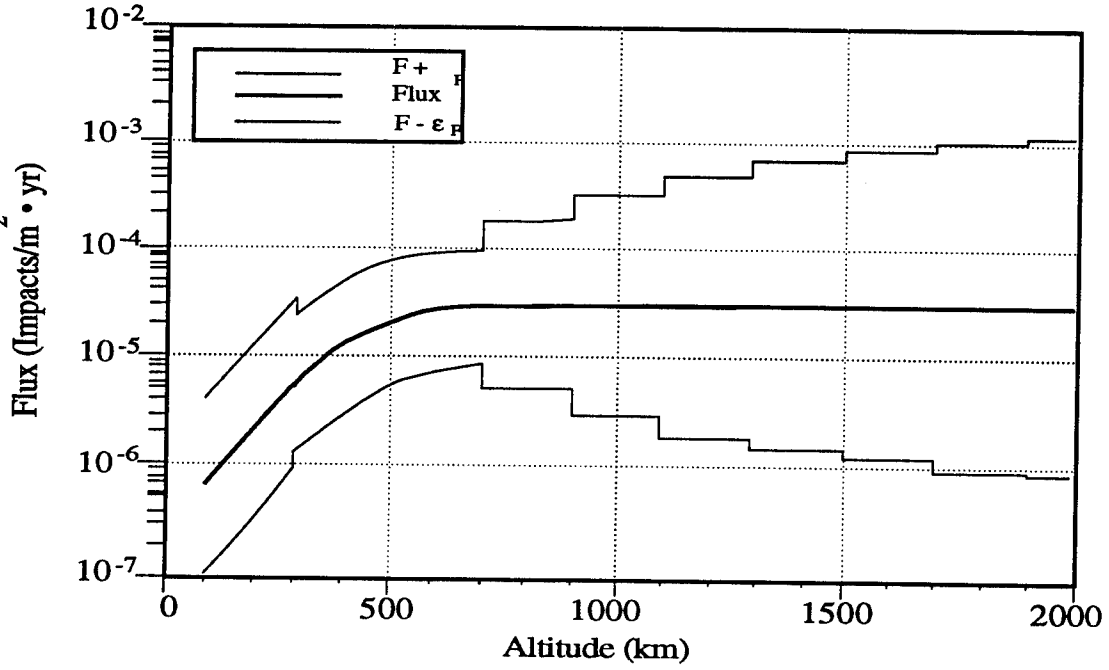

(c) d = 1.0 cm, t = 1995, and S = 90.

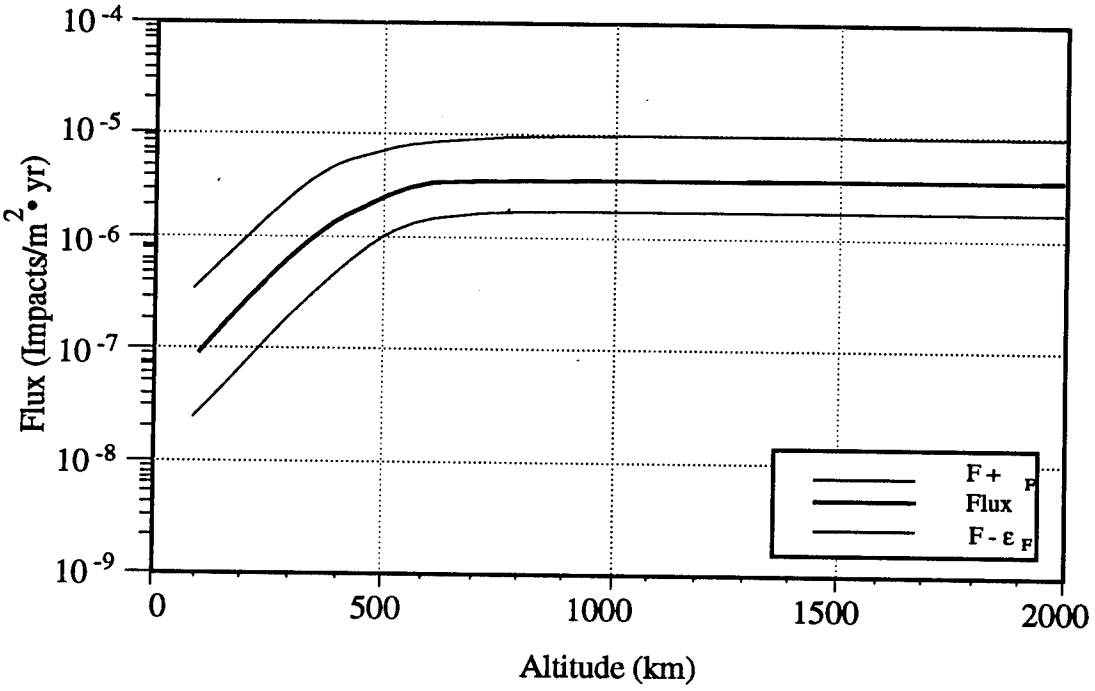

(d) d = 10 cm, t = 1995, and S = 90.

Figure 39. Concluded

7.3 UNCERTAINTY ASSESSMENT

Table 6 summarizes the uncertainties analyses presented for an orbital inclination of 95 deg and t = 1995 (S = 90) for the altitudes and diameters shown. Figure 40 presents the overall model uncertainty versus diameter and altitude for 1995 and an orbital inclination of 30 deg.

From Table 6, except for an altitude of 500 ± 200 km and diameters ≥10 cm, the model uncertainties are at least plus or minus an order of magnitude and increase as altitude approaches 2000 km. For all altitudes and debris particle sizes, the overall uncertainty, ε_F, is dominated by the uncertainty in the measurements, ε_{FM} and ε_{FH}. The small-particle growth uncertainty, $(\partial F/\partial q)\varepsilon_q$, is significant for the small particles, d < 10 cm, while the large-particle growth uncertainty, $(\partial F/\partial p)\varepsilon_p$, gains importance as particle size increases beyond d ≥ 10 cm. The relative influence of solar activity, as measured by the value of S, increases as altitude decreases (for a given size particle) for altitudes <1000 km. Above these altitudes the influence of the atmosphere is negligible, regardless of the value of S, on the overall flux uncertainty.

Table 6. Orbital-debris flux uncertainty
(i = 95 deg, t = 1995, S=90).

h(km)	d(cm)	ε_{FM}	ε_{FH}	$\left(\frac{\partial F}{\partial p}\varepsilon_p\right)$	$\left(\frac{\partial F}{\partial q}\varepsilon_q\right)$	$\left(\frac{\partial F}{\partial S}\varepsilon_S\right)$	ε_F	$\frac{F+\varepsilon_F}{F}$
500	0.01	1.51	$7.55(10^{-1})$	*	1.86	1.21	2.79	2.85
	0.10	$9.55(10^{-3})$	$2.39(10^{-3})$	*	$5.90(10^{-3})$	$3.84(10^{-3})$	$1.21(10^{-2})$	3.53
	1.00	$4.16(10^{-5})$	$1.04(10^{-5})$	*	$2.41(10^{-5})$	$1.67(10^{-5})$	$5.19(10^{-5})$	3.50
	10.00	$1.34(10^{-6})$	$2.69(10^{-6})$	$6.62(10^{-7})$	$1.64(10^{-7})$	$2.16(10^{-6})$	$3.76(10^{-6})$	2.40
	100.00	$2.31(10^{-7})$	$4.63(10^{-7})$	$1.20(10^{-7})$	*	$3.72(10^{-7})$	$6.48(10^{-7})$	2.40
1000	0.01	2.17	19.5	*	2.68	*	19.8	10.10
	0.10	$1.37(10^{-2})$	$6.18(10^{-2})$	*	$8.48(10^{-3})$	*	$6.38(10^{-2})$	10.30
	1.00	$5.98(10^{-5})$	$2.69(10^{-4})$	*	$3.46(10^{-5})$	*	$2.78(10^{-3})$	10.30
	10.00	$1.93(10^{-6})$	$3.86(10^{-5})$	$9.52(10^{-7})$	$2.53(10^{-7})$	*	$4.43(10^{-6})$	2.15
	100.00	$3.33(10^{-7})$	$6.65(10^{-7})$	$1.72(10^{-7})$	*	*	$7.63(10^{-7})$	2.15
1500	0.01	2.17	52.1	*	2.68	*	52.2	25.10
	0.10	$1.37(10^{-2})$	$1.65(10^{-1})$	*	$8.49(10^{-3})$	*	$1.66(10^{-1})$	25.10
	1.00	$5.99(10^{-5})$	$7.18(10^{-4})$	*	$3.47(10^{-5})$	*	$7.22(10^{-4})$	25.10
	10.00	$1.93(10^{-6})$	$3.87(10^{-6})$	$9.53(10^{-7})$	$2.36(10^{-6})$	*	$4.43(10^{-6})$	2.15
	100.00	$3.33(10^{-7})$	$6.66(10^{-7})$	$1.73(10^{-7})$	*	*	$7.64(10^{-7})$	2.15

Note: * Small Relative to Other Terms

Figure 40 shows the regions where the flux model gives the best prediction. The uncertainty factor, $[(F + \varepsilon_F)/F]$, versus diameter and altitude for i = 30 deg, t = 1995, and S = 90. The most precise predictions are at an altitude of 500 km (±200 km) or for the large particles, $d \geq 5$ cm. These results are consistent with the greatest availability of data, Solar Max and for these size particles, USSPACECOM. The uncertainty increases as particle size decreases or as altitude increases away from these nominal values. The overall uncertainty for these latter regions is shown to be at least plus or minus an order of magnitude.

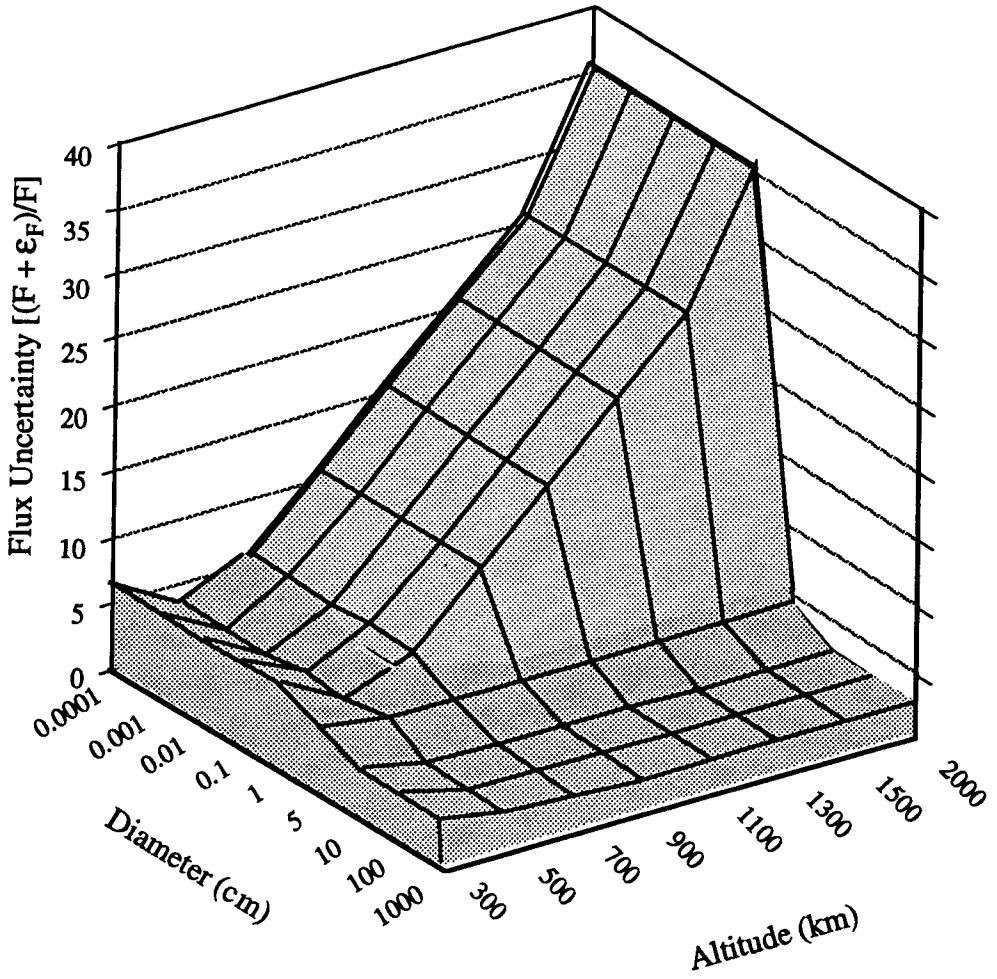

Figure 40. Flux model uncertainty versus diameter and altitude (i = 30 deg, t = 1995, S =90).

As shown by the examples in Subsection 7.2 and as depicted in Table 6 and Figure 40, the overall uncertainty of this model is consistently dominated by the uncertainties in the measured environment, ε_{FM} and ε_{FH}. If one could improve the space debris measurements, i.e., reduce

these uncertainties, especially ε_{FH} with respect to altitude, then the overall model uncertainty could be reduced. This assumes that the model accurately predicts the environment to begin with and that the improved measurements are consistent with the model predictions (there exists the possibility that improved measurements could invalidate the model). With improved measurements, reduction in the uncertainties are possible for both the large- and small-particle growth, ε_p and ε_q. For example, an order of magnitude reduction in ε_{FM} and ε_{FH} would result in the following for a particle size of 0.1 cm at 30-deg orbital inclination and altitudes of 1000 and 1500 km (Table 7).

Table 7. Improved flux predictions.

	d(cm)	h(km)	ε_{FM}	ε_{FH}	ε_F	F	$(F+\varepsilon_F)/F$
Current	0.1	1000	$8.15(10^{-3})$	$3.67(10^{-2})$	$3.79(10^{-2})$	$4.07(10^{-3})$	10.3
		1500	$8.16(10^{-3})$	$9.79(10^{-2})$	$9.84(10^{-2})$	$4.08(10^{-3})$	25.1
Improved	0.1	1000	$8.15(10^{-4})$	$3.67(10^{-3})$	$6.28(10^{-3})$	$4.07(10^{-3})$	2.54
		1500	$8.16(10^{-4})$	$9.79(10^{-3})$	$1.10(10^{-2})$	$4.08(10^{-3})$	3.71

Improving the measurement uncertainties by an order of magnitude can reduce the overall model uncertainty to a consistent factor for all altitudes and sizes and to values less than an order of magnitude.

8.0 CONCLUSION

The NASA 90 orbital-debris environment prediction model has been assessed. The model represents a smooth curve fit to the data. These data consist of USSPACECOM radar data, MIT/LL ETS and GEODSS optical data, returned spacecraft surface impact data (Solar Max), and recent radar data from Aricebo and Goldstone. Special purpose analytic/computational models were used by NASA to validate future traffic and growth studies. The USSPACECOM data were used primarily to establish altitude, velocity, and solar and orbital inclination effects for debris particles 10 cm or greater in diameter. Particle-size distribution was established by examining all data sets, but primarily relied on impact studies of returned spacecraft surfaces for the smaller-debris particles.

8.1 MODEL DEVELOPMENT

NASA believes that the NASA 90 model is valid only for spacecraft in LEO and through the year 2010. The validity of the model rests on the fundamental assumptions made in the derivation of this model. Other than the assumptions concerning the validity of the data or the specific uses of those data in the model formulation, perhaps the most fundamental or key observation concerning this model is with respect to that data base. The model was derived to fit the data that represent a historic record of man's first space operations. If these operations should change dramatically, then the basis for this model may no longer be valid. For example, the model assumes certain growth rates, breakup rates, and has inherent debris concentrations, $\Psi(i)$, built into it. If any of these drastically change, the model may not be adjustable to account for these changes (nor may the model be used to assess potential space architectures where these ground rules change significantly). Even now there are significant altitudes where the smoothed NASA model does not fit the debris environment by one to two orders of magnitude because of breakups at these altitudes and inclinations. The model accuracy is fundamentally tied to the accuracy of the data base. The data base is most accurate for altitudes on the order of 500 km and debris particles >10 cm in diameter. The model accuracy can only be improved by an increase in the accuracy of the data, assuming any new or improved data can be incorporated easily into the model. For example, the function H(d) was developed to account for improved knowledge of the environment for particles >8 cm (although extrapolated to smaller sizes). Future fixes may not be as easily developed or incorporated to improve the model's performance. Perhaps the most controversial and uncertain part of the model is in predicting the future. There simply is not enough of a historic record to see the future trends or growth rates to accurately project whether these are indeed linear or compounded growth curves.

The most unsatisfactory parts of this model are the collision-velocity impact distributions, velocity direction, and the particle-density estimates. The collision-velocity impact distribution is a complicated function of orbital inclination and has no discernible link to physical reality in its presented form. The direction of impact model assumes circular orbits only and does not allow for elliptical orbit out-of-plane impacts. This may not be a bad assumption as a first approximation since most LEO-region debris orbits will be nearly circular. The particle-density function assumes spherical particles and has little data to support its formulation, especially for the smaller sizes. Each of these expressions are restricted due to limited data. Improving these expressions, or knowledge of these environments, will only come with improved measurements and experiments. The user is cautioned that these particular expressions in the NASA 90 model are particularly weak.

8.2 SENSITIVITY ANALYSIS

The NASA 90 orbital-debris flux prediction model,

$$F(d, h, i, t, S) = H(d)\,\Phi(h, S)\,\Psi(i)\,[F_1(d)\,g_1(t) + F_2(d)\,g_2(t)]$$

has been shown to be most sensitive to changes in the orbital-debris particle diameter, d. The changes in flux are most sensitive to diameters <0.05 cm, with the overall sensitivity increasing as particle size decreases. This sensitivity reflects the nature of the curve fit predictions, F_1 (d) and F_2 (d). The flux model is relatively insensitive to the large diameters >1 cm.

Next in relative importance is the model sensitivity with respect to the small-particle growth rate, q, followed by the sensitivities with respect to large-particle growth, p, and inclination, i. The model sensitivity increases as q increases, which reflects the nature of the assumed compounded growth, $g_1(t)$, for the small particles. Changes in the value of p do not influence the model sensitivity, reflecting the nature of the assumed linear growth, $g_2(t)$, for the large particles. This difference in sensitivity illustrates the distinction between whether debris growth is assumed to be linear or compounded. Neither linear nor compounded growth for the large-particles is substantiated by the data. There is essentially no data to base the small-particle growth rate. If the actual growth rates are found to be compounded for p and q, then the choice of the growth rate (5 percent versus 10 percent) will influence the resulting prediction. If the growth is linear, then the actual value of the growth rate becomes less important. The sensitivity with respect to orbital inclination reflects

the $\Psi(i)$ distribution defining regions of increased and decreased sensitivity as the inclination is varied for altitudes <1000 km.

The flux model sensitivity to time (t) and level of solar activity (S) are relatively equal in importance. The least sensitive parameter is altitude (h). Beyond 800 to 1000-km altitude, the flux model predicts a cloud of orbital debris that remains constant with increasing altitude. This does not fit physical intuition nor does it comply with the data as shown in Figure 3. In Figure 3, the debris flux environment peaks at 800, 1000, and 1500 km because of known breakups at these altitudes, which the model clearly does not predict. Disregarding these peaks, the general trend for the actual debris flux is to decrease at altitudes beyond 800 to 1000 km. The flux model, Equation 6, does not predict this decrease and is insensitive to changes at altitudes >1000 km. The NASA 90 model applications should be restricted to altitudes <1000 km. This flux model does not *explicitly* account for variations in the ballistic coefficient of fragments which affects their orbital lifetime. This is done implicitly in the solar activity term.

In rank order, the relative NASA 90 model sensitivities (and comments pertaining thereto) with respect to the variables d, h, i, t, S, p, and q are as follows:

Parameter	Comments
• diameter, d	Reasonable; however, model flux becomes undefined (infinite) as $d \rightarrow 0$. Recommend limiting model application to specific range of debris sizes, for example $10^{-4} \leq d \leq 10^{3}$ cm.
• small-particle growth rate, q	Reasonable. Sensitivity increases with growth rate.
• orbital inclination, i large-particle growth rate, p	Reasonable. Model sensitivity reflects variation with respect to debris concentration, Ψ (i). Model is sensitive to choice of growth (linear or compounded).
• time, t solar activity, S	Reasonable. Model sensitivities reflect response or changes with respect to t and S.

• orbital altitude, h	Unreasonable. Model predicts essentially constant flux beyond 1000 km with increasing insensitivity as altitude increases. Limit model application to altitudes <1000 km.

8.3 UNCERTAINTY ANALYSIS

Except for altitudes of 500 km (±200 km) and debris sizes >10 cm, the flux model predictions and resultant uncertainties have been shown to be plus or minus one order of magnitude at a 90-percent confidence. The best measured data are at 500 km and for sizes ≥10 cm. The flux model predictions at this altitude and size range are within a factor of 2 to 4. The major contributor to the overall model uncertainty is the uncertainty in the measured flux environment. Reducing only the measurement uncertainties, ε_{FM} and ε_{FH}, by an order of magnitude for all altitudes and diameters can reduce the overall flux prediction uncertainty to a factor of 2 to 4 consistent with 500 km and d ≥ 10 cm. This assumes the model itself can be adjusted to account for any improved data or improved knowledge of the actual environment. The current uncertainty bound of at least plus or minus one order of magnitude (except at 500 km and d > 10 cm) is significant. It is recommended the model be used only for other than conceptual design studies.

8.4 RESULTS/RECOMMENDATIONS

As a result of this study, the following conclusions and recommendations are made:

- The NASA 90 model is an engineering model for the prediction of long-term, orbital-debris environments for spacecraft in LEO only. It is an empirical relationship derived from curve fits to the data. It meets NASA's objective for a design model that is easy to use. The model has been instrumental in leading to increased understanding of the orbital-debris environment.

- It is recommended this model only be used to establish the order of magnitude of the orbital-debris hazard environment for spacecraft in LEO, specifically h ≤ 1000 km, for studies only through the year 2010 and for present space operations. The model should not be used in space architecture studies where the space operations change significantly. The model should be restricted to the data base, 10^{-4} cm ≤ d ≤ 10^{3} cm.

- The collision-velocity impact distribution and direction of impact algorithm are not recommended for quantitative use. The velocity distribution used in this model represents the expected distribution only at one altitude (500 km) and for a given snapshot in time. The estimated relationship for particle mass rests on very little data and represents a gross approximation of the environment.

- The model does not operate with high accuracy except at 500-km altitude or for sizes where $d \geq 10$ cm. For all other regions, the model uncertainty is at least one order of magnitude. The model may not benefit from new debris measurements to improve the model accuracy if those new measurements significantly alter the predicted environment. Presently, the model does not reproduce the measured environment beyond 1000 km.

- It is recommended that the AF examine and assess more sophisticated physics-based computational models to meet the goals of developing an AF, long-term debris model that can

    - operate with high accuracy at the relevant altitudes (LEO) and orbital parameters
    - benefit from new debris measurements
    - accommodate current and future AF space scenarios and architectures

- In the effort to develop more accurate long-term, orbital-debris models, ORION recommends that the AF pursue a vigorous program to measure the debris environment with high accuracy in LEO for all particle sizes.

As a final note, the LEO debris environment is largely a man-made environment. As obvious as this statement may seem, the development of any model which attempts to predict the future consequences of man's activities must inherently be uncertain.

REFERENCES

1. Kessler, D. J., Reynolds, R. C. and Anz-Meador, P. D., Orbital Debris Environment for Spacecraft Designed to Operate in Low Earth Orbit, NASA TM 100471, April 1989.

2. Proposed Revision to Section 8, "Meteoroids and Orbital Debris," SSP 30425, Space Station Program, Natural Environment Definition for Design, September 1990.

3. Jackson, P. A., Major (USAF), "Space Surveillance Satellite Catalog Maintenance," AIAA 90-1339, April 1990.

4. Taff, L.G. and Jonuskis, D.M., "Results and Analysis of a Bi-Telescopic Survey of Low Altitude Orbital Debris," Advances Space Res., Vol. 6, No. 7, pp. 131-137, 1986.

5. Henize, K. G., and Stanley, J. F., "Optical Observations of Space Debris," AIAA 90-1340, April 1990.

6. Laurance, M.R. and Brownlee, D.E., "The Flux of Meteoroids and Orbital Space Debris Striking Satellites in Low Earth Orbit," Nature, Vol. 323, 11 September 1986.

7. Zook, H. A., McKay, D. S., and Bernhard, R. P., "Results from Returned Spacecraft Surfaces," AIAA 90-1349, April 1990.

8. Kessler, D. J., "Orbital Debris Environment for Spacecraft in Low Earth Orbit," AIAA 90-1353, April 1990.

9. Thompson, T. W. and Goldstein, R., "Radar Measurements of Small Debris. Arecibo and Goldstone Radars," AIAA 90-1342, April 1990.

10. Reynolds, R. C. and Potter, A. E., Jr., Orbital Debris Research at NASA Johnson Space Center, 1986-1988, NASA TM 102155, September 1989.

11. de Jonge, A.R.W. and Wesselus, P.R., "Detecting Space Debris Above 900 km Using IRAS," AIAA 90-1341, April 1990.

12. Badhwar, G. D., and Anz-Meador, P. D., "Relationship of Radar Cross Section to the Geometric Size of Orbital Debris," AIAA-90-1347, April 1990.

13. Johnson, N.L. and Nauer, D.J., "Orbital Debris Detection: Techniques and Issues," AIAA 90-1330, April 1990.

14. Kessler, D. J., and Anz-Meador, P. D., "Effects on the Orbital Debris Environment Due to Solar Activity," AIAA 90-0083, January 1990.

15. Walterscheid, R.L., "Solar Cycle Effects on the Upper Atmosphere: Implications for Satellite Drag," J Spacecraft, Vol. 26, No. 6, Nov - Dec 1989.

16. Withbroe, G. L., "Solar Activity Cycle: History and Predictions," J. Spacecraft, Vol. 26, No. 6, Nov - Dec 1989.

17. McIntosh, P. S., "Did Sunspot Maximum Occur in 1989?", Sky & Telescope, January 1991.

18. Johnson, N. L., and McKnight, D. S., Artificial Space Debris, Orbit Book Company, Malabar, Florida, 1987.

19. Space Debris, A Report from the ESA Space Debris Working Group, European Space Agency, 1988.

20. Report on Orbital Debris, Interagency Group (Space) for the National Security Council, Washington D.C., February 1989.

21. Badhwar, G. D., and Anz-Meador, P. D., "Determination of the Area and Mass Distrubution of Orbital Debris Fragments," Earth, Moon, and Planets 45: pp 29-51, Kluwer Academic Publishers, Netherlands, 1989.

22. Rex, D., Eichler, P., Soppa, U., Zuschlag, J., and Bade, A., "Space Debris - Origin, Evolution and Collision Mechanics," Acta Astronautica, Pergammon Press, Great Britian, Vol. 20, pp. 209-216, 1989.

23. Reynolds, R. C., "A Review of Orbital Debris Environment Modeling at NASA/JSC," AIAA-90-1355, April 1990.

24. DoD Space Transportation Mission Requirements Definition, Volume I: Discussion, Aerospace Report No. TOR-0086A (2460-01)-1, Vol. I, 12 December 1986.